The Discontinuous Galerkin Trefftz Method

Vom Fachbereich Elektrotechnik und Informationstechnik der Technischen Universität Darmstadt genehmigte Dissertationsschrift zur Erlangung des akademischen Grades Doktor-Ingenieur (Dr.-Ing.) von Dipl. Phys. Fritz Kretzschmar geboren am 5 Dezember 1984 in Frankfurt am Main

Tag der Einreichung: 13 April 2015, Tag der Prüfung: 16 Juli 2015
Darmstadt 2015 — D 17

1. Gutachten: Prof. Thomas Weiland
2. Gutachten: Prof. Herbert Egger

TECHNISCHE UNIVERSITÄT DARMSTADT

GRADUATE SCHOOL
computational engineering

The Discontinuous Galerkin Trefftz Method

Genehmigte Dissertationsschrift von Dipl. Phys. Fritz Kretzschmar geboren am 5 Dezember 1984 in Frankfurt am Main

1. Gutachten: Prof. Thomas Weiland
2. Gutachten: Prof. Herbert Egger

Tag der Einreichung: 13 April 2015
Tag der Prüfung: 16 Juli 2015

Darmstadt 2015 — D 17

Bitte zitieren Sie dieses Dokument als:
URN: urn:nbn:de:tuda-tuprints-51668
URL: http://tuprints.ulb.tu-darmstadt.de/5166

Dieses Dokument wird bereitgestellt von tuprints,
E-Publishing-Service der TU Darmstadt
http://tuprints.ulb.tu-darmstadt.de
tuprints@ulb.tu-darmstadt.de

Plan difficult tasks through the simplest tasks
Achieve large tasks through the smallest tasks
The difficult tasks of the world
Must be handled through the simple tasks
The large tasks of the world
Must be handled through the small tasks.

Eidesstattliche Erklärung

Ich erkläre hiermit an Eides statt, dass ich meine Dissertation selbständig und nur mit den angegebenen Hilfsmitteln angefertigt habe. Alle Stellen, die aus Quellen entnommen wurden, sind als solche kenntlich gemacht. Diese Arbeit hat in gleicher oder ähnlicher Form noch keiner Prüfungsbehörde vorgelegen.

Darmstadt, den 13 April, 2015

(Fritz Kretzschmar)

Zusammenfassung

Das Ziel der nachfolgenden Arbeit ist die Entwicklung einer neuartigen numerischen Methode, welche zur Approximation der zeitabhängigen Maxwellschen Gleichungen verwendet wird. Die genannte Methode kombiniert eine bereits bestehende diskontinuierliche Galkerkin (DG) Methode mit sogenannten polynomialen Trefftz Funktionen, welche die zeitabhängigen Maxwellschen Gleichungen exakt lösen.

Zunächst werden polynomialen Trefftz Funktionen entwickelt, wobei hier zwei verschiedene Konstruktionsmechanismen dargelegt werden. Im ersten Konstruktionsmechanismus werden die polynomialen Trefftz Funktionen durch die widerholte Verwendung von Rekursionsgleichungen, welche in diesem Kontext entwickelt wurden, aus einer schon existierenden Basis hergeleitet. Im zweiten Konstruktionsmechanismus werden die polynomialen Trefftz Funktionen durch polynomiale ebene Wellen ausgedrückt. Zusätzlich werden Grundlegende Eigenschaften der so konstruierten Basen, d.h. Dimension und Energietransport, beschrieben.

Nachfolgend wird die DG Methode eingeführt in welcher die genannten polynomialen Trefftz Funktionen verwendet werden. Eine anknüpfende Analyse zeigt, dass die entstehende DG-Trefftz Methode stabil ist, eindeutige Lösungen hat und somit wohldefiniert ist.

Die durchgeführten numerischen Studien der Methode zeigen, dass spektrale Konvergenz des L_2-Norm Fehlers in der betrachteten Raum-Zeit Domäne $\Omega \times I$ unter Anheben der polynomialen Approximationsordnung p erreicht wird. Es folgt, dass die Methode Lösungen die von hoher Ordnung in der Zeit sind, produziert. Unter h-Verfeinerung ergeben sich die erwarteten Konvergenzraten von $p + 1$. Zusätzlich weist die DG-Trefftz ein gutes Dispersionsverhalten auf. Der Vergleich mit einer herkömmlichen DG Methode zeigt, dass mit der DG-Trefftz Methode vergleichbare Lösungen mit einer deutlich geringeren Anzahl von Basisfunktionen simuliert werde können. Die Anzahl der betrachteten Freiheitsgrade verringert sich von $\mathcal{O}(p^4)$ auf $\mathcal{O}(p^3)$.

Im letzten Teil der Arbeit wird eine neuartige transparente Randbedingung im Rahmen der DG-Trefftz Methode entwickelt, die zur Simulation von unendlich ausgedehnten Domänen verwendet werden kann. In dieser Randbedingung werden in die Domäne laufende Wellen direkt in der Basis unterdrückt, was möglich ist, da die Richtungen der polynomialen Trefftz Funktionen bekannt sind.

Abstract

In the following work we develop a novel numerical method, which is used to approximate time-dependent Maxwell's equations. The method combines an already existing discontinuous Galerkin (DG) method with polynomial Trefftz functions. These polynomial Trefftz functions exactly solve Maxwell's equations in an element-wise fashion.

In the first part of this work we develop polynomial Trefftz functions. Here, we introduce two different construction mechanisms. First, we transform already existing polynomial functions into polynomial Trefftz functions by applying newly developed recurrence relations. In the second mechanism, we directly construct the polynomial Trefftz functions in terms of polynomial plane waves. Subsequently, basic properties of the resulting bases, i.e. dimension and energy transport, are discussed.

We then introduce the underlying DG-method and combine it with the polynomial Trefftz functions. A subsequent analysis shows that the method is stable and has unique solutions, which implies that the method is well-defined.

The numerical studies show that the method exhibits spectral convergence of the L_2-norm error under p-enrichment in the whole space-time domain of interest $\Omega \times I$. Therefore, high-order time-integration is an inherent feature of the method. Under h-refinement the method produces the expected $p+1$ convergence rates. In addition the method exhibits a good dispersion behavior. A comparison with a comparable non-Trefftz method shows that the DG-Trefftz method produces the same results with a lower number of basis functions. The number of degrees of freedom is decreased from $\mathcal{O}(p^4)$ to $\mathcal{O}(p^3)$.

In the last part of the work we introduce a novel transparent boundary condition in the context of the DG-Trefftz method. This boundary condition exploits the knowledge of the direction of propagation of the basis and directly penalizes basis functions that correspond to wave that are going into the domain.

Curriculum Vitae

Personal

Date of Birth	December 5th 1984, son of Rüdiger Kretzschmar and Barbara Kretzschmar in Frankfurt am Main , Germany
Adress	Kiesstrasse 21 – 64283 Darmstadt, Germany

Education

1991–1995	**Elementary School** Gerhardt Hauptmann Schule Dreieich, Germany
1995–2001	**Middle School** Weibelfeld Schule Dreieich, Germany
2001–2004	**High School** Weibelfeld Schule Dreieich, Germany
2004–2010	**Diploma/Magister Studies** Frankfurt University Frankfurt, Germany (Specialized in Physics and Philosophy)
2010–2012	**Doctoral Studies** DUKE University Durham, NC, United States (Specialized in High Energy Physics)
2012–2014	**Doctoral Studies** TU Darmstadt Darmstadt, Germany (Specialized in Computational Engineering)

Abitura

Date	May 2004
Specialization	Chemistry and History

Diploma Thesis

Title	**Dispersion Relations in Abelian and Non-Abelian Plasmas**
Supervisors	Prof. Adrian Dumitru and Prof. Carsten Greiner
Description	In this thesis we investigated the dispersion of the collective modes in a quark gluon plasma in the hard thermal loop limit.

Current Work

Topics	Computational Electrodynamics, Wave Propagation Problems, Discontinuous Galerkin Methods, Trefftz Methods
Supervisors	Prof. Thomas Weiland, Prof Herbert Egger, and Dr. Sascha Schnepp

Contents

List of Figures

List of Tables

1 Introduction

Nowadays, modeling and precisely predicting the behaviour of electromagnetic fields that accompany the propagation of electromagnetic waves has become a fundamental requirement for various academic disciplines including engineering, bio-medicine, and physics, where common problems tend to involve a high degree of complexity. As a result, satisfactory solutions can usually not be obtained in an analytic fashion anymore but must be numerically approximated on a computer instead. For this purpose, various existing numerical methods such as Finite Difference Time Domain (FDTD) methods and Finite Element Methods (FEM) have been adopted to the area of electromagnetism. These well established methods already work with great success in most scenarios. However, for certain applications that require extremely precise solutions it can be difficult to obtain the desired solutions (at least not in a reasonable time). Scenarios of this kind arise for example in bio-medical applications, such as simulations of the interaction of the retina with electromagnetic radiation or the modeling of a optical nerve; in physical applications such as the modeling of meta-materials as well as photonic crystals; and in engineering applications such as the simulation of optical instruments. Here, limiting factors can be due to inherent numerical artifacts of the established methods that can cause, for instance, high numerical dispersion errors or by applying low order time integrators that thereby limit the precision. Many of the numerical artifacts can be minimized by applying problem specific versions of the established methods. Here, Trefftz methods are one class of these problem specific methods that employ basis functions that exactly solve the underlying Partial Differential Equation (PDE) equations. In the case of time dependent Maxwell's equations employing Trefftz functions is automatically accompanied by using a method that is defined in space-time. If the employed basis functions are high order in time, these methods are suitable for high order time integration. Though widely studied in mechanics and fluid dynamics, Trefftz functions have been seldomly applied in methods that solve time dependent Maxwell's equations so far.

In this dissertation, we present a novel method that combines a space-time Discontinuous Galerkin (DG) method with polynomial Trefftz functions which are polynomial basis functions that exactly solve Maxwell's equations. By doing so, many of the mentioned numerical artifacts are considerably minimized so that

highly accurate results in space-time can be obtained. In connection to the development of the Discontinuous Galerkin Trefftz (DGT) method we also show stability and well-posedness of the scheme and we provide numerical evidence its properties.

The dissertation is organized in following three main parts: introduction, methodology, and numerical experiments.

Chapter 2 provides an introduction to the subfield of electromagnetism that we consider in this work. We start by introducing Maxwell's equations as well as the considered constitutive laws. After that, we introduce the concept of energy balance that will be used in the further chapters. We discuss special solutions of Maxwell's equations namely plane waves. The remainder of this chapter deals with the application of Maxwell's equations to finite domains. In particular, we discuss continuity requirements as well as boundary conditions.

Chapter 3 gives an introduction to Trefftz methods. In this context, we first outline the original Trefftz method and subsequently discuss the progress of its developement since then. Afterwards, we outline the development of the new DGT method and classify it in this context.

Chapter 4 contains the first essential building block for the DGT method: polynomial Trefftz functions. These build up the polynomial Trefftz space which we introduce as a new concept here. To this end, we treat them in a rigorous fashion: we first characterize their temporal behavior, and from this characterization, in combination with standard arguments for polynomial spaces, determine the dimension of the polynomial Trefftz space. This dimension is only dependent on the spatial dimension. Subsequently, we comment on the energy transport of these functions. In the final part of the chapter we then introduce two different ways to construct a polynomial Trefftz basis: first by transforming polynomial non-Trefftz basis functions into polynomial Trefftz basis functions by applying appropriate recurrence relations; secondly by constructing a Trefftz basis in terms of transport polynomials.

Chapter 5 is concerned with developing the method. To this end, we first introduce an abstract DG framework in which we employ trial and test function from a general vector space. From this preliminary discussion we obtain some of the essential properties of the method that are: consistency and stability. In the second step we then derive the DGT method from this template by constraining the vector space to the polynomial Trefftz space. We show that this method is well-posed and outline a numerical implementation.

Chapter 6 provides first qualitative results. More precisely, we study the propagation of plane waves through various media that are homogeneous, piece-wise

homogeneous, and inhomogeneous. We also discuss a novel type of Trefftz basis functions that are tailored to media with material jumps (in a one-dimensional scenario). In the remainder of this chapter we show the simulations of single-slit and double-slit diffraction experiments.

Chapter 7 contains the numerical study of the error behavior of the DGT method. To this end, we first study the contribution of numerical dispersion and numerical dissipation to the error with a simple example. After that, we conduct a series of numerical convergence studies. More precisely, we investigate the error convergence under p-enrichment and h-refinement for two distinct scenarios. Hereby, we obtain spectral convergence in the whole space-time domain and optimal convergence rates. Subsequently, we outline a comparison of the efficiency of the DGT method (in a one-dimensional scenario) to that of established methods and thereby confirm its validity. In the final part of the chapter we compare the error of a simulation produced with the space-time DGT method to that of a similar DG method that uses a standard non-Trefftz basis.

Chapter 8 introduces another feature of the DGT method, namely a novel type of transparent boundary condition. These boundary conditions exploit the knowledge of the direction of propagation in the basis functions by splitting them into incoming and outgoing parts at the boundary and then penalizing the incoming parts. The new transparent boundary condition shows the potential to serve as a replacement for some commonly applied boundary conditions, as we show in an attached error study.

2 Formulation of Continuous Electrodynamics

"The theory I propose may therefore be called a theory of the Electromagnetic Field, because it has to do with the space in the neighborhood of the electric or magnetic bodies, and it may be called a Dynamical Theory, because it assumes that in that space there is matter in motion, by which the observed electromagnetic phenomena are produced."

James Clerk Maxwell (1865)

The study of electromagnetic[1] phenomena has a long history. Our modern perspective on electromagnetism is based upon the works of James Clerk Maxwell [62, 63] who combined and completed the theoretical outcome of the experiments that were conducted by his scientific predecessors into "*a dynamical theory of the electromagnetic field*".

In this chapter we introduce the necessary physical framework that we will use. Following Jackson [37] (Chapter 1), we start by introducing the electromagnetic fields as well as their governing equations, i.e. Maxwell's equations in the continuum in Section 2.1. To this description we add material equations in Section 2.2. In Section 2.3 we derive an energy balance that follows from the considered system. In the fashion of Landau [54] (Chapter 6) we then introduce a simple way to solve Maxwell's equations.

Following Stratton [87] (Chapter 5), we extend our discussion to finite domains. To this end we derive the necessary continuity requirements of the fields at medium interfaces in Section 2.5 and consequently discuss their behavior at domain boundaries in Section 2.6.

[1] The name **electromagnetism** is a combination of the Greek words λίτος Μαγνῆτις (English.: "*magnesian stone*") and ήλεκτρον (English.: "*amber*").

2.1 Maxwell's Equations

We start by motivating the governing equations of the electromagnetic fields. For details, we refer to [37, 54, 87]. Motivated from experimental observations they read as follows:

Faraday's induction law: when a permanent magnet is moved through a wire loop surrounding an area S it induces an electromotive force which is related to the magnetic flux through this area by

$$\int_{\partial S} \mathbf{E}(\mathbf{r},t)\cdot\boldsymbol{\tau}\,\mathrm{d}l = -\frac{d}{dt}\int_S \mathbf{B}(\mathbf{r},t)\cdot\mathbf{n}\,\mathrm{d}S, \tag{2.1a}$$

where, $\mathbf{E}$ is the electric field strength, and $\mathbf{B}$ the magnetic induction. Note that we designate vectors by bold letters. In addition $\mathbf{r}\in\mathbb{R}^3$ is the position vector, $t\in\mathbb{R}$ the time. $\mathbf{n}$ denotes the outward normal direction on S, ∂S a closed loop around S, and $\boldsymbol{\tau}$ a tangential vector. Here, $\mathbf{n}$ and $\boldsymbol{\tau}$ are chosen according to the right hand rule.

Ampere's law: a wire going through a surface S which carries an electric current produces a magnetic field in its surrounding. The relation between the field strength and the current density is given by

$$\int_{\partial S} \mathbf{H}(\mathbf{r},t)\cdot\boldsymbol{\tau}\,\mathrm{d}l = \int_S \left(\frac{d}{dt}\mathbf{D}(\mathbf{r},t)+\mathbf{J}(\mathbf{r},t)\right)\cdot\mathbf{n}\,\mathrm{d}S. \tag{2.1b}$$

Here, $\mathbf{H}$ is the magnetic field, $\mathbf{D}$ the electric displacement field, and $\mathbf{J}$ the current density. The displacement current term $\frac{d}{dt}\mathbf{D}$ has been added by Maxwell.

Gauss' law for magnetism: it has been observed in experiments that magnetic field lines are always closed so that no magnetic monopoles can exist. This observation can be expressed by

$$\int_{\partial V} \mathbf{B}(\mathbf{r},t)\cdot\mathbf{n}\,\mathrm{d}S = 0, \tag{2.1c}$$

where ∂V is the surface of an arbitrary volume V.

Gauss' law: an electric charge generates an electric field. The relation between the charge density ρ and the displacement field $\mathbf{D}$ is given by

$$\int_{\partial V} \mathbf{D}(\mathbf{r},t)\cdot\mathbf{n}\,\mathrm{d}S = \int_V \rho(\mathbf{r},t)\,\mathrm{d}V. \tag{2.1d}$$

We summarize the fields as well as their Systeme International (SI) units in Table 2.1

Symbol	Name	SI Unit
$\mathbf{E}(\mathbf{r},t)$	Electric field	[V/m]
$\mathbf{H}(\mathbf{r},t)$	Magnetic field	[A/m]
$\mathbf{D}(\mathbf{r},t)$	Electric displacement field	[As/m^2]
$\mathbf{B}(\mathbf{r},t)$	Magnetic induction	[Vs/m^2]
$\mathbf{J}(\mathbf{r},t)$	Current density	[A/m^2]
$\rho(\mathbf{r},t)$	Charge density	[C/m^3]

Table 2.1.: Electromagnetic fields and their units.

It is often more convenient to work with a system of PDEs instead of integral equations. Therefore, we derive Maxwell's equations in their differential form. To this end we apply Stokes' theorem and an exchange of integration and time derivative to (2.1a), yielding

$$-\int_S \frac{d}{dt}\mathbf{B}(\mathbf{r},t)\cdot\mathbf{n}\,\mathrm{d}S = \int_{\partial S}\mathbf{E}(\mathbf{r},t)\cdot\boldsymbol{\tau}\,\mathrm{d}l = \int_S \boldsymbol{\nabla}\times\mathbf{E}(\mathbf{r},t)\ \cdot\mathbf{n}\,\mathrm{d}S.$$

Since this holds for arbitrary surfaces S, one obtains the differential form of Faraday's law

$$\boldsymbol{\nabla}\times\mathbf{E}(\mathbf{r},t) = -\frac{d\mathbf{B}}{dt}(\mathbf{r},t), \tag{2.2a}$$

and by a similar application of Stokes' theorem to Ampere's law (2.1b), one finds

$$\boldsymbol{\nabla}\times\mathbf{H}(\mathbf{r},t) = \frac{d\mathbf{D}}{dt}(\mathbf{r},t) + \mathbf{J}(\mathbf{r},t). \tag{2.2b}$$

By applying Gauss' theorem on Gauss' law for magnetism (2.1c) we obtain

$$0 = \int_{\partial V}\mathbf{B}(\mathbf{r},t)\cdot\mathbf{n}\,\mathrm{d}S = \int_V \boldsymbol{\nabla}\cdot\mathbf{B}(\mathbf{r},t)\,\mathrm{d}V.$$

Since this holds for arbitrary volumes V, we obtain the differential form of Gauss' law for magnetism

$$\boldsymbol{\nabla}\cdot\mathbf{B}(\mathbf{r},t) = 0, \tag{2.2c}$$

and by a similar application of Gauss' theorem on Gauss' law (2.1d), we set

$$\nabla \cdot \mathbf{D}(\mathbf{r}, t) = \rho(\mathbf{r}, t). \tag{2.2d}$$

The differential form of Maxwell's equations (2.2a)-(2.2d) is equivalent to the integral form (2.1a)-(2.1d) in all situations where the conditions for applications of Stokes' and Gauss' theorem are fullfilled.

Charge continuity equation: let us apply a time derivative on (2.2d) and a divergence operator on (2.2b). This yields

$$\frac{d\nabla \cdot \mathbf{D}}{dt} = \frac{d\rho}{dt} \qquad \text{and} \qquad \frac{d\nabla \cdot \mathbf{D}}{dt} = -\nabla \cdot \mathbf{J}.$$

By combining the two equations, we obtain

$$\nabla \cdot \mathbf{J} + \frac{d\rho}{dt} = 0 \qquad \text{or} \qquad \frac{d}{dt}\int_V \rho \mathrm{d}V = -\int_{\partial V} \mathbf{J} \cdot \mathbf{n}\,\mathrm{d}S. \tag{2.3}$$

Therefore, no net charge can be produced. This is a fundamental principle in physics which is implicitly included in Maxwell's equations as has been shown.

As a direct consequence of (2.3) we see that (2.2b) is not independent of (2.2d). By similar reasoning one also obtains that (2.2a) must be connected to (2.2c). Assuming that charge conservation (2.3), Faraday's law (2.2a), and Ampere's law (2.2b) hold, then Gauss' law (2.2c) and Gauss' law for magnetism (2.2d) hold for all times if they hold for one time e.g. $t_0 = 0$. Consequently, if the fields $\mathbf{D}$ and $\mathbf{B}$ are divergence free at one instance in time, then, in the absence of currents $\mathbf{J} = 0$, they remain divergence free for all time.

Let us now comment on the unknowns of the system. The four fields $\mathbf{E}, \mathbf{D}, \mathbf{B}$ and $\mathbf{H}$ result in a total of 12 field components, whereas the sources $\mathbf{J}$ and ρ result in four components. Time dependent Maxwell's equations (2.2a) and (2.2b) provide 6 equations whereas (2.3) provides one more equation. Therefore, the system is under specified.

2.2 Material Laws

As has been stated in the previous section, we need additional equations to complete our description of the propagation of electromagnetic waves. The fields $\mathbf{E}$ and $\mathbf{D}$ as well as $\mathbf{B}$ and $\mathbf{H}$ are connected through material laws. In this work we

restrict our investigations to material laws which model **linear**, **isotropic**, **non-dispersive**, **loss-free** materials without **time dependency**, of the form

$$\mathbf{D}(\mathbf{r},t) = \epsilon(\mathbf{r})\mathbf{E}(\mathbf{r},t), \tag{2.4a}$$

$$\mathbf{B}(\mathbf{r},t) = \mu(\mathbf{r})\mathbf{H}(\mathbf{r},t). \tag{2.4b}$$

In addition, the current $\mathbf{J}$ is assumed to be connected to the electric field $\mathbf{E}$ through Ohms law which we consider to be of the form

$$\mathbf{J}(\mathbf{r},t) = \kappa(\mathbf{r})\mathbf{E}(\mathbf{r},t). \tag{2.4c}$$

Here, the permittivity $\epsilon = \epsilon_0\epsilon_r$ and the permeability $\mu = \mu_0\mu_r$ characterize the electric and the magnetic properties of the medium, respectively. The material constants of the vacuum are ϵ_0, μ_0, and the vacuum speed of light is $c = 1/\sqrt{\epsilon_0\mu_0}$. Their values are summarized in Table 2.2. With these additional 9 equations (2.4a)-(2.4c) the system (2.2a)-(2.2d) is now properly specified. Note that for the considered case ϵ and μ are scalar functions and the conductivity is zero. For more complicated materials ϵ, μ and κ could be tensorial with non-linear dependencies.

Property	Value	SI units
ϵ_0	$\sim 8.854 \cdot 10^{-12}$	[A s /(V m)]
μ_0	$4\pi \cdot 10^{-6}$	[Vs/(Am)]
c	299792458	[m/s]

Table 2.2.: Numerical values and SI units of the fundamental constants.

From this point on we cast the equations into a dimensionless form (see. Appendix A). In this form, the medium specific speed of light $v = 1/\sqrt{\epsilon\mu}$ is free of units.

2.3 Poynting's Theorem

Let us now discuss the conservation of the electromagnetic energy. To derive this we respectively multiply (2.2a) with $\mathbf{H}$ and (2.2b) with $\mathbf{E}$, yielding

$$\nabla \times \mathbf{E} \cdot \mathbf{H} = -\frac{d\mathbf{B}}{dt} \cdot \mathbf{H} = -\frac{1}{2}\frac{d(\mathbf{B}\cdot\mathbf{H})}{dt},$$

$$\nabla \times \mathbf{H} \cdot \mathbf{E} - \mathbf{J} \cdot \mathbf{E} = \frac{d\mathbf{D}}{dt} \cdot \mathbf{E} = \frac{1}{2}\frac{d(\mathbf{D}\cdot\mathbf{E})}{dt}.$$

Now, we subtract the first identity from the second yielding

$$\frac{1}{2}\frac{d}{dt}(\mathbf{B}\cdot\mathbf{H}+\mathbf{E}\cdot\mathbf{D})-\mathbf{J}\cdot\mathbf{E}=\nabla\times\mathbf{H}\cdot\mathbf{E}-\nabla\times\mathbf{E}\cdot\mathbf{H}=\nabla\cdot\mathbf{H}\times\mathbf{E}.$$

Let us denote the energy density and the energy flux density, respectively by

$$\mathscr{E}=\frac{1}{2}(\mathbf{D}\cdot\mathbf{E}+\mathbf{H}\cdot\mathbf{B}) \qquad \text{and} \qquad \mathbf{S}=\mathbf{E}\times\mathbf{H}. \tag{2.5}$$

We now may cast the previous equality into the following form

$$\frac{d\mathscr{E}}{dt}=-\nabla\cdot\mathbf{S}-\mathbf{J}\cdot\mathbf{E}. \tag{2.6}$$

This is the energy balance in its differential form. By integrating (2.6) and applying Gauss' theorem we obtain the energy balance

$$\frac{d}{dt}\int_V \mathscr{E}\,\mathrm{d}V=-\int_{\partial V}\mathbf{S}\cdot\mathbf{n}\,\mathrm{d}S-\int_V \mathbf{J}\cdot\mathbf{E}\,\mathrm{d}V, \tag{2.7}$$

in its integral form, also known as **Poynting's theorem**, which states that the total electromagnetic energy in V in the absence of currents only changes due to an inflow or an outflow of energy through the boundaries ∂V.
We will make extensive use of (2.7) later in the analysis of the numerical approximation.

2.4 Plane Waves

Let us now discuss a specific type of solutions of Maxwell's equations. We consider a homogeneous medium with $\epsilon=\mu=$const and $\kappa=0$ in the absence of charges $\rho=0$ and currents $\mathbf{J}=0$ described by

$$\nabla\times\mathbf{E}=-\mu\frac{d\mathbf{H}}{dt}, \tag{2.8a}$$

$$\nabla\times\mathbf{H}=\epsilon\frac{d\mathbf{E}}{dt}, \tag{2.8b}$$

$$\nabla\cdot\mathbf{H}=0, \tag{2.8c}$$

$$\nabla\cdot\mathbf{E}=0. \tag{2.8d}$$

In this scenario, we can combine Faraday's law (2.8a) and Ampere's law (2.8b) into a homogeneous wave equation. We apply a **curl** operator to (2.8a) as well as a vector identity yielding,

$$\nabla(\nabla\cdot\mathbf{E})-\boldsymbol{\nabla}^2\mathbf{E}=\boldsymbol{\nabla}\times(\boldsymbol{\nabla}\times\mathbf{E})=-\mu\frac{d\boldsymbol{\nabla}\times\mathbf{H}}{dt}=-\frac{1}{v^2}\frac{d^2\mathbf{E}}{dt^2}.$$

In the last step we additionally applied Ampere's law (2.8b). Since $\boldsymbol{\nabla}\cdot\mathbf{E}=0$ (in the considered setting) this reduces to

$$\boldsymbol{\nabla}^2\mathbf{E}-\frac{1}{v^2}\frac{d^2\mathbf{E}}{dt^2}=0. \tag{2.9}$$

This equation is for instance solved by functions of the form

$$\mathbf{u}^E(\mathbf{r},t)=\mathbf{e}\,\psi(\mathbf{d}\cdot\mathbf{r}-vt)\qquad\text{where}\qquad|\mathbf{e}|=|\mathbf{d}|=1. \tag{2.10}$$

Since the values of these functions are constant on planes perpendicular to $\mathbf{d}$ they are called plane wave solutions. Plugging $\mathbf{u}^E$ instead of $\mathbf{E}$ into (2.9), yields

$$\begin{aligned}\boldsymbol{\nabla}^2\mathbf{u}^E=&\mathbf{e}\,\mathbf{d}^2\left(\psi''(\mathbf{d}\cdot\mathbf{r}-vt)\right)\\=&\frac{1}{v^2}\left(v^2\mathbf{d}\,\psi''(\mathbf{d}\cdot\mathbf{r}-vt)\right)=\frac{1}{v^2}\frac{d^2\mathbf{u}^E}{dt^2}.\end{aligned}$$

This shows that $\mathbf{u}^E$ solves the wave equation. In order for $\mathbf{u}^E$ and $\mathbf{u}^H$ to also fulfill Ampere's law (2.8b) these functions must be coupled. To show this let us plug $\mathbf{u}^E$ and $\mathbf{u}^H$ into Ampere's law (2.8b), resulting in

$$\mathbf{d}\times\mathbf{u}^E=\boldsymbol{\nabla}\times\mathbf{u}^E=\mu\frac{d\mathbf{u}^H}{dt}=\frac{1}{Z}\mathbf{u}^H.$$

This allows to determine $\mathbf{u}^H$ from $\mathbf{u}^E$. Here, $Z=\sqrt{\mu/\epsilon}$ is the intrinsic wave impedance. By similar reasoning, (2.8a) and (2.8b) can be formulated into the conditions

$$\mathbf{d}\cdot\mathbf{u}^E=0\qquad\text{and}\qquad\mathbf{d}\cdot\mathbf{u}^H=0,$$

respectively. The resulting plane waves have electric and magnetic fields tangential to the direction of propagation. Summarizing we find

Theorem I (Plane Wave Solutions of Maxwell's Equations)
Let $\mathbf{d} \in \mathbb{R}^3$ *with* $|\mathbf{d}| = |\mathbf{e}| = |\mathbf{h}| = 1$ *as well as* $\mathbf{d} \cdot \mathbf{e} = 0$, $\mathbf{d} \cdot \mathbf{h} = 0$ *and* $\mathbf{d} \times \mathbf{e} = Z^{-1}\mathbf{h}$. *Then plane waves of the form*

$$\mathbf{u}^E = \mathbf{e}\,\psi(\mathbf{d}\cdot\mathbf{r} - v\,t) \qquad \text{and} \qquad \mathbf{u}^H = \frac{\mathbf{h}}{Z}\,\psi(\mathbf{d}\cdot\mathbf{r} - v\,t),$$

satisfy (2.8a)-(2.8d).

Proof. By plugging these solutions into (2.8) we show that this ansatz fulfills Maxwell's equations.

1 Since $\mathbf{d} \cdot \mathbf{h} = 0$, the ansatz fulfills magnetic Gauss' law

$$\nabla \cdot \mathbf{u}^H = \mathbf{d} \cdot \mathbf{h}\,\psi'(\mathbf{r}, t) = 0.$$

2 Since $\mathbf{d} \cdot \mathbf{e} = 0$, the ansatz fulfills Gauss' law in the absence of charges

$$\nabla \cdot \mathbf{u}^E = \mathbf{d} \cdot \mathbf{e}\,\psi'(\mathbf{r}, t) = 0.$$

3 Using $\mathbf{d} \times \mathbf{e} = Z^{-1}\mathbf{h}$, we see that the ansatz fulfills Faraday's law

$$\nabla \times \mathbf{u}^E = \mathbf{d} \times \mathbf{e}\psi'(\mathbf{r}, t) = \frac{\mu v}{Z}\mathbf{d} \times \mathbf{e}\psi'(\mathbf{r}, t) = \mu v \mathbf{h}\psi'(\mathbf{r}, t) = \mu \frac{d\mathbf{u}^H}{dt}.$$

4 Finally, the ansatz fulfills current free Ampere's law in the absence of currents

$$\nabla \times \mathbf{u}^H = \frac{1}{Z}\mathbf{d} \times \mathbf{h}\psi'(\mathbf{r}, t) = v\epsilon\,\mathbf{e}\psi'(\mathbf{r}, t) = -\epsilon \frac{d\mathbf{u}^E}{dt}.$$

Therefore the whole system of Maxwell's equations (2.8a)- (2.8d) is fulfilled. □

A plane wave satisfies Maxwell's equations (2.8a)-(2.8c) and Gauss' law(2.8d) in the absence of charges $\rho = 0$ with electric and magnetic fields perpendicular to the direction of propagation $\mathbf{d}$. Moreover, the Poynting vector is given by

$$\mathbf{S} = \mathbf{e} \times \mathbf{h} = \mathbf{d}\,|\mathbf{e}|\,|\mathbf{h}|.$$

Let us finally note that by the **superposition principle** for homogeneous linear equations, also linear combinations of plane waves solve (2.8a)-(2.8d).

2.5 Behavior of Electromagnetic Fields at Interfaces

So far we have discussed electromagnetic fields in a homogeneous continuum. Let us now investigate their behavior at interfaces between two materials. To this end we consider Maxwell's equations (2.1a)-(2.1d) in their integral form over a spatial domain of interest $\Omega \subseteq \mathbb{R}^3$. Let this domain be divided by an interface Γ into two sub-domains Ω_1 and Ω_2 with different constant materials (ϵ_1, μ_1) and (ϵ_2, μ_2), respectively.

For magnetic Gauss law (2.1c) we consider an integration over the surface $\partial\Omega$ of Ω as is depicted in Fig. 2.1 (left). To derive the behavior of the fields at the interface, we take the limit $\Delta h_1 \to 0$ from the left and $\Delta h_2 \to 0$ from the right. By doing so the contributions from surfaces $\partial\Omega$ that are orthogonal to the interface vanish. What remains is

$$(\mathbf{n}_1\mathbf{B}_1 + \mathbf{n}_2\mathbf{B}_2)A = 0,$$

where A is the considered contact area of the domains. For Faraday's law (2.1a) we consider an integration over a contour τ of a plane S orthogonal to the interface. By the limiting process $\Delta h_1 \to 0$ and $\Delta h_2 \to 0$ from the left and right respectively, now the contributions on parts of S that are orthogonal to the interface vanish. As a result we obtain

$$(\mathbf{n}_1 \times \mathbf{E}_1 + \mathbf{n}_2 \times \mathbf{E}_2)\, l = 0,$$

From these findings we deduce that the normal component of $\mathbf{B}$ and the tangential component of $\mathbf{E}$ must be continuous, i.e.,

$$\mathbf{n}_1 \cdot \mathbf{B}_1 + \mathbf{n}_2 \cdot \mathbf{B}_2 = 0 \tag{2.11a}$$
$$\mathbf{n}_1 \times \mathbf{E}_1 + \mathbf{n}_2 \times \mathbf{E}_2 = 0, . \tag{2.11b}$$

where l is the contactline between the two areas. A similar investigation of (2.1c) and (2.1b) reveals that the normal component of $\mathbf{D}$ and the tangential component of $\mathbf{H}$ will jump

$$\mathbf{n}_1 \cdot \mathbf{D}_1 + \mathbf{n}_2 \cdot \mathbf{D}_2 = \sigma, \tag{2.12a}$$
$$\mathbf{n}_1 \times \mathbf{H}_1 + \mathbf{n}_2 \times \mathbf{H}_2 = \mathbf{L}, \tag{2.12b}$$

if there is a surface charge density σ and surface current density $\mathbf{L}$ present. For the considered scenario (2.8) $\sigma = 0$ and $\mathbf{L} = 0$, meaning that the normal component of $\mathbf{D}$ and the tangential component of $\mathbf{H}$ are continuous, too.

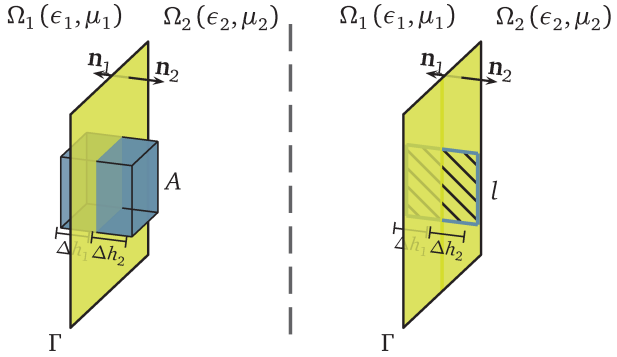

Figure 2.1.: Illustration to derive the continuity of the normal and tangential components of a field through an interface (green area) between the two domains Ω_1 and Ω_2 with outward normals $\mathbf{n}_1$ and $\mathbf{n}_2$. The left side displays a closed integration area (blue area) with normal width Δh and area A; and the right side a closed contour (blue line) with normal length l.

2.6 Boundary Conditions

Let us now consider a finite spatial domain of interest Ω. In this case we must also provide conditions at the boundary $\partial\Omega$ of Ω. To complete the description of the considered system we assume idealized materials at the exterior of Ω and derive the necessary requirements on the fields via the continuity conditions (2.11) from the previous section. Let us illustrate this procedure for the four Boundary Conditions (BC) that we will use.

Perfect Electric Conductor Boundary Conditions: these boundary conditions describe a Perfect Electric Conductor (PEC) in which the conductivity is $\kappa \to \infty$. From Ohms' law (2.4c) it follows that the electric field in the conductor must vanish in order for $\mathbf{J}$ to be finite. At the boundaries of a PEC, we obtain from (2.11b) that

$$\mathbf{n} \times \mathbf{E} = 0. \tag{2.13}$$

Let us discuss the behavior of a plane wave inpinging at such a boundary. Due to the continuity requirements (2.11b) and (2.12b) the tangential component of the electric field of the incoming wave changes its sign (at the impact) while that of the magnetic field does not. As a result the outgoing wave heads away from the

boundary. Therefore, the wave is reflected at the boundary.

Perfect Magnetic Conductor Boundary Conditions: In analogy to PEC, we can define Perfect Magnetic Conductor (PMC) materials. At the PMC boundaries we obtain from (2.12a) that the magnetic field fulfills

$$\mathbf{n} \times \mathbf{H} = 0. \tag{2.14}$$

This PMC condition is typically used to express symmetry.

According to (2.7), both PEC and PMC boundary conditions yield

$$\begin{aligned} \mathbf{S} \cdot \mathbf{n} &= (\mathbf{E} \times \mathbf{H}) \cdot \mathbf{n} \\ &= (\mathbf{n} \times \mathbf{E}) \cdot (\mathbf{n} \times \mathbf{H}) \times \mathbf{n} = 0, \end{aligned}$$

and thus no energy flux through the boundaries.

Periodic Boundary Conditions: Some physical structures, e.g. photonic crystals, exhibit a natural periodic structure. Such a scenario can be realized by Periodic Boundary Conditions (PBC) of the form

$$\mathbf{n} \times \mathbf{E}|_{\partial\Omega_-} = \mathbf{n} \times \mathbf{E}|_{\partial\Omega_+} \qquad \text{and} \qquad \mathbf{n} \times \mathbf{H}|_{\partial\Omega_-} = \mathbf{n} \times \mathbf{H}|_{\partial\Omega_+}. \tag{2.15}$$

Here, fields that impinge a boundary at $\partial\Omega_-$ leave the domain and re-enter at the opposite side $\partial\Omega_+$. The inspection of the Poynting vector yields that the total energy is conserved.

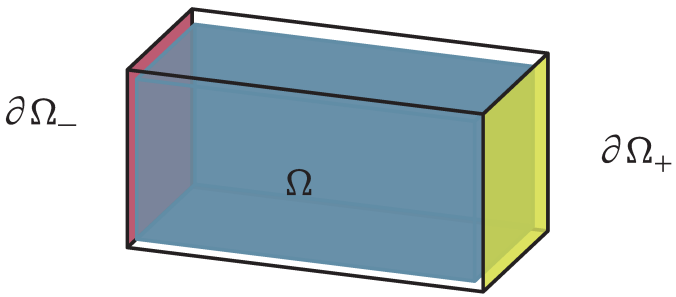

Figure 2.2.: Illustration of periodic boundaries. Fields that impinge a boundary at $\partial\Omega_+$ (green shaded area) leave the domain and re-enter at the opposite side $\partial\Omega_-$ (red shaded area) and vice versa.

Open Boundary Conditions: In some wave propagation scenarios it is necessary to consider a domain which is embedded in a larger domain that is not simulated. An optimal way to achieve this would be boundaries through which a wave passes unaffected. These idealized Transparent Boundary Conditions (TBC) are difficult to achieve in practice. At large distances the scattered field shows a behavior that is described by the Silver-Müller radiation condition [6, 55, 70]

$$\mathbf{r}\big(\mathbf{n}\times\mathbf{E}-Z^{-1}\,\mathbf{n}\times(\mathbf{n}\times\mathbf{H})\big)\to 0 \qquad \text{for} \qquad r\to\infty.$$

This motivates to use Silver Müller Boundary Conditions (SM) of the form

$$\mathbf{n}\times\mathbf{E}-Z^{1}\,\mathbf{n}\times(\mathbf{n}\times\mathbf{H})=0, \tag{2.16}$$

as an approximation of finite $\partial\Omega$. If the direction of propagation of the outgoing wave $\mathbf{d}$ is normal to the boundary (i.e. $\mathbf{n}\cdot\mathbf{d}=0$) these SM result in a good approximation that worsens for steeper angles between $\mathbf{n}$ and $\mathbf{d}$.
In conclusion we can cast all boundary conditions into a generalized form

$$\alpha^{E}\,\mathbf{n}\times\mathbf{E}-\beta^{E}\,\mathbf{n}\times(\mathbf{n}\times\mathbf{H})=\mathbf{n}\times\mathbf{g}(\mathbf{r},t)\,, \tag{2.17a}$$

or alternatively

$$\alpha^{H}\,\mathbf{n}\times\mathbf{H}+\beta^{H}\,\mathbf{n}\times(\mathbf{n}\times\mathbf{E})=\mathbf{n}\times\mathbf{g}'(\mathbf{r},t)\,. \tag{2.17b}$$

In here, $\alpha_E, \alpha_H, \beta_E$, and β_H usually are constants (exept for changing boundary conditions) whereas $\mathbf{g}(\mathbf{r},t)$ and $\mathbf{g}'(\mathbf{r},t)$ are functions of space and time. The functions $\mathbf{g}(\mathbf{r},t)$ and $\mathbf{g}'(\mathbf{r},t)$ denote possible energy fluxes at the boundaries.

Chapter Resumé

In this chapter we have introduced the underlying equations and physical principles of this work. Let us summarize the outcome in the following problem definition that we will consider in the remainder of this work.

Problem I (Three Dimensional Scenario)
Solutions $(\mathbf{E}, \mathbf{H})$ *of time-dependent Maxwell's equations for linear, loss-free, non-dispersive, time-invariant, isotropic media*

$$\nabla \times \mathbf{E} = -\mu \frac{d\mathbf{H}}{dt},$$
$$\nabla \times \mathbf{H} = \epsilon \frac{d\mathbf{E}}{dt},$$

subject to appropriate boundary conditions such as

$$\alpha^E \mathbf{n} \times \mathbf{E} - \beta^E \mathbf{n} \times (\mathbf{H} \times \mathbf{n}) = \mathbf{n} \times \mathbf{g}(\mathbf{r}, t) \quad \text{on} \quad \partial\Omega \times I,$$

as well as initial conditions

$$\mathbf{E}(0) = \mathbf{E}_0 \qquad \text{and} \qquad \mathbf{H}(0) = \mathbf{H}_0 \qquad \text{on} \quad \Omega \times t_0,$$

constrained by

$$\nabla \cdot \mathbf{E_0} = 0 \qquad \text{and} \qquad \nabla \cdot \mathbf{H_0} = 0,$$

describe the propagation of electromagnetic waves in the absence of charges and currents.

Part I.
Methodology

3 Trefftz Methods

"Wir kommen sofort zu einem Analogon des Ritzschen Verfahrens, indem wir die Lösung nicht wie bei Ritz durch Funktionen approximieren, welche den Randbedingungen genügen, aber die Differentialgleichung nicht erfüllen, sondern solche Funktionen nehmen, welche die Differentialgleichung befriedigen, aber nicht die Randbedingungen".

Erich Trefftz (1926)

In the last century, the development of methods to approximate the solution of PDE systems has played a very important role in academia. Here, problem specific methods, such as the Trefftz methods, have gained a lot of attention by engineers due to their good approximation behavior.

In this chapter, we introduce the basic concepts of Trefftz methods and motivate the procedure that we use to develop a Trefftz method in the context of electrodynamics. To this end, we first introduce the original Trefftz method in Section 3.1. Subsequently, we survey some of the existing Trefftz methods in Section 3.2 and classify our new method in this context in Section 3.3.

3.1 The Original Trefftz Method

One of the first systematic methods to approximate the solutions of complicated physical problems has been developed in 1909 by Walter Ritz [80]. The **Ritz method** is a variational method which is used to solve an underlying differential equation given by

$$\mathscr{D}(\mathbf{u}) = \mathbf{f} \quad \text{in} \quad \Omega, \tag{3.1a}$$

$$\mathscr{B}(\mathbf{u}) = \mathbf{y} \quad \text{on} \quad \partial\Omega. \tag{3.1b}$$

Here, $\mathscr{D}$ is the corresponding differential operator that is approximated by trial functions $\mathbf{u}$, $\mathbf{f}$ is a right hand side, $\mathscr{B}$ is a boundary condition, and $\mathbf{y}$ a function on the boundary. To solve the equation Ritz applied a testing testing procedure in which he employed test functions $\mathbf{w}$. Here, both $\mathscr{B}(\mathbf{u}) = \mathbf{y}$ and $\mathscr{B}(\mathbf{w}) = 0$ satisfy boundary conditions.

A few years later, in 1926, Erich Trefftz adopted the original idea of Ritz but modified it slightly yielding a new method [88]. In his counter-piece to the original Ritz method, Trefftz required trial and test functions to fulfill the underlying homogeneous differential equation, i.e. $\mathscr{D}(\mathbf{u}) = \mathscr{D}(\mathbf{w}) = 0$ and $\mathbf{f} = 0$. Today, this method is known as the Trefftz method.

At this point we can already deduce two necessary requirements to formulate a Trefftz method:

1. Trial and test functions that exactly solve the underlying homogeneous partial differential equation. The test functions must therefore lie in the Null-space of $\mathscr{D}$. The mentioned functions incorporate knowledge of the underlying problem and are therefore problem specific. We will call these functions **Trefftz functions**.

2. An underlying **methodological framework** that supports the application of the previously mentioned Trefftz functions.

From this it is obvious that Trefftz methods can only be formulated if the underlying differential operator has known elementary solutions. This is not possible for all differential operators. In some scenarios a problem can be split into a part for which solutions exist and another part for which no solutions exist. The first part is then solved by Trefftz functions and the second part by non-Trefftz functions[1].

3.2 Survey of Trefftz Methods

Since its first application to structural mechanics problems (i.e. the calculation of stresses of various beams) the Trefftz method has been extended to various fields in **mechanics** and **fluid dynamics**: there exist Trefftz methods for plate bending as well as thick plate problems [39–41], elasticity problems [77, 86], problems governed by the Poisson equation [96], heat conduction problems [42] and recently wave propagation problems [74, 92]. In combination to these rather applied works, a bunch of purely **theoretical** results [23, 24, 26, 95] are available. Let us summarize some of the major contributions of the mentioned works.

[1] Methods of this type are sometimes called *"hybrid Trefftz methods"*; since this name is ambiguous we will not use it.

In his PhD thesis in 1973 [86] Erwin Stein created a modern version of the Trefftz method. Herein, Stein incorporated the Trefftz method into a FEM framework in order to precisely calculate the stresses acting on plates.
Shortly after that Jirousek constructed a new Trefftz FEM method in [41] and [39] that employs coordinate functions which locally satisfy the underlying (non-homogeneous) Lagrange equation in an element-wise fashion. These element-wise solutions are glued together with generalized (not necessarily local) inter-element boundary condition functions that connect adjacent nodes. In Jirouseks notation these functions are called "*frame functions*". Since these initial works were restricted to plate bending problems, Jirousek generalized the approach in [40]. In the context of his work he pointed out that the solutions of the underlying problem are solely defined on the frame of the mesh. Trefftz methods that are based on Jirouseks approach are referred to as **direct Trefftz methods**.
In [96] and [95] Zielinski and Herrera have constructed a boundary based FEM Trefftz method (originally for the Poisson equation). The method uses a decomposition of the domain into sub-domains as is elaborated in [23] and [24]. Due to the nature of the employed "*Trefftz complete*" functions the method only receives contributions on the skeleton of the resulting mesh. This results in two solutions at every element-interface from the two adjacent elements which are then fitted by a collocation method. Due to the nature of the boundary fitting process, methods of this kind are called **indirect Trefftz methods**. The difference between the direct and indirect methods was later elaborated by Herrera in [26].
In [77] Piltner incorporated a representation of singular and non-singular solutions of a crack propagation problem into a variational scheme. The development of these solutions has been previously outlined in [76]. In particular, Piltner was able to formulate a systematic approach to expand the solutions in terms of harmonic polynomials, suitable for a Gaussian integration in the numerical scheme.
In [75] Petrolito applied polynomial and non-polynomial Trefftz functions to a FEM method used for thick plate bending processes. By the application of Trefftz functions, Petrolito was able to *a priori* avoid some of the problems that have previously limited the numerical simulations.
Let us turn our attention to the works of Farhat, Petersen, Wang, and Tezaur. In [74] Farhat, Petersen and Tezaur developed a $(1+1)$-dimensional[2] space-time method that employs "*transport polynomials*", i.e. polynomial plane waves, in order to solve the acoustic wave equation. The method is formulated in the context a the DG framework. Farhat et al. decided to implement the inter-element continuity in terms of Lagrange multipliers. As a result, the contributions from the constant

[2] We use the notation $(d+1)$-dimensional to emphasize that a space-time method with d spatial dimensions and one time dimension is used.

element-basis functions need to be globally reconstructed in a post-processing step. In the follow-up work [92], Farhat, Wang, and Tezaur have extended the method to a (2+1)-dimensional (and partially to a (3+1)-dimensional) setting. The latter work contains a discussion on some of the properties of the applied transport polynomial basis, such as a prove of their linear independence.

In addition to these "*strict*" Trefftz methods, numerous methods that partially apply Trefftz functions have been developed. For instance Novak et al. [72] have developed an approach to the propagation of cracks in concrete. The cracks have been simulated as perturbances on top of a mean-field simulation that employs Trefftz functions similar to those of Piltner.

In the context of the Poisson equation Chen et al. [12] have been able to show an equivalence between the solution obtained with a Trefftz method and that obtained by means of Greens functions. The result is based on the similarity of the applied fundamental solutions.

Let us now turn to Trefftz methods in the context of **electrodynamics**. There exist some works on **frequency-domain** problems governed by the homogeneous Helmholtz equation [31, 68, 69] as well as Maxwell's equations [5, 32, 33, 38, 68, 90]; and on **time-domain** problems governed by Maxwell's equations [14, 15, 47, 48]. Let us discuss the contributions of the authors once again a little more detailed.

In [90] Igor Tsukerman incorporated several types of Trefftz functions into the Flexible Local Approximation Method (FLAME) framework which was previously developed in [89]. The Trefftz functions employed here are solely evaluated at the nodes of the numerical grid. Note that the resulting Trefftz-FLAME method is a non-variational FDTD method. Tsukerman et al. obtained very rapid convergence, in particular a sixth order convergence for specific scattering problems using a n-point stencil. In addition to this basic version of Trefftz-FLAME, Tsukerman et al. developed several extensions such as an adaptive version in [38].

Moiola, Hiptmair, and Perugia established a frequency-domain Trefftz method for the Helmholtz equation in [31]. They employed non-polynomial plane wave solutions that were previously introduced in [69] as Trefftz functions. In this work *a priori* error estimates in the case of p-refinement were developed. The analysis leads to best approximation errors. In the two-dimensional case these errors are independent of the choice of directions of the plane waves, whereas in the three-dimensional case only specific directional choices are allowed. In later works the analysis was extended to Maxwell's equations in [32]. In addition locally refined meshes were considered in [33]. Here, the error was found to be dependent on the frequency ω and the spatial size of the cell h (but works for all ωh). The PhD thesis of Andrea Moiola [68] summarizes all important findings and provides background

information.
Independently from the works of Moiola et al., Badics et al. [5] have developed another frequency-domain Trefftz method. In this method Badics also employs plane waves as Trefftz functions. However, a non-specified polynomial version of the plane waves is used. The implementation is subsequently analyzed in terms of performance.

Before we conclude this survey chapter, let us mention that there already exists a number of different surveys and overviews of different Trefftz methods that were developed in the time between 1973 and 2000. In particular the detailed works by Ruge [82], Jirousek [43], and Herrera [25], as well as the summary work by Kita et al. [46] provide a good overview.

3.3 A Trefftz Method for Maxwell's Equations

The work [48] is the beginning of our contribution to the topic. Herein, a (1+1)-dimensional DG Trefftz method for time-domain electromagnetic problems was introduced. The employed Trefftz functions are polynomial plane waves similar to those applied by Farhat et al. The method exhibits exponential convergence of the approximation error in the L_2-norm under p-refinement and optimal convergence rates under h-refinement. In addition to these numerical convergence experiments, a Trefftz basis for non-homogeneous materials was developed here. In [15], the previously discovered method is extended to a (3+1)-dimensional version and subsequently classified into a general DG framework. Furthermore, substantial properties such as stability and well-posedness have been shown. In addition a general construction procedure for polynomial basis functions is proposed. In [14], we have proposed a new type of TBC in the DG-Trefftz context; by exploiting essential knowledge of the transport basis functions, i.e. knowledge of their directions, we were able to obtain transparent boundaries with very small errors due to reflections. In a cooperation with Moiola and Perugia [47], we compared the Trefftz method with a non Trefftz method. The Trefftz method outperforms the conventional method due to a smaller number of Degrees of Freedom (DoF) for equivalent relative errors. In addition to this comparison *a priori* error estimates for the (1+1)-dimensional Maxwell system have been developed in [47].

Let us put our contributions into the general context of Trefftz methods: The underlying equations significantly influence the type of the used Trefftz method because they determine which Trefftz functions are used. From this point of view, our method is different from those applied by Jirousek, Herrera, Zielinski, Petrolino and Piltner, since we are considering Maxwell's equations. In addition, we implement Trefftz functions into a DG framework which has not been done by the

mentioned authors. For the latter reason the Trefftz FLAME framework by Tsukerman et al. is also different to our method, since a non-variational FDTD formulation has been used here. The DG methods by Moiola and Farhat however show significant similarities to our method. Let us now shortly outline the development of the Trefftz method in this work as discussed in Section 3.1, every Trefftz method needs two essential building blocks: Trefftz functions and a suitable underlying framework. In Chapter 4 we will therefore develop polynomial Trefftz functions that solve Problem I and combine them with a suitable DG method in Chapter 5. The procedure follows our approach from [15].

4 Polynomial Solutions of Maxwell's Equations

The choice of an appropriate basis is an essential task in the formulation of a numerical method. For this purpose, polynomial basis functions are particularly attractive, since they can be integrated exactly. In this chapter we will develop polynomial functions that solve Maxwell's equations, proceeding as follows:

We first survey some of the already existing procedures to develop such functions in Section 4.1. Consequently, in Section 4.2 we discuss some of the basic properties of the resulting basis as well as a way to generate polynomial solutions from already existing polynomials. In Section 4.3 we then introduce a second way to directly generate a Trefftz basis in terms of polynomial plane waves.

4.1 Survey of Polynomial Trefftz Basis Sets

There exist various types of basic sets of polynomials that solve certain underlying equations. These include polynomial solutions for the wave equation [34, 57, 58, 61, 64, 65], the heat equation [2, 49, 81], the plate vibration equation [50, 60], the beam vibration equation [3], and thermoelasticity equations [59]. In addition to that some authors have focused on developing techniques to generate solving polynomials for general differential equations [34, 66, 81]. Let us summarize some of the major contributions of the corresponding works in the following.

In 1955 Miles and Williams developed a basic set of harmonic polynomials of order p with k variables that solve the Laplace equation [64, 65]. Subsequently, associated polynomials that solve a homogeneous wave equation were derived. Here, the maximum number of polynomials was found to depend on the number of variables k and the order p. In the proceeding work [66], Miles and Williams developed a procedure to construct polynomials that solve partial differential equations which are described by an abstract differential operator. These solving polynomials can be constructed from any polynomial by iteratively applying the underlying differential operator n-times until the original polynomial vanishes. The sum of these n intermediate results then constitutes the solving polynomial.

A few years, later in [34] Horvat unified the approach of Miles and Williams with

some already existing approaches to an algebraic method. As a result, recurrence formulas between solution polynomials could be calculated.
In [81] Rosenbloom has developed a technique to derive associated functions that solve the heat equation. These associated functions consist of a combination of fundamental solutions and "*heat polynomials*", i.e. polynomials that satisfy the heat equation. Here, the heat polynomials are found by a power series expansion of a suitable generating function, that solves the heat equation.
Just a few years ago Maciag et al. [61] further developed Rosenblooms approach. In addition to the construction of solving polynomials from a generating function by a power series, they added a second procedure in which a Taylor series expansion is applied instead. This approach has then been applied by Maciag et al. to several applications [2, 3, 49, 50, 59, 60], including wave propagation problems [57, 58, 61]. In [61], "*wave polynomials*", i.e. polynomials that solve the wave equation, as well as recurrence relations, were constructed for a two-dimensional wave equation. The construction has then been extended to the three-dimensional wave equation in [57], and used in several applications including inverse problems [58].

In this work we introduce two different ways to construct a polynomial Trefftz basis for Maxwell's equations. First, we show how to derive a suitable polynomial Trefftz basis from an already existing polynomial basis (containing basis functions that do not solve the underlying equations). This approach is very closely related to that of Miles [66], and can be seen as an extension of it to Maxwell's equations. Secondly, we directly generate polynomial solutions from the already known plane wave functions (see Theorem I). Since we apply no expansion here, this approach is different to that of Maciag et al. [61].

4.2 Polynomial Trefftz Spaces

In this section we summarize some of the findings of [15]. Here, we introduce the space of polynomials that solve Problem I in an abstract manner first. We call this space the polynomial Trefftz space corresponding to Problem I[1].

Trefftz space: Before we start with the discussion of the polynomial Trefftz space, let us define the term "*Trefftz space*". Assume a certain physical problem that is described by a homogeneous PDE containing a known differential operator over a space time domain of interest.

[1] For the sake of simplicity we will omit the explicit notion of the underlying Problem from now on.

Definition I (Space Time Domain)
Let $\Omega \subseteq \mathbb{R}^d$ be the spatial domain of interest and $I \subseteq \mathbb{R}$ the considered time interval, then $Q = \Omega \times I$ is called the space-time domain of interest.

The Trefftz space corresponding to this problem is composed of all functions $\mathbf{u}$ that solve this PDE system (in our case Maxwell's equations); therefore, these $\mathbf{u}$ lie in the null-space of the differential operator. For our considered Problem I we can explicitly state the Trefftz space as

Definition II (Trefftz Space)
The Trefftz Space corresponding to Problem I in the space-time domain $Q = \Omega \times I$, is

$$T(Q) \equiv \Big\{ \mathbf{F}(\mathbf{E},\mathbf{H}) : \Omega \times \mathbf{I} \longrightarrow \mathbb{R}^l \quad \text{with} \quad \nabla \times \mathbf{E} + \frac{d}{dt}(\epsilon \mathbf{H}) = 0,$$
$$\nabla \times \mathbf{H} - \frac{d}{dt}(\epsilon \mathbf{E}) = 0, \quad \nabla \cdot \mathbf{E}_0 = 0 \quad \text{and} \quad \nabla \cdot \mathbf{H}_0 = 0 \Big\}.$$

The functions $\mathbf{F} \in T(Q)$ that lie in this space are called **Trefftz functions**.

Polynomial Trefftz space: Let us now proceed to the discussion of the "*polynomial Trefftz space*". This is the subspace of a Trefftz space which only contains polynomials. For Problem I it reads

Definition III (Polynomial Trefftz Space)
The polynomial version of the Trefftz Space from Definition II with functions of maximum order p in the discrete space-time domain $Q = \Omega \times I$ where $\Omega \subset \mathbb{R}^d$,

$$\mathbb{T}_p(Q) \equiv \Big\{ \mathbf{F} \in \big[\mathbb{P}_p(Q)\big]^l : \mathbf{F} \in T(Q) \Big\},$$

is composed of all possible polynomial Trefftz functions $\mathbf{F}^p \in \mathbb{T}_p(Q)$ with l vectorial components.

The functions $\mathbf{F}^p \in \mathbb{T}_p(Q)$ lying in this space are called **polynomial Trefftz functions**. As we will see in a moment, these functions need to be vectorial functions.

Notation: We denote a polynomial space defined over a set $D \subseteq \mathbb{R}^d$ by $[\mathbb{P}_p(D)]^l$. Here, p denotes the maximum order of the constituting polynomials with l vectorial components and d is the dimension of the underlying set. Following the reasoning

of [34], this polynomial space can be spanned by linearly independent combinations of monomials. For instance, in a two-dimensional space depending on x and y these would read

$$\begin{array}{ccccccccc} & & & & 1 & & & & \text{p=0} \\ & & & x & & y & & & \text{p=1} \\ & & x^2 & & xy & & y^2 & & \text{p=2} \\ & x^3 & & x^2y & & xy^2 & & y^3 & \text{p=3} \\ \iddots & & & & \vdots & & & \ddots & \vdots \end{array}$$

This leads to a linear system of equations; the total number of possible equations determines the dimension and reads

$$\dim \mathbb{P}_p(D)^l = l \cdot \begin{pmatrix} p+d \\ d \end{pmatrix} \qquad \text{where} \qquad D \subseteq \mathbb{R}^d. \tag{4.1}$$

In the remainder of this work we consider polynomials that are defined in a reference cell $Q^n = K \times I^n$; where, $I^n = [t^{n-1}, t^n]$ is the considered time interval and $K \subset \mathbb{R}^d$ is a (discrete) spatial cell. Let us restrict our considerations to a (3+1)-dimensional setting, i.e. $l = 6$ from now on[2].

Characterization: let us characterize the behavior of the fields that satisfy Maxwell's equations in the following Lemma

Lemma I (Characterization) (see Theorem 8 of [15])
For every $\tilde{\mathbf{F}} = \left(\tilde{\mathbf{E}}, \tilde{\mathbf{H}}\right)^6 \in \mathbb{P}_p(K)$ *there exists a unique* $\mathbf{F} = (\mathbf{E}, \mathbf{H}) \in \mathbb{T}_p(Q^n)$ *with* $\mathbf{E}\left(t^{n-1}\right) = \tilde{\mathbf{E}}$ *and* $\mathbf{H}(t^n) = \tilde{\mathbf{H}}$.

Proof. Let $\mathbf{F} = (\mathbf{E}, \mathbf{H})$ be in $\mathbb{T}_p(Q^n)$. Then, $\mathbf{E}$ and $\mathbf{H}$ can be expanded as

$$\mathbf{E}(\mathbf{r}, t) = \sum_{m=0}^{p} \mathbf{e}_{p-m}(\mathbf{r}) \left(v\left(t - t^n\right)\right)^m \quad \text{and} \quad \mathbf{H}(\mathbf{r}, t) = \sum_{m=0}^{p} \mathbf{h}_{p-m}(\mathbf{r}) \left(v\left(t - t^n\right)\right)^m,$$

where $\mathbf{e}_{p-m}(\mathbf{r}), \mathbf{h}_{p-m}(\mathbf{r}) \in \mathbb{P}^3_{p-m}(K)$ are spatial polynomials of order m. Let us use the definition $\mathbf{E}(t^n) = \tilde{\mathbf{E}}$ and $\mathbf{H}(t^n) = \tilde{\mathbf{H}}$ to write

$$\mathbf{e}_p(\mathbf{r}) = \mathbf{E}(\mathbf{r}, t^n) \qquad \text{and} \qquad \mathbf{h}_p(\mathbf{r}) = \mathbf{H}(\mathbf{r}, t^n).$$

[2] For two and one dimensional spatial domains, the number of vectorial components is $l = 3$ and 2, respectively.

If we insert this and the temporal derivatives

$$\frac{d\mathbf{E}}{dt} = \sum_{m=0}^{p} m v \mathbf{e}_m(\mathbf{r})\,(v\,(t-t^n))^{m-1} \quad \text{and} \quad \frac{d\mathbf{H}}{dt} = \sum_{m=0}^{p} m v \mathbf{h}_m(\mathbf{r})\,(v\,(t-t^n))^{m-1},$$

into Maxwell's equations, and compare powers of t we obtain

$$m v \epsilon \mathbf{e}_{p-m} = \boldsymbol{\nabla} \times \mathbf{h}_{p-m+1} \qquad \text{and} \qquad m v \epsilon \mathbf{h}_{p-m} = -\boldsymbol{\nabla} \times \mathbf{e}_{p-m+1},$$

for all $m = 1 \dots p$. □

This means that we can pick fields $(\mathbf{E}(t^n), \mathbf{H}(t^n))$ at one instance in time t^n and then propagate them in time. Therefore, we separate the temporal and the spatial parts of the fields. As a result we can efficiently generate a Trefftz basis in the following manner; first, we choose a Trefftz basis for the values $\tilde{\mathbf{F}} = (\tilde{\mathbf{E}}, \tilde{\mathbf{H}}) \in \mathbb{P}(K)^6$ at an initial time and then propagate all fields of the constituting basis functions in time. This construction reveals, that the number of basis functions needed to span the Trefftz space does not change with time and that the fields $\mathbf{E}$ and $\mathbf{H}$ must be coupled. Let us elucidate these two findings that determine the dimension as well as the construction of one possible basis in the following.

Dimension: in the field expansion of the proof of Theorem I the time variable has been separated from the spatial part and remained as a multiplicative propagation factor. Therefore, the number of basis functions needed to span the Trefftz space does not change with time. Consequently, the dimension of $\mathbb{T}_p(Q)$ is solely determined by the spatial part. In the absence of constraints this dimension can be determined by setting $d = 3$ and $l = 6$ in (4.1). The resulting dimension is

Theorem II (Dimension) (see Theorem 13 of [15])
The Trefftz space $\mathbb{T}_p(Q)$ corresponding to Problem I with p being the maximum order of the constituting Trefftz functions and $Q = K \times I$ being the considered space-time domain over a spatial domain of interest $K \subset \mathbb{R}^3$ has the dimension

$$\dim \mathbb{T}_p(Q) = \frac{(p+2)(p+1)}{3}(2p+9).$$

Proof. In the absence of constraints we consider (4.1) with p, $d = 3$ and $l = 6$. This yields a total of

$$(p+3)(p+2)(p+1),$$

equations. From $\mathbf{E}_0 \in \mathbb{P}_p(K)^3$ we deduce $\boldsymbol{\nabla} \cdot \mathbf{E}_0 \in \mathbb{P}_{p-1}(K)$. Therefore we must consider (4.1) with $p-1$, $d=3$ and $l=1$ resulting in

$$\frac{1}{6}(p+2)(p+1)p,$$

equations. The same is true for $\boldsymbol{\nabla} \cdot \mathbf{H}_0 = 0$, yielding a total of $(p+2)(p+1)p/3$ constraints. By subtracting this number from $(p+3)(p+2)(p+1)$ we obtain the assumption. □

Note that this dimension is a general result and must hold for every polynomial Trefftz space (with $d=3$ and $l=6$). The number of basis functions for a fixed order p is consequently given by

$$\dim \mathbb{T}_p(Q) - \dim \mathbb{T}_{p-1}(Q) = 2\,(p+1)\,(p+3)\,. \tag{4.2}$$

Construction: following the proof of Theorem I, every polynomial Trefftz basis function $\mathbf{F}^p = (\mathbf{E}, \mathbf{H}) \in \mathbb{T}_p(Q)$ can be constructed by an expansion

$$\mathbf{F}^p\,(\mathbf{r}, t) = \sum_{m=0}^{p} \begin{pmatrix} \mathbf{e}_{p-m}(\mathbf{r}) \\ \\ Z^{-1}\,\mathbf{h}_{p-m}(\mathbf{r}) \end{pmatrix} (vt)^m\,. \tag{4.3}$$

The spatial parts of the Trefftz functions $\mathbf{e}_m$ and $\mathbf{h}_m$ are connected via the recurrence relations

$$\mathbf{e}_{p-m} = \frac{1}{m}\boldsymbol{\nabla} \times \mathbf{h}_{p-m+1} \qquad \text{and} \qquad \mathbf{h}_{p-m} = -\frac{1}{m}\boldsymbol{\nabla} \times \mathbf{e}_{p-m+1}. \tag{4.4}$$

This allows to consequtively compute $\mathbf{e}$ and $\mathbf{h}$ by

$$\tilde{\mathbf{E}} = \mathbf{e}_p \to \mathbf{h}_{p-1} \to \mathbf{e}_{p-2} \to \mathbf{h}_{p-3} \to \mathbf{e}_{p-4} \ldots$$
$$\tilde{\mathbf{H}} = \mathbf{h}_p \to \mathbf{e}_{p-1} \to \mathbf{h}_{p-2} \to \mathbf{e}_{p-3} \to \mathbf{h}_{p-4} \ldots.$$

Let us illustrate how to construct a Trefftz basis from a set of linearly independent polynomials that are exactly of order p.

For order $p = 0$ we require a total of six basis functions according to (4.2). Here, the expansion (4.4) reads

$$\mathbf{F}^0(\mathbf{r}, t) = \begin{pmatrix} \mathbf{e}_0(\mathbf{r}) \\ \\ Z^{-1}\,\mathbf{h}_0(\mathbf{r}) \end{pmatrix},$$

and the Trefftz basis is directly given by the six constant polynomials in Table 4.1 without any manipulations.

i	1	2	3	4	5	6
$\mathbf{e}_i^0$	$\begin{pmatrix}1\\0\\0\end{pmatrix}$	$\begin{pmatrix}0\\1\\0\end{pmatrix}$	$\begin{pmatrix}0\\0\\1\end{pmatrix}$	$\begin{pmatrix}0\\0\\0\end{pmatrix}$	$\begin{pmatrix}0\\0\\0\end{pmatrix}$	$\begin{pmatrix}0\\0\\0\end{pmatrix}$
$\mathbf{h}_i^0$	$\begin{pmatrix}0\\0\\0\end{pmatrix}$	$\begin{pmatrix}0\\0\\0\end{pmatrix}$	$\begin{pmatrix}0\\0\\0\end{pmatrix}$	$\begin{pmatrix}1\\0\\0\end{pmatrix}$	$\begin{pmatrix}0\\1\\0\end{pmatrix}$	$\begin{pmatrix}0\\0\\1\end{pmatrix}$

Table 4.1.: Polynomial Trefftz functions that constitute a zero order Trefftz basis.

For order $p = 1$ the dimension following from (4.2) is 16. In this case the summation (4.4) contains two terms

$$\mathbf{F}^1(\mathbf{r}, t) = \begin{pmatrix} \mathbf{e}_1(\mathbf{r}) \\ \\ Z^{-1}\,\mathbf{h}_1(\mathbf{r}) \end{pmatrix} + \begin{pmatrix} \mathbf{e}_0(\mathbf{r}) \\ \\ Z^{-1}\,\mathbf{h}_0(\mathbf{r}) \end{pmatrix} (vt)^1 .$$

Here, the divergence free polynomial functions in Table 4.2 constitute a basis, that is however not yet a Trefftz basis.

i	1	2	3	4	5	6	7	8
$\mathbf{e}_i^1$	$\begin{pmatrix}0\\x\\0\end{pmatrix}$	$\begin{pmatrix}0\\0\\x\end{pmatrix}$	$\begin{pmatrix}y\\0\\0\end{pmatrix}$	$\begin{pmatrix}0\\0\\y\end{pmatrix}$	$\begin{pmatrix}z\\0\\0\end{pmatrix}$	$\begin{pmatrix}0\\z\\0\end{pmatrix}$	$\begin{pmatrix}x\\-y\\0\end{pmatrix}$	$\begin{pmatrix}0\\-y\\z\end{pmatrix}$
$\mathbf{h}_i^1$	$\begin{pmatrix}0\\0\\0\end{pmatrix}$	$\begin{pmatrix}0\\0\\0\end{pmatrix}$	$\begin{pmatrix}0\\0\\0\end{pmatrix}$	$\begin{pmatrix}0\\0\\0\end{pmatrix}$	$\begin{pmatrix}0\\0\\0\end{pmatrix}$	$\begin{pmatrix}0\\0\\0\end{pmatrix}$	$\begin{pmatrix}0\\0\\0\end{pmatrix}$	$\begin{pmatrix}0\\0\\0\end{pmatrix}$
$\dots$	9	10	11	12	13	14	15	16
$\dots$	$\begin{pmatrix}0\\0\\0\end{pmatrix}$	$\begin{pmatrix}0\\0\\0\end{pmatrix}$	$\begin{pmatrix}0\\0\\0\end{pmatrix}$	$\begin{pmatrix}0\\0\\0\end{pmatrix}$	$\begin{pmatrix}0\\0\\0\end{pmatrix}$	$\begin{pmatrix}0\\0\\0\end{pmatrix}$	$\begin{pmatrix}0\\0\\0\end{pmatrix}$	$\begin{pmatrix}0\\0\\0\end{pmatrix}$
$\dots$	$\begin{pmatrix}0\\x\\0\end{pmatrix}$	$\begin{pmatrix}0\\0\\x\end{pmatrix}$	$\begin{pmatrix}y\\0\\0\end{pmatrix}$	$\begin{pmatrix}0\\0\\y\end{pmatrix}$	$\begin{pmatrix}z\\0\\0\end{pmatrix}$	$\begin{pmatrix}0\\z\\0\end{pmatrix}$	$\begin{pmatrix}x\\-y\\0\end{pmatrix}$	$\begin{pmatrix}0\\-y\\z\end{pmatrix}$

Table 4.2.: Linearly independent polynomials that form a basis of order one.

Let us now explicitly execute the Trefftz function construction procedure for the first basis function of Table 4.2. Here, $\mathbf{e}_1^1 = (0,x,0)^T$ and $\mathbf{h}_1^1 = (0,0,0)^T$. By application of the recurrence relations (4.4) we obtain $\mathbf{e}_1^0 = (0,0,0)^T$ and $\mathbf{h}_1^0 = (0,0,-1)^T$. The resulting polynomial Trefftz basis function is therefore given by $\mathbf{F}_1^1 = (\mathbf{E}_1^1, \mathbf{H}_1^1)^T = ((0,x,0),(0,0,-vt))^T$ All other Trefftz basis functions that follow these functions are listed in Table 4.3.

i	1	2	3	4	5	6	7	8
$\mathbf{E}_i^1$	$\begin{pmatrix}0\\x\\0\end{pmatrix}$	$\begin{pmatrix}0\\0\\x\end{pmatrix}$	$\begin{pmatrix}y\\0\\0\end{pmatrix}$	$\begin{pmatrix}0\\0\\y\end{pmatrix}$	$\begin{pmatrix}z\\0\\0\end{pmatrix}$	$\begin{pmatrix}0\\z\\0\end{pmatrix}$	$\begin{pmatrix}x\\-y\\0\end{pmatrix}$	$\begin{pmatrix}0\\-y\\z\end{pmatrix}$
$Z\mathbf{H}_i^1$	$\begin{pmatrix}0\\0\\-vt\end{pmatrix}$	$\begin{pmatrix}0\\vt\\0\end{pmatrix}$	$\begin{pmatrix}0\\0\\vt\end{pmatrix}$	$\begin{pmatrix}-vt\\0\\0\end{pmatrix}$	$\begin{pmatrix}0\\-vt\\0\end{pmatrix}$	$\begin{pmatrix}vt\\0\\0\end{pmatrix}$	$\begin{pmatrix}0\\0\\0\end{pmatrix}$	$\begin{pmatrix}0\\0\\0\end{pmatrix}$
$\dots$	9	10	11	12	13	14	15	16
$\dots$	$\begin{pmatrix}0\\0\\vt\end{pmatrix}$	$\begin{pmatrix}0\\-vt\\0\end{pmatrix}$	$\begin{pmatrix}0\\0\\-vt\end{pmatrix}$	$\begin{pmatrix}vt\\0\\0\end{pmatrix}$	$\begin{pmatrix}0\\vt\\0\end{pmatrix}$	$\begin{pmatrix}-vt\\0\\0\end{pmatrix}$	$\begin{pmatrix}0\\0\\0\end{pmatrix}$	$\begin{pmatrix}0\\0\\0\end{pmatrix}$
$\dots$	$\begin{pmatrix}0\\x\\0\end{pmatrix}$	$\begin{pmatrix}0\\0\\x\end{pmatrix}$	$\begin{pmatrix}y\\0\\0\end{pmatrix}$	$\begin{pmatrix}0\\0\\y\end{pmatrix}$	$\begin{pmatrix}z\\0\\0\end{pmatrix}$	$\begin{pmatrix}0\\z\\0\end{pmatrix}$	$\begin{pmatrix}x\\-y\\0\end{pmatrix}$	$\begin{pmatrix}0\\-y\\z\end{pmatrix}$

Table 4.3.: Polynomial Trefftz basis functions of order one.

For order $p = 2$ we need 30 basis functions (according to (4.2)). The expansion (4.3) for each polynomial Trefftz basis function reads

$$\mathbf{F}^1(\mathbf{r},t) = \begin{pmatrix} \mathbf{e}_2(\mathbf{r}) \\ \\ Z^{-1}\,\mathbf{h}_2(\mathbf{r}) \end{pmatrix} + \begin{pmatrix} \mathbf{e}_1(\mathbf{r}) \\ \\ Z^{-1}\,\mathbf{h}_1(\mathbf{r}) \end{pmatrix} (vt)^1 + \begin{pmatrix} \mathbf{e}_0(\mathbf{r}) \\ \\ Z^{-1}\,\mathbf{h}_0(\mathbf{r}) \end{pmatrix} (vt)^2 .$$

An appropriate basis function is composed of $\mathbf{e}_1^2 = (0, x^2, 0)$ and $\mathbf{h}_1^2 = (0,0,0)$. By using the recurrence relations (4.3) we obtain $\mathbf{e}_1^1 = (0,0,0)$ and $\mathbf{h}_1^1 = (0,0,-2x)$ and, subsequently $\mathbf{e}_1^0 = (0,1,0)$ and $\mathbf{h}_1^0 = (0,0,0)$. The resulting polynomial Trefftz basis function is $\mathbf{F}_1^2 = (\mathbf{E}_1^2, \mathbf{H}_1^2)^T = ((0, x^2 + (vt)^2, 0), (0,0,-2vxt))^T$. A complete list of the order two basis functions and the corresponding Trefftz basis functions can be found in Appendix B. This Trefftz basis construction procedure can now be simply applied on basis sets of $p > 2$; With this we can construct Trefftz basis functions for arbitrary orders p.

Stability: in the final part of this chapter we comment on stability over a time-slab. To this end, we consider a spatial partition of the domain $\Omega_h \equiv \mathscr{T}(\Omega)$ over a time interval I^n and investigate the evolution of the electromagnetic energy in an arbitrary spatial element $K \in \Omega_h$ over a time interval I^n. Note that $\|\cdot\|_K$ and $\|\cdot\|_{K\times I^n}$ denote the L_2-norms over K and $K \times I^n$, respectively.

Theorem III (Stability) (see Theorem 11 of [15])
Let $K \in \Omega_h$ be an arbitrary regular, geometry-conforming, nonoverlapping element and $Q^n = K \times I^n$ denote the corresponding space-time element. Then for all $(\mathbf{E}^n, \mathbf{H}^n) \in \mathbb{T}_p(Q^n)$ there holds

$$\epsilon\|\mathbf{E}^n\|^2_{K\times I^n} + \mu\|\mathbf{H}^n\|^2_{K\times I^n} \leq C(p,K,I^n)\left(\epsilon\|\mathbf{E}(t^{n-1})\|^2_K + \mu\|\mathbf{H}(t^{n-1})\|^2_K\right)$$

with a constant $C(p,K,I^n)$ only depending on the polynomial degree, the spatial element, the size of the time interval, and the material parameters.

Proof. The energy argument yields

$$\begin{aligned}\frac{1}{2}\frac{d}{dt}\Big(\epsilon\|\mathbf{E}\|^2_K + \mu\|\mathbf{H}\|^2_K\Big) &= (\boldsymbol{\nabla}\times\mathbf{H},\mathbf{E})_K - (\boldsymbol{\nabla}\times\mathbf{E},\mathbf{H})_K \\ &= (\mathbf{n}\times\mathbf{H},\mathbf{E})_{\partial K} \leq \|\mathbf{H}\|_{\partial K}\|\mathbf{E}\|_{\partial K} \leq c\Big(\epsilon\|\mathbf{E}\|^2_K + \mu\|\mathbf{H}\|^2_K\Big).\end{aligned}$$

For the last estimate, we used a discrete trace inequality [27] and Young's inequality.

By employing Gronwall's lemma, we obtain

$$\epsilon\|\mathbf{E}(t)\|_K^2 + \epsilon\|\mathbf{H}(t)\|_K^2 \leq e^{c|t-t^{n-1}|}\big(\epsilon\|\mathbf{E}(t^{n-1})\|_K^2 + \epsilon\|\mathbf{H}(t^{n-1})\|_K^2\big).$$

The assertion of the theorem follows by integration with respect to the time variable. □

Note, that this result is the first step to derive a stability estimate for the numerical method in the next chapter.

4.3 Transport Polynomials

In the following, we discuss a direct construction of a Trefftz basis in terms of polynomial plane waves that are polynomial versions of the electromagnetic plane waves introduced in Definition I. This construction procedure is different to that described in the previous Section 4.2. Note at this point, that Farhat et al. have employed a similar form of these solutions for acoustic wave problems [74, 92]. In this context the polynomial plane waves are scalar functions that exhibit a transport character $(\mathbf{d}\cdot\mathbf{r}-v\,t)$ in direction $\mathbf{d}$; For this reason these functions are called **transport polynomials**.

Suitable polynomial solutions for Problem I can be derived from Definition I. In contrast to their accoustic counterparts, the transport polynomials required here need to be vector valued functions with coupled electric and magnetic fields corresponding to propagating plane waves.

Definition IV (Transport Polynomials)
For a given order p the transport polynomial that describes the propagation of a plane wave in direction $\mathbf{d}_i$ with $|\mathbf{d}_i| = 1$ reads

$$\mathbf{F}(\mathbf{r},t)_i^p = \begin{pmatrix} \mathbf{e}_i \\ Z^{-1}\mathbf{h}_i \end{pmatrix} \phi(\mathbf{r},t)_i^p \qquad \text{where} \qquad \phi(\mathbf{r},t)_i^p = (\mathbf{d}_i\cdot\mathbf{r}-v\,t)^p\,. \tag{D IV}$$

Here, the electric and magnetic field vectors fulfill $\mathbf{e}_i\cdot\mathbf{d}_i = \mathbf{h}_i\cdot\mathbf{d}_i = 0$ and $\mathbf{d}_i\times\mathbf{e}_i = Z^{-1}\mathbf{h}_i$.

Theorem IV (Solutions of Maxwell's Equations)
Let $\mathbf{F}(\mathbf{r},t)_i^p$ be a transport polynomial as defined in Definition IV, then it solves Problem I.

Proof. The assumption directly follows from Theorem I by inserting $\mathbf{F}(\mathbf{r},t)_i^p$. □

In Definition IV the properties of the material, i.e. ϵ and μ enter the basis function through the velocity $v = 1/\sqrt{\epsilon\mu}$ and the intrinsic impedance $Z = \sqrt{\mu/\epsilon}$. Here the transport character is expressed by the scalar function $\phi(\mathbf{r},t)_i^p$ and the vectorial character by $(\mathbf{e}_i, Z^{-1}\mathbf{h}_i)^T$. Note that these transport polynomials can also be written in terms of the monomial functions from the previous section.

4.4 Construction of a Basis in terms of Transport Polynomials

Let us introduce one way to systematically assemble appropriate transport polynomials for a basis. According to Definition IV the three constituting vectors of each transport polynomial $\mathbf{F}_i^p$ must fulfill $\mathbf{d}_i \cdot \mathbf{e}_i = \mathbf{d}_i \cdot \mathbf{h}_i = 0$ and $\mathbf{d}_i \times \mathbf{e}_i = Z^{-1}\mathbf{h}_i$. This is the case if $\mathbf{e}_i$, $\mathbf{h}_i$ and $\mathbf{d}_i$ lie on the x,y and z axis of a right handed Cartesian coordinate system for instance. From this initial constellation we can generate appropriate constituting vectors for transport polynomials in other directions by applying three Eulerian rotations. Here, we first apply a rotation around the z axis with an angle α_i, followed by a rotation around the y axis with an angle β_i and a final rotation around the z axis with an angle α_i, as depicted in Fig. 4.1 The resulting vectors read

$$\mathbf{e}_i = \begin{pmatrix} \cos^2(\beta_i) - \sin^2(\beta_i)\cos(\alpha_i) \\ -\cos(\beta_i)\sin(\beta_i)(1+\cos(\alpha_i)) \\ -\sin(\alpha_i)\sin(\beta_i) \end{pmatrix}, \tag{4.5a}$$

for the electric field and

$$\mathbf{h}_i = \begin{pmatrix} \cos(\beta_i)\sin(\beta_i)(1+\cos(\alpha_i)) \\ -\sin^2(\beta_i) + \cos^2(\beta_i)\cos(\alpha_i) \\ \sin(\alpha_i)\cos(\beta_i) \end{pmatrix}, \tag{4.5b}$$

for the magnetic field, which results in a direction of propagation

$$\mathbf{d}_i = \begin{pmatrix} -\sin(\alpha_i)\sin(\beta_i) \\ -\sin(\alpha_i)\cos(\beta_i) \\ \cos(\alpha_i) \end{pmatrix}. \tag{4.5c}$$

Note, that this is not the only choice of $\mathbf{e}_i$ and $\mathbf{h}_i$ for a certain direction $\mathbf{d}_i$ since $\mathbf{e}_i$ and $\mathbf{h}_i$ can lie in the whole plane orthogonal to $\mathbf{d}_i$. Assuming that we already picked one set of suitable fields for a direction by the described procedure, then only one more linearly independent choice $\mathbf{e}_i'$ and $\mathbf{h}_i'$ can be picked; For instance one can choose the vectors $\mathbf{e}_i'$ and $\mathbf{h}_i'$ for a different polarization by an additional rotation of $\pi/2$ in the green plane. However, if one is interested in only one polarization it makes more sense to enrich the basis with functions that contain more directions, of course.

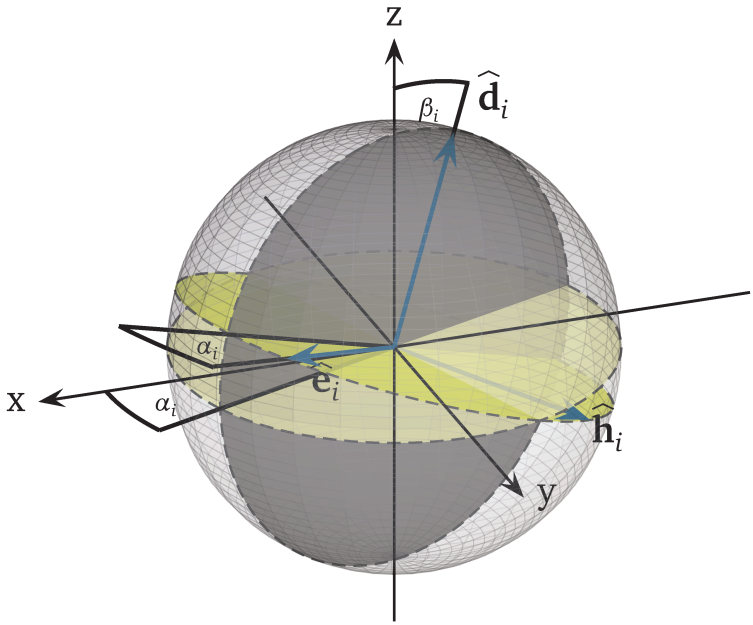

Figure 4.1.: Construction of constituting vectors $\mathbf{d}_i$, $\mathbf{e}_i$ and $\mathbf{h}_i$ for transport polynomials. We start from initial $(\widehat{\mathbf{e}}, \widehat{\mathbf{h}}, \widehat{\mathbf{d}})$ defined on the (x, y, z) axis. To obtain different directions we apply three Eulerian rotations. First we rotate all vectors by the angle α_i in the dark gray shaded rotation plane, after that by an angle β_i in the light gray shaded plane and finally by α_i in the green area.

Basis: In order to construct a basis one can assemble transport polynomials with different directions $\mathbf{d}_i$. For every order p their maximum number is given by (4.2), which particularly means that one also can choose less than the maximally allowed basis functions[3]

Moiola et al. have extensively studied the choice of suitable directions for non-polynomial plane waves in [68]. However, there exists no maximum number for these non-polynomial functions. Therefore, one could theoretically enrich the basis with plane waves in infinitely many directions. The approximation behavior under this **d**-enrichment was studied by Moiola. Here, **d**-enrichment improves the

[3] This has already been pointed out by Farhat et al. in [92] for instance.

approximation, but worsens the conditioning of the update matrix (of the linear system) at the same time. A suitable compromise has been to choose directions in layered structures. An optimized, but more complicated choice has been developed by Sloan [84].

For transport polynomials there exists a maximal number of basis functions for a given order. However, there exists no *a-priori* optimal choice for the directions of the basis functions inside this basis. If there is no distinguished direction present, one could for instance select directions according to Moiolas or Sloans procedure. If on the other hand a distinguished direction is present, e.g. in a wave-guide, choosing the directions of the transport polynomials that constitute a basis according to this direction can be more efficient. One possible choice of angles is listed in Table 4.4 and depicted in Fig. 4.2.

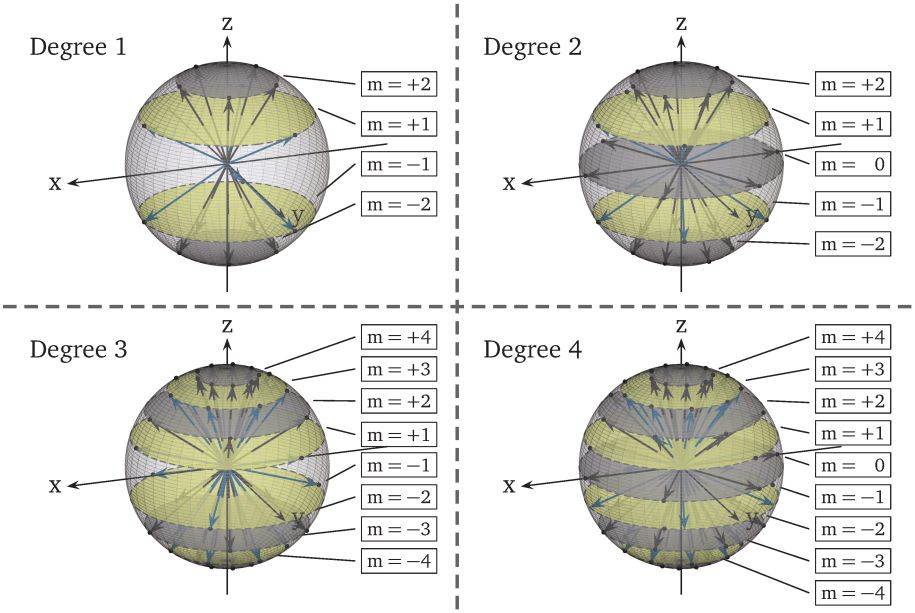

Figure 4.2.: Construction of the basis in terms of polynomial Trefftz functions for orders $p = 1, 2, 3, 4$ corresponding to Table 4.1. The directions of specific basis functions are depicted by blue and gray arrows. Here the basis functions are grouped together according to their layer number $m = 0, \pm 1, \pm 2 \ldots$ and sorted are sorted in green and gray layers.

Order	Layer	β_i	α_j	# Transport Polynomials	
p=1	m=1	$\pm\frac{1}{6}\pi$	$0, \frac{2}{3}\pi, \frac{4}{3}\pi$	$2\cdot 3 = 6$	16
	m=2	$\pm\frac{2}{6}\pi$	$0, \frac{2}{5}\pi, \frac{4}{5}\pi, \frac{6}{5}\pi, \frac{8}{5}\pi$	$2\cdot 5 = 10$	
p=2	m=0	$\frac{3}{6}\pi$	$0, \frac{2}{3}\pi, \frac{4}{3}\pi$	6	30
	m=1	$\pm\frac{1}{6}\pi$	$0, \frac{2}{5}\pi, \frac{4}{5}\pi, \frac{6}{5}\pi, \frac{8}{5}\pi$	$2\cdot 5 = 10$	
	m=2	$\pm\frac{2}{6}\pi$	$0, \frac{2}{7}\pi, \frac{4}{7}\pi, \frac{6}{7}\pi, \frac{8}{7}\pi, \frac{10}{7}\pi, \frac{12}{7}\pi$	$2\cdot 7 = 14$	
p=3	m=1	$\pm\frac{1}{9}\pi$	$0, \frac{2}{3}\pi, \frac{4}{3}\pi$	$2\cdot 3 = 6$	48
	m=2	$\pm\frac{2}{9}\pi$	$0, \frac{2}{5}\pi, \frac{4}{5}\pi, \frac{6}{5}\pi, \frac{8}{5}\pi$	$2\cdot 5 = 10$	
	m=3	$\pm\frac{3}{9}\pi$	$0, \frac{2}{7}\pi, \frac{4}{7}\pi, \frac{6}{7}\pi, \frac{8}{7}\pi, \frac{10}{7}\pi, \frac{12}{7}\pi$	$2\cdot 7 = 14$	
	m=4	$\pm\frac{4}{9}\pi$	$0, \frac{2}{9}\pi, \frac{4}{9}\pi, \frac{6}{9}\pi, \frac{8}{9}\pi, \frac{10}{9}\pi, \frac{12}{9}\pi, \frac{14}{9}\pi, \frac{16}{9}\pi$	$2\cdot 9 = 18$	

Table 4.4.: A possible choice of suitable angles for a basis in terms of transport polynomials corresponding to plane waves with one polarization.

Two-dimensional scenario: In the two-dimensional case Definition IV reduces to

$$\mathbf{F}^{2\mathrm{d}}(x,y,t)_i^p = \begin{pmatrix} \mathbf{e}^{2\mathrm{d}} \\ Z^{-1}\mathbf{h}^{2\mathrm{d}} \end{pmatrix} \left(\mathbf{d}^{2\mathrm{d}} - vt\right)^p . \tag{4.6}$$

Here, we consider both $\mathbf{d}^{2\mathrm{d}} = (d_x, d_y)^T$ and $\mathbf{h}^{2\mathrm{d}} = (h_x, h_y)^T$ to be in the xy-plane $\mathbf{r}^{2\mathrm{D}} = (x,y)^T$ and consequently $\mathbf{e}^{2\mathrm{d}} = e_z$. The two-dimensional polynomial space over $Q^n = K \times I^n$ with $K \subset \mathbb{R}^2$ has dimension

$$\dim \mathbb{T}_p(Q) = (p+3)(p+1), \tag{4.7}$$

and consequently $2p+3$ basis functions for a certain oder p. One choice to construct a basis in terms of transport polynomials is to equidistantly distribute the directions of the basis functions in the xy-plane. This choice is depicted in Fig. 4.2 for the first four orders. As mentioned before this choice makes sense, if there is no prefered direction present.

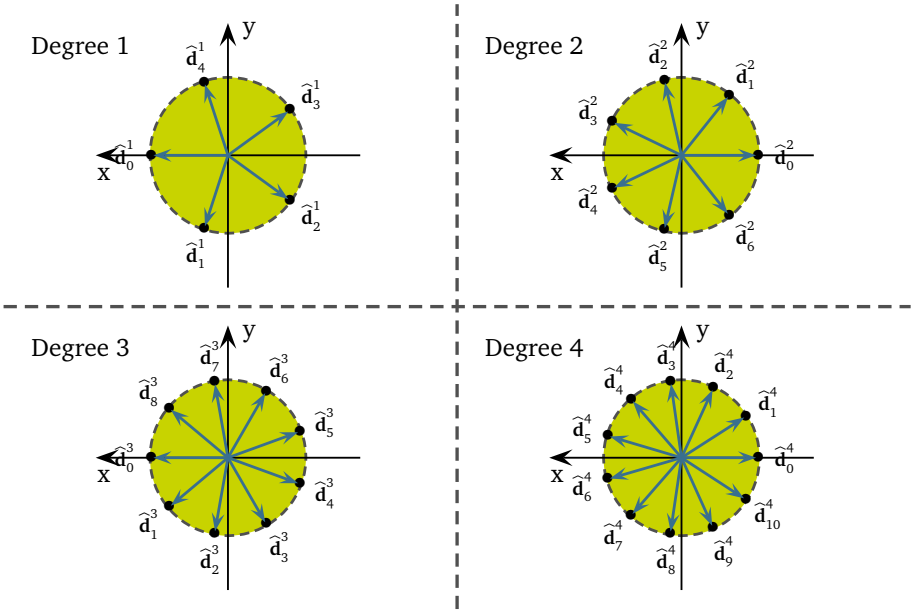

Figure 4.3.: Choice of directions for the two-dimensional basis in terms of transport polynomials for orders $p = 1, 2, 3, 4$. For a fixed order p there exists a total of $2p+3$ basis functions. The corresponding electric fields $\mathbf{e}^{2\mathrm{d}\,p}_{i}$ and magnetic $\mathbf{h}^{2\mathrm{d}\,p}_{i}$ fields can subsequently be constructed as shown in Fig. 4.1.

One-dimensional scenario: One-dimensional transport polynomials describe waves with two vectorial components traveling in one direction that can be x for instance (see. [48]). The two corresponding vectorial components can be $\mathbf{E}^{1\mathrm{d}} = E_z$ and $\mathbf{H}^{1\mathrm{d}} = H_y$ for instance. The resulting transport polynomial reads

$$\mathbf{F}^{1\mathrm{d}}(x,t)^{p}_{\pm} = \begin{pmatrix} \mathbf{e}^{1\mathrm{d}} \\ \pm Z^{-1}\mathbf{h}^{1\mathrm{d}} \end{pmatrix} (\pm x - vt)^{p}\,, \tag{4.8}$$

and corresponds to a wave that travels in direction $+x$ or $-x$. The basis contains $2(p+1)$ polynomials with 2 functions per order p.
Let us illustrate the effect of different media on the transport polynomials at this point. In a vacuum $\epsilon = \mu = 1$ the medium speed of light is $v = 1$. A plane wave propagates in free space at a 45 degree space-time angle. The basis that is suitable to describe this scenario is depicted in Fig. 4.4 (left side). In a medium with $\epsilon = 4$ and $\mu = 1$ the medium speed of light is $v = 1/2$. In this medium space-time angle

of a propagating wave decreases to 22.5 degrees. For this scenario the basis is depicted in Fig. 4.4 (right side).

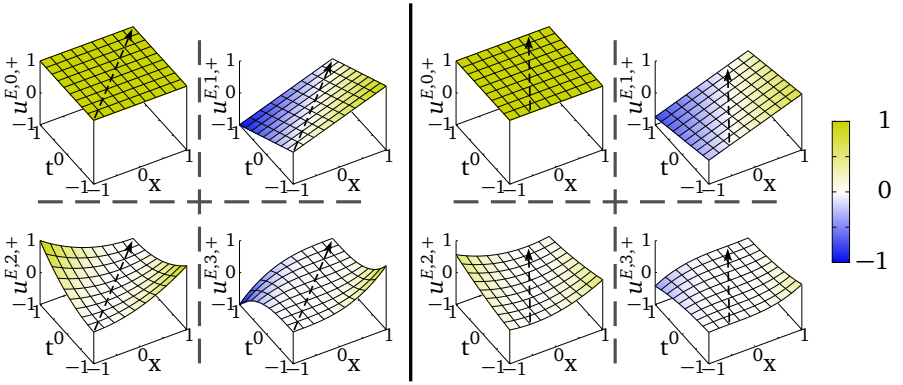

Figure 4.4.: Electric fields of the one-dimensional transport polynomials of orders $p = 0, 1, 2, 3$; in a vacuum (i.e. $\epsilon = 1$ and $\mu = 1$) on the left and a medium (i.e. $\epsilon = 4$ and $\mu = 1$) on the right.

Chapter Resumé

In this chapter we have discussed polynomial Trefftz type basis functions corresponding to Problem I and introduced two possible ways to systematically construct them. In the remainder of this work we will apply a Trefftz basis in terms of transport polynomials.

To this end we have first defined the appropriate Trefftz space in Definition II and the corresponding polynomial Trefftz space in Definition III. Then we have characterized the behavior of the considered fields in Lemma I. From this we have obtained the dimension of the polynomial Trefftz space in Theorem II; And a procedure to construct a polynomial Trefftz basis from a already existing polynomial basis by an expansion of the constituing fields (4.3) and application of derived recurrence relations (4.4).

In the final part of this chapter we have introduced our Trefftz basis of choice, that is in terms of transport polynomials (see Definition IV) as well as one possible way of construction. Subsequently, we have outlined two- and one-dimensional versions.

5 Discrete Approximations of Maxwell's Equations

In this chapter we introduce the framework for the DGT method. To this end, we proceed as follows.

In the first Section 5.1 we create a short survey of some popular numerical frameworks. From these possibilities, we select the DG framework to be suited for our endeavor. In Section 5.2, we then state our underlying DG method in an abstract manner and introduce some of its inherent properties. Subsequently, we combine this DG method with the previously developed polynomial Trefftz basis in Section 5.3. In Section 5.4 we will then explicitly state a numerical scheme based on this method.

5.1 Survey of Numerical Methods

Let us discuss some of the frequently used methods in computational electromagnetism. Before we start, let us remark that there exists no "*best method*" in general. A certain method can only be well suited for a considered application.

Yee scheme: one of the first schemes in computational electromagnetism is the scheme developed by Kane Yee in 1966 [94]. The Yee-scheme is an FDTD method in which the electric field **E** and the magnetic field **H** are discretized on the edges and faces of a hexaherdal grid. In the original version Yee applied a "*leap-frog*" time stepping scheme for the time update and first order difference quotients for the spatial derivatives. Due to its local, explicit structure, the Yee scheme is very fast and well suited for parallelization. However, high precision and the treatment of complicated geometries are problematic.

Finite Integration Technique: another widely used method that has been developed by Thomas Weiland in 1977 [93] is the Finite Integration Technique (FIT). In FIT, the fields are implemented as integrated quantities. Here, the fields **E** and **B** are defined on the edges and faces of a primal grid and the fields **H** and **D** on the edges and faces of a dual grid. In FIT all benefits of the Yee scheme are prevailed. For hexahedral grids the method is second order. However, difficult geometries remain a challenge.

Finite Element Method: a third class of methods are the FEM that have been developed by pioneers such as Olgried Zienkiewicz [97] in the fifties. In FEM the underlying equation system is transformed into a weak formulation by first multiplying the original equation by trial functions, then integrating over elements of a mesh and finally approximating the physical fields by basis functions. This procedure leads to a linear system that is then solved. In contrast to the previously discussed three methods, FEM (potentially) is a high order method that is applicable to complicated geometries. However, to ensure continuity requirements of electromagnetic fields over the cell boundaries, usually special elements such as Nedelec elements [1] are applied in standard FEM.

5.2 A Discontinuous Galerkin Framework

In connection to the previous discussion, let us now state our method of choice. In order to employ the polynomial basis functions developed in the previous chapter, this method must be a high order method that allows the employment of locally defined basis functions[1]. By the first argument both the Yee-scheme and FIT disqualify as suitable choices. Herein, only FEM is a high-order method, but also not completely suited in its standard form, due to the additional continuity requirement to the elements.

A framework that drops this additional requirement is the DG framework that has been originally applied by Reed and Hill [79] as well as Raviart [53] in 1973 to the neutron transport equation. Just as in FEM, a weak formulation of the problem is derived. However, in DG the continuity requirements of the fields are weakly enforced by means of averaging flux terms at the traces of the elements. This makes the DG method highly flexible and particularly allows the employment of local basis functions. In this section we will introduce our specific DG method.

Constituents of the Discontinuous Galerkin Method

As a prelude of the complete discussion of the discontinuous Galerkin method let us shortly derive the element-wise constituents of the method in a local reference element K over a time interval I^n corresponding to Problem I. Following the

[1] Note that there also exist FDTD methods such as for instance the FLAME framework by Tsukerman et al. that employ Trefftz functions. However, we do not consider these methods here.

standard Galerkin construction, we multiply Maxwell's equations with sufficiently smooth test functions ($\mathbf{v}$, $\mathbf{w}$) and integrate the result over space and time

$$\int_{I^n}\int_K \left\{ \left(\nabla \times \mathbf{E} + \mu \frac{\partial \mathbf{H}}{\partial t} \right) \cdot \mathbf{w} - \left(\nabla \times \mathbf{H} - \epsilon \frac{\partial \mathbf{E}}{\partial t} \right) \cdot \mathbf{v} \right\} \mathrm{d}V \, \mathrm{d}t = 0. \tag{5.1}$$

Subsequently, we perform an integration by parts yielding

$$\int_{I^n}\int_K \left\{ (\mathbf{E} \cdot (\nabla \times \mathbf{w}) - \mathbf{H} \cdot (\nabla \times \mathbf{v})) - \left((\mu \mathbf{H}) \frac{\partial \mathbf{w}}{\partial t} + (\mu \mathbf{E}) \frac{\partial \mathbf{v}}{\partial t} \right) \right\} \mathrm{d}V \, \mathrm{d}t \tag{5.2}$$

$$+ \int_{I^n}\int_{\partial K} (\mathbf{n} \times \mathbf{E}^* \cdot \mathbf{w} - \mathbf{n} \times \mathbf{H}^* \cdot \mathbf{v}) \, dS \, \mathrm{d}t$$

$$+ \int_K \left(\mu \tilde{\mathbf{H}} \cdot \mathbf{w} + \epsilon \tilde{\mathbf{E}} \cdot \mathbf{v} \right) \Big|_{t^n}^{t^{n+1}} \mathrm{d}V = 0, \tag{5.3}$$

with $\mathbf{E}^*$ and $\mathbf{H}^*$ being the spatial fluxes and $\tilde{\mathbf{E}}$ and $\tilde{\mathbf{H}}$ the temporal fluxes. In the first line of (5.2) we identify four terms that are integrated over space and time whereas the second line contains two terms at the spatial and two terms at the temporal boundary, respectively. Following Monk [35, 36] we integrate (5.2) once again yielding the ultra-weak formulation

$$\int_{I^n}\int_K \left\{ \left(\nabla \times \mathbf{E} + \mu \frac{\partial \mathbf{H}}{\partial t} \right) \cdot \mathbf{w} + \left(\nabla \times \mathbf{H} - \epsilon \frac{\partial \mathbf{E}}{\partial t} \right) \cdot \mathbf{v} \right\} \mathrm{d}V \, \mathrm{d}t \tag{5.4}$$

$$+ \int_{I^n}\int_{\partial K} (\mathbf{n} \times (\mathbf{E}^* - \mathbf{E}) \cdot \mathbf{w} - \mathbf{n} \times (\mathbf{H}^* - \mathbf{H}) \cdot \mathbf{v})_{\partial K} \, dS \, \mathrm{d}t$$

$$+ \int_K \left(\mu \left(\tilde{\mathbf{H}} - \mathbf{H} \right) \cdot \mathbf{w} + \epsilon \left(\tilde{\mathbf{E}} - \mathbf{E} \right) \cdot \mathbf{v} \right) \Big|_{t^n}^{t^{n+1}} \mathrm{d}V = 0.$$

Notice, that the differential operators in the terms of the first line act on the fields and not on the test functions anymore. These new volume terms are just the original integrals from (5.1). In the second line we can identify the resulting spatial boundary terms and in the third line the temporal boundary terms. In the method we will choose fluxes that are centered in space and upwind in time. At an spatial interface between two cells this means

$$\mathbf{E}^* = \tfrac{1}{2}(\mathbf{E}_1 + \mathbf{E}_2) \qquad \text{and} \qquad \mathbf{H}^* = \tfrac{1}{2}(\mathbf{H}_1 + \mathbf{H}_2), \tag{5.5}$$

whereas at a temporal interface

$$\tilde{\mathbf{E}} = \mathbf{E} \qquad \text{and} \qquad \tilde{\mathbf{H}} = \mathbf{H}. \tag{5.6}$$

The Global Discontinuous Galerkin Method

Let us now introduce the resulting discontinuous Galerkin method. At this point we discuss some properties of the framework. To this end, we keep the spaces of the considered test and basis functions as general as possible. We just demand them to be in the space of piecewise smooth vector valued functions

$$\left(\mathcal{V}_n^E, \mathcal{V}_n^H\right) = \left[\mathbb{P}^p\left(Q^n\right)\right]^6, \tag{5.7}$$

at times $n \geq 1$. By combining the cell-wise contributions from (5.4) and including the boundary conditions at the global boundaries $\partial\Omega$.

Again we consider a spatial partition of the domain $\Omega_h = \mathcal{T}(\Omega)$ over a time interval I^n. The resulting space-time slab reads $Q_h^n = \Omega_h \times I^n$. At the interior boundaries we denote by $\mathcal{F}_i \equiv \{f = \partial K \cap \partial K',\ K \neq K' \in \Omega_h\}$ the set of element interfaces and at the boundaries by $\mathcal{F}_b \equiv \{f = \partial K \cap \partial\Omega,\ K \in \Omega_h\}$ the set of boundary faces.

On the interfaces between two elements $\partial K_1 \cap \partial K_2$ piecewise continuous functions have two values. The discontinuous Galerkin framework deals with this in terms of numerical fluxes. For further convenience we would like to introduce the tangential jump operator and the average operator at the interfaces between two neighboring cells K_1 and K_2

$$[\![\mathbf{n} \times \mathbf{E}]\!] = \mathbf{n} \times \mathbf{E}_2 - \mathbf{n} \times \mathbf{E}_1, \tag{5.8}$$

$$\{\!\{\mathbf{E}\}\!\} = \frac{1}{2}\left(\mathbf{E}_1 + \mathbf{E}_2\right). \tag{5.9}$$

Method I (Space-time DG method) (see Method 1 of [15])

Set $\mathbf{E}_h^0 = \mathbf{E}_0$, *and* $\mathbf{H}_h^0 = \mathbf{H}_0$, *and consecutively find* $(\mathbf{E}_h^n, \mathbf{H}_h^n) \in \mathcal{V}_n^E \times \mathcal{V}_n^H$ *for* $n \geq 1$, *such that*

$$A^n(\mathbf{E}_h, \mathbf{H}_h^n; \mathbf{v}, \mathbf{w}) = R^n(\mathbf{E}_h^{n-1}, \mathbf{H}_h^{n-1}; \mathbf{v}, \mathbf{w}), \tag{5.10}$$

for all $(\mathbf{v}, \mathbf{w}) \in \mathcal{V}_n^E \times \mathcal{V}_n^H$ *with bilinear forms* A^n *and* R^n *defined by*

$$\begin{aligned}
A^n(\mathbf{E}, \mathbf{H}; \mathbf{v}, \mathbf{w}) = \\
&\sum_{K \in \Omega_h} \int_{K \times I^n} (\epsilon \frac{\partial \mathbf{E}}{\partial t} - \boldsymbol{\nabla} \times \mathbf{H}) \cdot \mathbf{v} + (\mu \frac{\partial \mathbf{H}}{\partial t} + \boldsymbol{\nabla} \times \mathbf{E}) \cdot \mathbf{w} && \textit{(volume terms)} \\
&+ \sum_{K \in \Omega_h} \int_{K \times \partial I^n} \epsilon \mathbf{E}(t^{n-1}) \cdot \mathbf{v}(t^{n-1}) + \mu \mathbf{H}(t^{n-1}) \cdot \mathbf{w}(t^{n-1}) && \textit{(temporal interface terms)} \\
&+ \sum_{f \in \mathcal{F}_i} \int_{f \times I^n} \mathbf{n} \times (\mathbf{H} - \mathbf{H}^*) \cdot \mathbf{v} - \mathbf{n} \times (\mathbf{E} - \mathbf{E}^*) \cdot \mathbf{w} && \textit{(spatial interface terms)} \\
&+ \sum_{f \in \mathcal{F}_b} \int_{f \times I^n} \mathbf{n} \times \mathbf{E} \cdot \mathbf{v} - \beta^E \mathbf{n} \times (\mathbf{H} \times \mathbf{n}) \cdot \mathbf{v}, && \textit{(boundary terms)}
\end{aligned}$$

and

$$\begin{aligned}
R^n(\mathbf{E}, \mathbf{H}, \mathbf{v}, \mathbf{w}) = \\
&\sum_{K \in \Omega_h} \int_{K \times I^n} \epsilon \mathbf{E}(t^{n-1}) \cdot \mathbf{v}(t^{n-1}) + \mu \mathbf{H}(t^{n-1}) \cdot \mathbf{w}(t^{n-1}) && \textit{(temporal interface terms)} \\
&+ \sum_{f \in \mathcal{F}_b} \int_{f \times I^n} \mathbf{n} \times \mathbf{g}(\mathbf{r}, t) \cdot \mathbf{v}. && \textit{(boundary terms)}
\end{aligned}$$

On internal faces $f \in \mathcal{F}_i$ *between adjacent elements, we set centered fluxes*

$$\mathbf{E}^* = \{\!\{\mathbf{E}\}\!\}, \qquad \mathbf{H}^* = \{\!\{\mathbf{H}\}\!\}.$$

On global boundaries $f \in \mathcal{F}_b$ *we use pec boundary conditions* $\mathbf{n} \times \mathbf{E}^* = 0$ (2.17a). *An equivalent version can be formulated with pmc boundary conditions* $\mathbf{n} \times \mathbf{H}^* = 0$ (2.17b).

From the definition of Method I some important properties directly follow. The first property of our method is that it is implicit.

Theorem V (Implicitness – DG) (see Theorem 2 of [15])
Assume that the variational problem (5.10) *is solvable for every* $n \geq 1$. *Then Method I defines an implicit time stepping scheme.*

Proof. In the definition of Method I, the bilinear from A^n contains the fields defined at t^n and R^n those defined at time t^{n-1}. The fields $(\mathbf{E}_h^n, \mathbf{H}_h^n)$ can therefore be calculated from $(\mathbf{E}_h^{n-1}, \mathbf{H}_h^{n-1})$ by solving a non trivial system of equations under consderation of $\mathbf{g}(\mathbf{r}, t)$. Therefore, one has an implicit method. □

In Section 5.4 we will introduce a numerical scheme with this property. In addition Method I is consistent with the initial value Problem I. In particular it is consistent with the considered boundary conditions.

Theorem VI (Consistency – DG) (see Theorem 3 of [15])
Let $(\mathbf{E}, \mathbf{H})$ *be a sufficiently smooth solution of the continuous Problem I. Then*

$$A^n(\mathbf{E}, \mathbf{H}; \mathbf{v}, \mathbf{w}) = R^n(\mathbf{E}, \mathbf{H}; \mathbf{v}, \mathbf{w}),$$

for all piecewise smooth test functions $\mathbf{v}$, $\mathbf{w}$ *and all* $n \geq 1$.

Proof. We split the proof in four parts.

(i) The boundary terms satisfy (2.17). Therefore, they cancel out.

(ii) Since, $(\mathbf{E}, \mathbf{H})$ are solutions of Problem I, all volume terms in Method I trivially vanish.

(iii) Due to continuity of the fields at the temporal interfaces, the field terms yield $\mathbf{E}^{n-1}(t^{n-1}) = \mathbf{E}^n(t^{n-1})$ and $\mathbf{H}^{n-1}(t^{n-1}) = \mathbf{H}^n(t^{n-1})$, respectively. Therefore, the contributions in A^n and R^n cancel each other.

(iv) By a similar argument as in (iii), namely the tangential continuity (2.11) of $\mathbf{n} \times \mathbf{E} = \mathbf{n} \times \mathbf{E}^*$ and $\mathbf{n} \times \mathbf{H} = \mathbf{n} \times \mathbf{H}^*$ also the spatial interface terms cancel out.

It follows that Method I is consistent with Problem I. □

Here, we assumed a general type of boundary conditions as defined in Section 2.6. In order to develop energy estimates in the following sections, let us show that there holds a kind of coercivity estimate for Method I.

Theorem VII (Stability – DG) (see Theorem 4 of [15])
Let $(\mathcal{V}_n^E, \mathcal{V}_n^H)$ *be piecewise smooth approximation spaces on* $Q_h^n = \Omega_h \times I^n$, $n \geq 1$. *Then*

$$A^n(\mathbf{v},\mathbf{w};\mathbf{v},\mathbf{w}) \geq \tfrac{1}{2}|||(\mathbf{v},\mathbf{w})|||^2_{Q_h^n} \quad \textit{for all } \mathbf{v} \in \mathcal{V}_n^E,\ \mathbf{w} \in \mathcal{V}_n^H,$$

with the semi-norm

$$\begin{aligned}|||(\mathbf{v},\mathbf{w})|||^2_{Q_h^n} &= \|\epsilon^{1/2}\mathbf{v}(t^n)\|^2_{\Omega_h} + \|\mu^{1/2}\mathbf{w}(t^n)\|^2_{\Omega_h} \\ &\quad + \|\epsilon^{1/2}\mathbf{v}(t^{n-1})\|^2_{\Omega_h} + \|\mu^{1/2}\mathbf{w}(t^{n-1})\|^2_{\Omega_h} + 2\beta^E\|\mathbf{n}\times\mathbf{H}\|^2_{\partial\Omega_h\times I^n}.\end{aligned}$$

Proof. Let us consider the left hand side term A^n and specify $\mathbf{v} = \mathbf{E}_h^n$ and $\mathbf{w} = \mathbf{H}_h^n$. By doing so, the volume terms in element K read

$$\int_{K\times I^n}\left(\frac{d(\epsilon\mathbf{E}_h^n\cdot\mathbf{E}_h^n)}{dt} + \frac{d(\mu\mathbf{H}_h^n\cdot\mathbf{H}_h^n)}{dt}\right) + \int_{K\times I^n}(\boldsymbol{\nabla}\times\mathbf{E}_h^n\cdot\mathbf{H}_h^n - \boldsymbol{\nabla}\times\mathbf{H}_h^n\cdot\mathbf{E}_h^n).$$

This equation can be transformed into a form, similar to Poyntings' Theorem (2.7), by application of Stokes' theorem and the product rule. We get

$$\int_{I^n}\frac{1}{2}\frac{d}{dt}\left(\|\epsilon^{1/2}\mathbf{E}_h^n(t)\|^2_K + \|\mu^{1/2}\mathbf{H}_h^n(t)\|^2_K\right) + \int_{\partial K\times I^n}\mathbf{E}_h^n\times\mathbf{H}_h^n\cdot\mathbf{n}.$$

A subsequent inclusion of the boundary conditions copes with the spatial flux terms at the boundaries. All that remains here is the time derivative term. At the internal interfaces $f = K_1 \cap K_2$ we obtain terms of the form

$$-(\mathbf{E}_1\times\mathbf{H}_1\cdot\mathbf{n}_1 + \mathbf{E}_2\times\mathbf{H}_2\cdot\mathbf{n}_2).$$

By combining the time derivative term, the interface conditions with the initial values, one gets, after a summation over all elements and a subsequent time integration over the considered time slab

$$\begin{aligned}A^n(\mathbf{E},\mathbf{H};\mathbf{E},\mathbf{H}) &= \sum_{K\in\Omega_h}\|\epsilon^{1/2}\mathbf{E}(t^n)\|^2_K + \|\mu^{1/2}\mathbf{H}(t^n)\|^2_K \\ &\quad + \sum_{K\in\Omega_h}\|\epsilon^{1/2}\mathbf{E}(t^{n-1})\|^2_K + \|\mu^{1/2}\mathbf{H}(t^{n-1})\|^2_K \\ &\quad + \sum_{f\in\mathcal{F}_i}\int_{f\times I^n}2\beta^E\|\mathbf{n}\times\mathbf{H}\|^2.\end{aligned}$$

□

In Theorem VII and the subsequent proof the bilinear form $A^n(\mathbf{v},\mathbf{w};\mathbf{v},\mathbf{w})$ can only be estimated by a semi-norm (instead of a norm), since $\mathbf{v}$ and $\mathbf{w}$ belong to abstract vector spaces $\mathscr{V}_n^E$ and $\mathscr{V}_n^H$ that can contain zero contributions. As a final result we comment on the behavior of energy in Method I. Here, the total energy contained in Ω is denoted by $\frac{1}{2}\int_\Omega(\epsilon\|\mathbf{E}(t)\|^2+\mu\|\mathbf{H}(t)\|^2)\,d\Omega$. From the previous discussion we directly obtain

$$\frac{1}{2}(\|\epsilon^{1/2}\mathbf{E}(t)\|_\Omega^2+\|\mu^{1/2}\mathbf{H}(t)\|_\Omega^2)\Big|_{t^{n-1}}^{t^n}=-\int_{\partial\Omega\times I^n}\mathbf{n}\times\mathbf{E}\cdot\mathbf{H}.$$

This asserts that the electromagnetic energy changes due to the flux $\mathbf{S}\cdot\mathbf{n}$ over the global boundary of the domain Ω. A similar relation holds for every solution of Method I independent of the approximation spaces used.

Theorem VIII (Energy Balance – DG) (see Theorem 6 of [15])
Let $(\mathbf{E}_h^n,\mathbf{H}_h^n)$ be a solution of Method I. Then

$$\begin{aligned}\frac{1}{2}\left(\|\epsilon^{1/2}\mathbf{E}_h^n\|_{\Omega_h}^2+\|\mu^{1/2}\mathbf{H}_h^n\|_{\Omega_h}^2\right)\Big|_{t^{n-1}}^{t^n}&=-\int_{\partial\Omega_h\times I^n}\left(\beta^E|\mathbf{n}\times\mathbf{H}_h^n|^2+\mathbf{n}\times\mathbf{g}(\mathbf{r},t)\cdot\mathbf{H}_h^n\right)\\&\quad-\tfrac{1}{2}\|\epsilon^{1/2}\left(\mathbf{E}_h^n(t^{n-1})-\mathbf{E}_h^{n-1}(t^{n-1})\right)\|_{\Omega_h}^2\\&\quad-\tfrac{1}{2}\|\mu^{1/2}\left(\mathbf{H}_h^n(t^{n-1})-\mathbf{H}_h^{n-1}(t^{n-1})\right)\|_{\Omega_h}^2.\end{aligned}$$

Proof. Let us consider the right hand side term R^n in Method I and specify $\mathbf{v}=\mathbf{E}_h^n$ and $\mathbf{w}=\mathbf{H}_h^n$. We get,

$$\begin{aligned}R^n\left(\mathbf{E}_h^{n-1},\mathbf{H}_h^{n-1};\mathbf{E}_h^n,\mathbf{H}_h^n\right)&=-\sum_{f\in\mathscr{F}_b}\int_{f\times I^n}\mathbf{n}\times\mathbf{g}(\mathbf{r},t)\cdot\mathbf{H}_h^n\\&\quad+\sum_{K\in\Omega_h}\int_K\epsilon\mathbf{E}_h^{n-1}(t^{n-1})\cdot\mathbf{E}_h^n(t^{n-1})+\mu\mathbf{H}_h^{n-1}(t^{n-1})\cdot\mathbf{H}_h^n(t^{n-1})\\&=-\sum_{f\in\mathscr{F}_b}\int_{f\times I^n}\mathbf{n}\times\mathbf{g}(\mathbf{r},t)\cdot\mathbf{H}_h^n\\&\quad+\frac{1}{2}\sum_{K\in\Omega_h}\int_K\left(\epsilon\|\mathbf{E}_h^{n-1}(t^{n-1})\|_K^2+\mu\|\mathbf{H}_h^{n-1}(t^{n-1})\|_K^2\right)\end{aligned}$$

$$+\frac{1}{2}\sum_{K\in\Omega_h}\int_K \left(\epsilon\|\mathbf{E}_h^n(t^{n-1})\|_K^2+\mu\|\mathbf{H}_h^n(t^{n-1})\|_K^2\right)$$
$$-\frac{1}{2}\sum_{K\in\Omega_h}\int_K \left(\epsilon\|\mathbf{E}_h^{n-1}(t^{n-1})-\mathbf{E}_h^n(t^{n-1})\|_K^2+\mu\|\mathbf{H}_h^{n-1}(t^{n-1})-\mathbf{H}_h^n(t^{n-1})\|_K^2\right),$$

where, we applied

$$\int_K \mathbf{E}_h^{n-1}\cdot\mathbf{E}_h^n=\frac{1}{2}\|\mathbf{E}_h^n\|_K^2+\frac{1}{2}\|\mathbf{E}_h^{n-1}\|_K^2+\frac{1}{2}\|\mathbf{E}_h^{n-1}-\mathbf{E}_h^n\|_K^2,$$

and a similar equality for the respective $\mathbf{H}_h^n$ and $\mathbf{H}_h^{n-1}$. If we now set $A^n\left(\mathbf{E}_h^n,\mathbf{H}_h^n;\mathbf{E}_h^n,\mathbf{H}_h^n\right)=R^n\left(\mathbf{E}_h^{n-1},\mathbf{H}_h^{n-1};\mathbf{E}_h^n,\mathbf{H}_h^n\right)$ and use the second part of Theorem VII we get the expression to be proven. □

The first four terms in the theorem directly correspond to the expected terms from Poynting's theorem (2.7). The additional terms appear due to the implicit nature of the time stepping discretization and result in an artificial decrease of the energy. For increasing approximation orders the effect of numerical dissipation decreases and makes the effect negligible for high order approximations. A direct result of this theorem is that the energy in the considered domain has uniform bounds. In the following section we will use this property together with the coercivity estimate to show the uniqueness of the solution for the method.

5.3 The Discontinuous Galerkin Trefftz Method

Let us now define the discontinuous Galerkin Trefftz method. To this end, we will fix the vector spaces $\mathcal{V}_n^E\times\mathcal{V}_n^H$ to that of the Trefftz functions defined in Definition II. Therefore, we consider piecewise continuous Trefftz functions $(\mathbf{E}^n,\mathbf{H}^n)\in\mathbb{T}_p(Q_h^n)$ from now on. Note that in the three-dimensional case the number of DoF on every space-time element $Q^n=K\times I^n$, of this basis is proportional to $\mathcal{O}(p^3)$ instead of the usual $\mathcal{O}(p^4)$ for the commonly applied tensorial basis. This means that we substantially decrease the number of DoF resulting in an increase of efficiency. The resulting discontinuous Galerkin Trefftz method reads

Method II (Space-Time DG Trefftz Method) (see Method 2 of [15])

Set $\mathbf{E}_h^0 = \mathbf{E}_0$, *and* $\mathbf{H}_h^0 = \mathbf{H}_0$ *and consecutively find* $(\mathbf{E}^n, \mathbf{H}^n) \in \mathbb{T}_p(Q_h^n)$ *for* $n \geq 1$, *such that*

$$A^n(\mathbf{E}_h^n, \mathbf{H}_h^n; \mathbf{v}, \mathbf{w}) = R^n(\mathbf{E}_h^{n-1}, \mathbf{H}_h^{n-1}; \mathbf{v}, \mathbf{w}) \tag{5.11}$$

for all $(\mathbf{v}, \mathbf{w}) \in \mathbb{T}_p(Q_h^n)$ *with bilinear forms* A^n *and* R^n *defined by*

$$\begin{aligned} A^n(\mathbf{E}, \mathbf{H}; \mathbf{v}, \mathbf{w}) = \\ &+ \sum_{K \in \Omega_h} \int_K \epsilon \mathbf{E}(t^{n-1}) \cdot \mathbf{v}(t^{n-1}) + \mu \mathbf{H}(t^{n-1}) \cdot \mathbf{w}(t^{n-1}) \quad \textit{(temporal interface terms)} \\ &+ \sum_{f \in \mathscr{F}_i} \int_{f \times I^n} [\![\mathbf{n} \times \mathbf{H}]\!] \cdot \{\!\{\mathbf{v}\}\!\} - [\![\mathbf{n} \times \mathbf{E}]\!] \cdot \{\!\{\mathbf{w}\}\!\} \quad \textit{(spatial interface terms)} \\ &+ \sum_{f \in \mathscr{F}_b} \int_{f \times I^n} \mathbf{n} \times \mathbf{E} \cdot \mathbf{v} - \beta^E \, \mathbf{n} \times (\mathbf{n} \times \mathbf{H}) \cdot \mathbf{v} \quad \textit{(boundary terms)} \end{aligned}$$

and

$$\begin{aligned} R^n(\mathbf{E}, \mathbf{H}, \mathbf{v}, \mathbf{w}) = \\ &+ \sum_{K \in \Omega_h} \int_K \epsilon \mathbf{E}(t^{n-1}) \cdot \mathbf{v}(t^{n-1}) + \mu \mathbf{H}(t^{n-1}) \cdot \mathbf{w}(t^{n-1}) \quad \textit{(temporal interface terms)} \\ &+ \int_{\partial\Omega \times I^n} \mathbf{n} \times \mathbf{g}(\mathbf{r}, t) \cdot \mathbf{v}. \quad \textit{(boundary terms)} \end{aligned}$$

Note that this method is equivalent to Method I for $\mathscr{V}_n^E, \mathscr{V}_n^H = \mathbb{T}(Q)$. However, by application of the Trefftz functions the volume terms in Method I trivially vanish and we are left with a method purely defined on the space-time skeleton of the mesh. This property is of vital importance for numerical implementations as we will see in Section 5.4. In the following we discuss the properties of this method. As a first observation, one can see that Method II is consistent with Problem I. This follows directly from Theorem VI. More precisely the volume terms were shown to vanish for solutions $(\mathbf{E}, \mathbf{H})$. Since Method II has no volume terms, the proof is a trivial version of that of Theorem VI. Let us now turn to the energy consideration. In contrast to Method I were we only observed a semi-norm $|||\mathbf{v}, \mathbf{w}|||_{Q_h^n}$ (see Theo-

rem VII) for the energy we can show that the equivalent for the functions in $\mathbb{T}_p(Q_h^n)$ is actually a norm.

Theorem IX (Stability – DG Trefftz) (see Theorem 17 of [15])
For all piecewise Trefftz-polynomials $(\mathbf{v},\mathbf{w}) \in \mathbb{T}_p(Q_h^n)$ *there holds*

$$|||(\mathbf{v},\mathbf{w})|||_{Q_h^n} \geq \sum_{K\in\Omega_h} \frac{1}{C(p,K,I^n)} \Big(\epsilon\|\mathbf{v}\|^2_{K\times I^n} + \mu\|\mathbf{w}\|^2_{K\times I^n}\Big),$$

with constant $C(p,Q_h^n)$ *taken from Theorem IX.*

Proof. Consider $|||(\cdot,\cdot)|||_{Q_h^n}$ from Theorem VII and omit the spatial interface term $(2\beta^E\|n\times\mathbf{H}\|^2_{\partial\Omega_h})$. By applying the estimate of Theorem IX on every element, and summing over all elements one obtains the assumption. □

In addition the method is energy dissipative

Theorem X (Energy Balance – DG Trefftz) (see Theorem 18 of [15])
Discrete solutions $(\mathbf{E}_h^n,\mathbf{H}_h^n) \in \mathbb{T}_p(Q_h^n)$ *of Method I satisfy the discrete energy dissipation relation of Theorem* (VIII).

$$\frac{1}{2}\Big(\|\epsilon^{1/2}\mathbf{E}_h^n\|^2_\Omega + \|\mu^{1/2}\mathbf{H}_h^n\|^2_\Omega\Big)\Big|_{t^{n-1}}^{t^n} = -\int_{\partial\Omega_h\times I^n} \beta^E|\mathbf{n}\times\mathbf{H}_h^n|^2 + \mathbf{n}\times\mathbf{g}(\mathbf{r},t)\cdot\mathbf{H}_h^n$$
$$-\sum_{K\in\Omega_h}\left(\frac{\epsilon}{2}\|[\mathbf{E}_h^n(t^{n-1}) - \mathbf{E}_h^{n-1}(t^{n-1})]\|^2_K + \frac{\mu}{2}\|\mathbf{H}_h^n(t^{n-1}) - \mathbf{H}_h^{n-1}(t^{n-1})]\|^2_K\right).$$

Proof. By Theorem IX and Theorem VII, we obtain

$$A^n(\mathbf{w},\mathbf{v};\mathbf{w},\mathbf{v}) \geq |||(\mathbf{v},\mathbf{w})|||^2_{Q_h^n} \geq c\Big(\|\epsilon^{1/2}\mathbf{v}\|^2_{\Omega\times I^n} + \|\mu^{1/2}\mathbf{w}\|^2_{\Omega\times I^n}\Big)$$

for all $(\mathbf{v},\mathbf{w}) \in \mathbb{T}_p(Q_h^n)$ with positive constant $c = \min_{K\in\Omega_h} C(p,Q_h^n) > 0$. □

It follows that the method is stable. Note that the dissipation here is due to the spatial flux terms $\beta^E|\mathbf{n}\times\mathbf{H}_h^n|^2$ (as well as boundary functions). However, the amplitude of this damping can be decreased by increasing the approximation precision. As a final result we obtain that the method has unique solutions

Theorem XI (Uniqueness of solutions – DG Trefftz)
The system (5.11) *in Method II is uniquely solvable for* $n > 1$.

Proof. The assumption directly follows from Theorem XI, since A^n is coercive on $\mathbb{T}_p(Q_h^n)$ and therefore uniquely solvable due to the Lax-Milgram lemma. □

Thus our method is well-defined and embedded in the context of DG methods. From here on one could start a systematic error convergence analysis as is done in a similar context by [19, 56]. However, we do not pursue this endeavor in this work.

5.4 A Numerical Implementation

In the final part of this chapter we state a corresponding numerical scheme that is operating on a uniform hexahedral mesh as depicted in Fig. 5.1. Following the usual Galerkin procedure, both the basis and the test functions are defined in the same space, that is in our case in the local Trefftz space $\mathbb{T}(Q_{\mathbf{k}}^n)$. In contrast to the previous discussion where we directly considered a global scheme for convenience, we will here discuss a construction of the scheme that is constituted from local building blocks. Therefore, the spatial position of the cell with respect to its neighbors must be explicitly given. We identify a certain space-time cell $Q_{\mathbf{k}}^n = \Omega_{\mathbf{k}} \times I^n$ by its temporal index n and its spatial multi-index $\mathbf{k}$. In our numerical scheme we consider a mesh that is constant in time. In particular we do not consider adaptations of the mesh here for the sake of simplicity. Note that there is no constraint to use time-dependent hp-adaptation. We approximate the fields cell-wise in terms of local Trefftz basis functions as

$$\mathbf{F}_{\mathbf{k}}^n(r_{\mathbf{k}}, t^n) = \begin{pmatrix} \mathbf{E}_{\mathbf{k}}^n \\ \\ \mathbf{H}_{\mathbf{k}}^n \end{pmatrix} \approx \sum_p^{p_{\max}} f_{\mathbf{k}}^{p,n} \begin{pmatrix} \mathbf{u}_{\mathbf{k}}^{\mathbf{E},p} \\ \\ \mathbf{u}_{\mathbf{k}}^{\mathbf{H},p} \end{pmatrix}, \tag{5.12}$$

up to a maximum order $p_{\max}$. Note that all information in the time-step is now solely contained in the coefficient. As a result, the original variational principle Method II reduces to a matrix form containing an "*Advanced*" flux matrix $\mathbf{A}$, a "*Retarded*" flux matrix $\mathbf{R}$ as well as some boundary functions $\mathbf{G}$

$$\mathbf{A}\mathbf{f}^n = \mathbf{R}\mathbf{f}^{n-1} + \mathbf{G}, \tag{5.13}$$

with coefficient vectors $\mathbf{f}^n$ and $\mathbf{f}^{n-1}$. $\mathbf{A}$ contains block diagonal entries by the space and time fluxes, as well as off block diagonal entries by the space fluxes. In contrast

to that **R** only contains block diagonal entries due to the time fluxes. The explicit forms of **A**, **R** and **G** are given in Appendix C. Both matrices **A** and **R** are sparse matrices. **R** is symmetric whereas **A** contains anti-symmetric entries from the space fluxes and symmetric entries from the time fluxes.

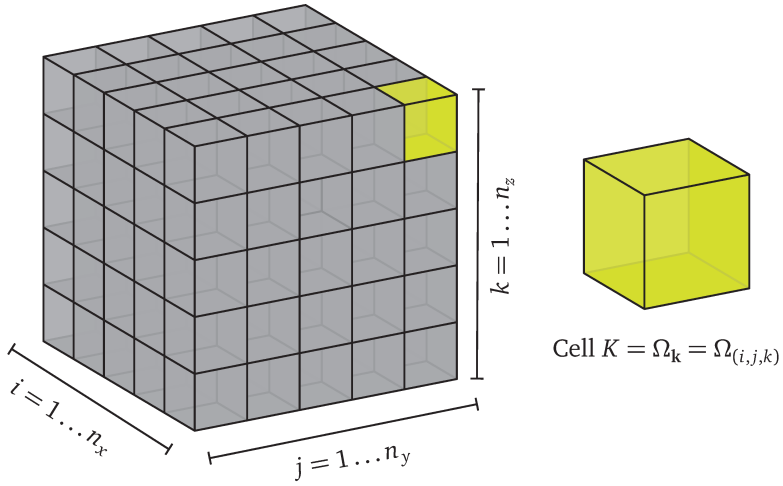

Figure 5.1.: Illustration of the hexahedral mesh applied in the numerical scheme. An example cell is identified by its spatial multiindex **k** consisting of three indices i,j and k denoting the number of cells in x,y and z direction.

At this point we would like to illustrate the stability of the method that follows from Theorem X with the help of the numerical implementation. In Fig. 5.2 we illustrate this property by plotting the eigenvalues of the update matrix[2] $\mathbf{U} = \mathbf{A}^{-1} \cdot \mathbf{R}$ for different orders $p = 0$ to 5. The plots directly illustrate that the scheme is energy-dissipative. In addition the energy dissipation decreases with increasing the order p. (This can not be directly obtained from Fig. 5.2 but has been checked.) The first observation can be directly obtained, since eigenvalues have an absolute value ≤ 1. Here, the eigenvalues that lie below the unit-circle correspond to damped modes. Eigenvalues that lying on the unit circle represent undamped modes. By increasing the order from $p = 0$ to $p = 5$ the number of eigenvalues on (and near) the unit circle increases absolutely and relatively. Note that we can not comment further on the nature of the damping at this point.

[2] The explicit calculation of the update matrix is only done for illustration here, but omitted in practice.

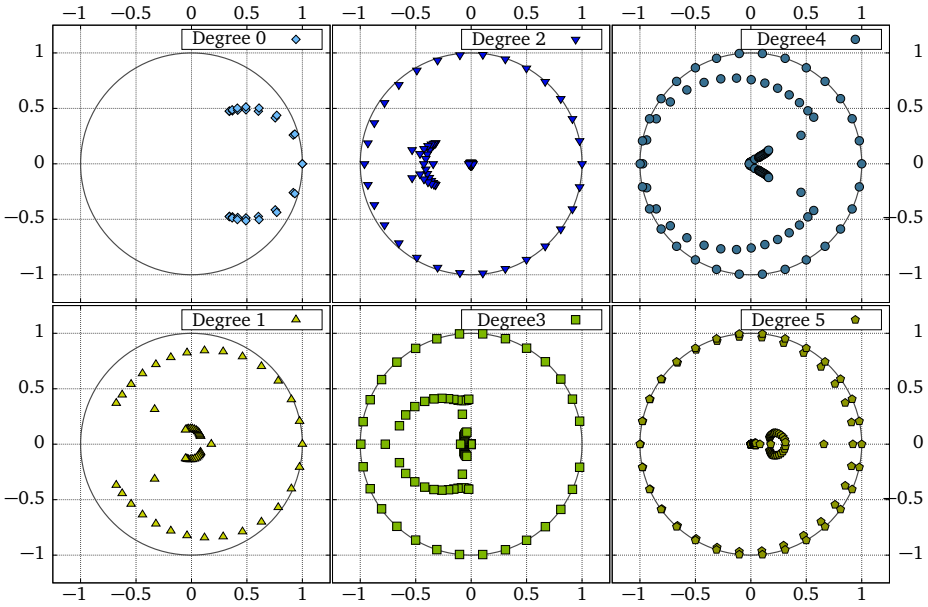

Figure 5.2.: Eigenvalues of update matrices for the one-dimensional discontinuous Galerkin Trefftz method in the complex plane for orders $p = 0, 1, 2, 3, 4, 5$. The gray solid line is the unit circle.

Chapter Resumé

In this chapter we have introduced our numerical method. To this end we have first surveyed three of the most commonly used methods namely FDTD, FIT, and FEM in Section 5.1. Starting from this we motivated the use of a discontinuous Galerkin framework for this work because of its high flexibility.

After this introduction we first indicated the derivation of the discontinuous Galerkin method in Section 5.2 and consequently introduced the complete discontinuous Galerkin method as Method I. The method uses an implicit time stepping scheme (see Theorem V) and is consistent with Problem I as has been shown in Theorem VI. In addition we asserted that the method is stable (see. Theorem VII) and made a statement on the behavior of the energy in Theorem VIII.

In Section 5.3 we introduced the discontinuous Galerkin Trefftz method as Method II, by restricting the test function spaces to that of the Trefftz spaces introduced in Sec-

tion 4. As a result we have obtained a (space-time) energy norm in Theorem IX instead of the seminorm in the previous method. The method was shown to be dissipative (see Theorem X). From coercivity and norm we obtained uniqueness of the solutions in Theorem XI. Therefore, the method is well-defined in the framework of discontinuous Galerkin methods.

In the last part of the chapter, i.e. Section 5.4, we have introduced our numerical scheme.

Part II.
Numerical Experiments

6 Physical Validation

Propagations of electromagnetic waves can be found in various applications such as the design of antennas [7, 67, 71], the analysis of phonic crystals [78, 91] and the design of particle accelerators [18] or other applications [11, 74, 92].

In this chapter we study the propagation of electromagnetic plane waves to numerically validate our method. Before we start with the actual experiments, we introduce the underlying scenarios in Section 6.1. Then we follow [48] and study propagations of plane waves through piecewise homogeneous and non-homogeneous materials in Section 6.2 and Section 6.3, respectively. In the final part of this chapter we report on our results of [15] and discuss various diffraction experiments.

6.1 Numerical Test Scenarios

According to Definition I (of Chapter 2) a plane wave propagates in a direction $\mathbf{d}$ with fields $\mathbf{E}$ and $\mathbf{H}$ orthogonal to $\mathbf{d}$. Depending on the direction of propagation $\mathbf{d}$ or, more specifically, the number of components of $\mathbf{d}$, one can consider the full three-dimensional scenario but also two-dimensional and one-dimensional ones. Let us elucidate these settings.

Two-Dimensional Setup: one possible scenario is the propagation of a wave in direction $\mathbf{d} = (d_x, d_y, 0)$, being a two-dimensional propagation in the $x-y$ plane. In this case, three field components are sufficient for a full description of the problem. For instance one can choose $\mathbf{E} = (0, 0, E_z)$ and $\mathbf{H} = (H_x, H_y, 0)$. Now we can write a reduced form of Problem I. In this case Maxwell's equations (2.8) read

$$\begin{pmatrix} \frac{\partial E_z}{\partial y} \\ -\frac{\partial E_z}{\partial x} \end{pmatrix} = -\mu \begin{pmatrix} \frac{\partial H_x}{\partial t} \\ \frac{\partial H_y}{\partial t} \end{pmatrix} \tag{6.1}$$

$$\text{and} \qquad \frac{\partial H_y}{\partial x} - \frac{\partial H_x}{\partial y} = \epsilon \frac{\partial E_z}{\partial t} \quad \text{on} \quad \Omega^{2\mathrm{d}} \times I.$$

For the fields to be divergence-free it sufficies to set $\nabla \cdot \mathbf{H}_0 = \nabla \cdot \mathbf{E}_0 = 0$. Scenarios of this kind can appear in various applications in which a symmetry in one direction

is present. Here, the considered spatial domain reads $\Omega^{2d} \subset \mathbb{R}^2$ over a time interval $I = (0, T)$. As a second possibility one can embed this two-dimensional domain into a three-dimensional one $\Omega = \Omega^{2d} \times R_z$. Along the symmetry direction R_z a repetition of the simulation or its 'collapse' at one instance $z_0 \in R$ is possible. Let us summarize this scenario

Problem II (Two Dimensional Scenario)
Solutions (H_x, H_y, E_z) *of time-dependent Maxwell's equations for linear, loss-free, non-dispersive, time-invariant, isotropic media*

$$\begin{aligned} \frac{\partial E_z}{\partial y} &= -\mu \frac{\partial H_x}{\partial t}, \\ \frac{\partial E_z}{\partial x} &= \mu \frac{\partial H_y}{\partial t}, \\ \frac{\partial H_y}{\partial x} - \frac{\partial H_x}{\partial y} &= \epsilon \frac{\partial E_z}{\partial t}. \end{aligned}$$

in a two dimensional domain Ω^{2d} *over a time I, subject to appropriate boundary conditions such as, PEC-like boundary conditions*

$$\alpha^E \begin{pmatrix} n_y \\ -n_x \end{pmatrix} E_z - \beta^E \left(\begin{pmatrix} H_x \\ H_y \end{pmatrix} - n_x n_y \begin{pmatrix} H_y \\ H_x \end{pmatrix} \right) = \begin{pmatrix} n_y \\ -n_x \end{pmatrix} g(x, y, t)$$

on $\partial\Omega^{2d} \times t$ *with normals* n_x *and* n_y *as well as initial conditions*

$$H_x(0) = H_{x,0}, \quad H_y(0) = H_{y,0} \quad \text{, and} \quad E_z(0) = E_{z,0} \qquad \text{on} \quad \Omega^{2d} \times t_0,$$

constrained by

$$\frac{\partial H_x}{\partial x} = \frac{\partial H_y}{\partial y} = \frac{\partial E_z}{\partial z} = 0,$$

describe the propagation of electromagnetic waves in the absence of charges and currents. Note that there is an equivalent version for PMC and PBC.

One-Dimensional Setup: An even simpler scenario is that of a propagating one-dimensional wave that can be for instance in direction $\mathbf{d} = (d_x, 0, 0)$. Here, only

two field components, e.g. $\mathbf{E} = (0, E_y, 0)$ and $\mathbf{H} = (0, 0, H_z)$ are sufficient. The reduced form of Problem I reads

$$\frac{\partial E_y}{\partial x} = -\mu \frac{\partial H_z}{\partial t} \qquad \text{and} \qquad -\frac{\partial H_z}{\partial x} = \epsilon \frac{\partial E_y}{\partial t} \quad \text{on} \quad \Omega^{1\mathrm{d}} \times I. \tag{6.2}$$

Scenarios of this kind could appear in applications in which symmetries in two coordinates are present. In accordance with the previously discussed two-dimensional scenario we write $\Omega^{1\mathrm{d}} \subset \mathbb{R}^1$ and $I = (0, T)$ or, as an embedded version $\Omega = \Omega^{1\mathrm{d}} \times R_y \times R_z$ with R_y being an additional symmetry direction.

Problem III (One Dimensional Scenario)
Solutions $E = E_y$, $H = H_z$ of time-dependent Maxwell's equations for linear, loss-free, non-dispersive, time-invariant, isotropic media

$$\frac{\partial E}{\partial x} = -\mu \frac{\partial H}{\partial t},$$
$$-\frac{\partial H}{\partial x} = \epsilon \frac{\partial E}{\partial t},$$

in a one dimensional domain $\Omega^{1\mathrm{d}}$ over a time I, subject to appropriate boundary conditions such as, PEC-like boundary conditions

$$\alpha^E n E - \beta^E H = n\, g\,(x, t) \qquad \text{on} \quad \partial\Omega^{1\mathrm{d}} \times t$$

as well as initial conditions

$$E(0) = E_0 \qquad \text{and} \qquad H(0) = H_0 \qquad \text{on} \quad \Omega^{1\mathrm{d}} \times t_0,$$

constrained by

$$\frac{\partial H_x}{\partial x} = \frac{\partial H_y}{\partial y} = \frac{\partial E_z}{\partial z} = 0,$$

describe the propagation of electromagnetic waves in the absence of charges and currents. Note that there is an equivalent version for PMC and PBC.

We specify the applied boundary conditions the context of the specific considered problem later on. However, let us state the analytic solution of two considered problems as well as the initial values.

Plane Waves with a Gaussian Form: Electromagnetic waves that have a Gaussian form are described by

$$\Psi^{\text{Gauss}}(\mathbf{r}, t) = \exp\left(-(\mathbf{d}\cdot\mathbf{r} - vt - \mathbf{r}_0)^2/\delta\right). \tag{6.3}$$

Here, δ is the width of the wave and $\mathbf{r}_0$ its offset. In addition one can control the direction of propagation by setting $\mathbf{d}$. The Gaussian form of the wave has a very high regularity. In this case the approximation error should decrease exponentially when increasing the order. For this to happen, the considered domain of interest should be sufficiently large. In particularly the boundary requirements should be approximately satisfied.

Plane Waves with a Box Form: Electromagnetic waves with a box form are described by

$$\Psi^{\text{Box}}(\mathbf{r}, t) = \Theta(\mathbf{d}\cdot(\mathbf{r} - \mathbf{r}_0) - vt) - \Theta(\mathbf{d}\cdot(\mathbf{r} - \mathbf{r}_0 - \delta) - vt), \tag{6.4}$$

where δ is the with of the box-wave and $\mathbf{r}_0$ its offset. Here, $\Theta(x - x_0)$ is the common Heaviside step function which has a straight jump from 0 to 1 at x_0. For a numerical approximation this waveform is an extreme case due to the missing regularities.

6.2 Propagation of a Wave through Piecewise Homogeneous Media

In our first test case, we consider Problem III with a plane wave of Gaussian form (6.3). The wave is traveling in a centered space-time domain $Q^{1d} = \Omega^{1d} \times I = (-20, 20) \times (0, 60)$ that has pec-boundaries (i.e. $\alpha^E = 1$, $\beta^E = 0$, and $g = 0$) and is filled with a material with $\epsilon = \mu = 1$ and $v = 1$. At t_0 we set $E_0 = -H_0 = \Psi^{\text{Gauss}}(\mathbf{r}, 0)$ with $\delta = 3$ and $x_0 = 0$ corresponding to a wave that is traveling leftwards. The results correspond to those of Sections 4.2 and 4.3 of [48]. Fig. 6.1 shows the electric field of the simulated plane wave, that is propagating as expected: first the wave is heading leftwards at a space-time angle of 45 degrees, then at time $t = 20$ the wave hits the (left) PEC boundary and is reflected back rightwards.

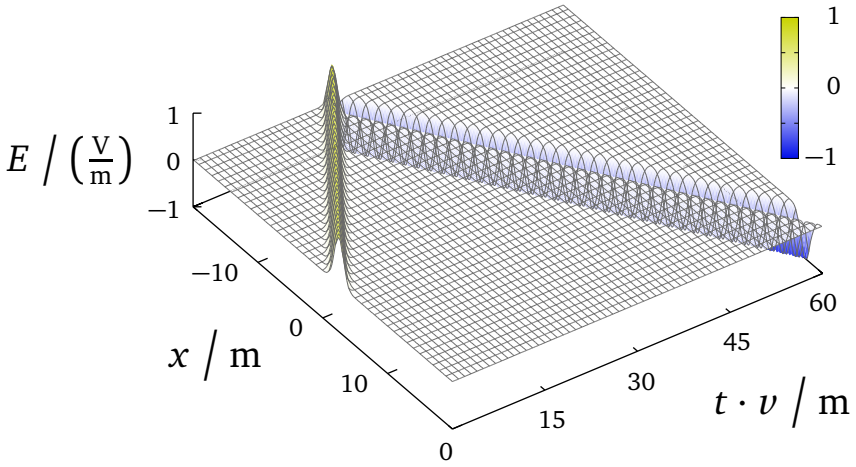

Figure 6.1.: Electric field of a plane wave with a Gaussian form propagating in a vacuum for Problem III. The solution in the whole space-time domain of interest $Q^{1d} = (-20, 20) \times (0, 60)$ is displayed. The wave with $\delta = 3$ starts at $x_0 = 0$, travels to the top edge, gets reflected and travels back.

In the second test case we again consider Problem III, but for a slightly more complicated setting: a space-time domain consisting of two sub-domains $Q_1^{1d} = (-10, 20) \times (0, 60)$ and $Q_2^{1d} = (-20, -10) \times (0, 60)$. In Q_1^{1d} the material is $\epsilon_1 = \mu_1 = 1$ whereas in Q_2^{1d} it is $\epsilon_2 = 4$ and $\mu_2 = 1$. Therefore, the resulting speed of light is $v_2 = 1/2$. We initialize a wave $E_0 = -H_0 = \Psi^{\text{Gauss}}(\mathbf{r}, 0)$ that is heading leftwards with width $\delta = 3$ and an offset $x_0 = 10$ to the right.

Fig. 6.2 displays the electric field component $\mathbf{E}_y$ of the simulated wave.

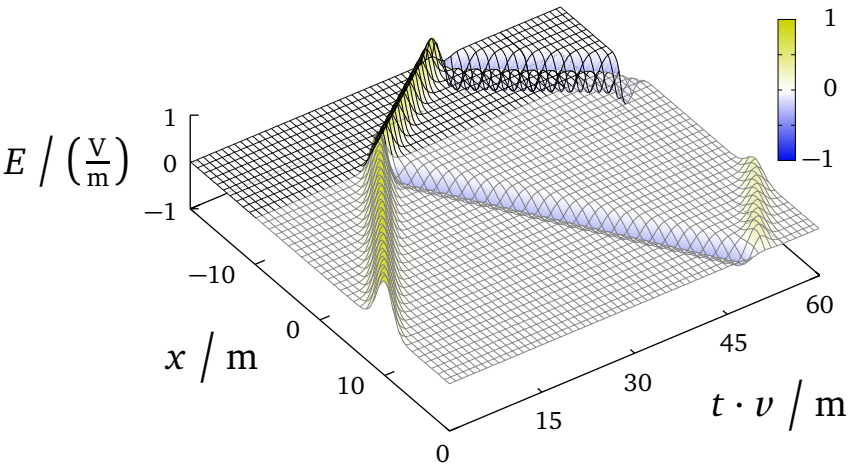

Figure 6.2.: Electric field of a one-dimensional wave with a Gaussian form propagating in a medium with a medium interface at $x_0 = -10$. The space-time domain of interest consists of two sub-domains $Q^{1d} = (-20, 20) \times (0, 60)$ $Q_1^{1d} = (-10, 20) \times (0, 60)$ and $Q_2^{1d} = (-20, -10) \times (0, 60)$ with material parameters $\epsilon_1 = \mu_1 = 1$, $\epsilon_2 = 4$, and $\mu_1 = 1$. The wave with $\delta = 3$ starts at $x_0 = 10$ and travels to the interface at $x = 10$. Here, one part of the wave is transmitted and travels trough the domain Ω_2 whereas another part is reflected back to domain Ω_1. Afterwards only reflections at the global boundaries occure.

At $t = 20$ the wave has reached the material interface. Here, a part of the impinging wave is transmitted, whereas the rest is reflected. The amplitudes of the reflected and transmitted waves can be calculated analytically are given by the reflection and transmission coefficients

$$R = \frac{Z_1 - Z_2}{Z_1 + Z_2}, \quad \text{and} \quad T = \frac{2Z_2}{Z_1 + Z_2}. \tag{6.5}$$

We observe that the numerical value of the amplitude of the reflected wave is very close to the expected value $R = 1/3$. The same is true for the transmitted wave with $T = 2/3$. We see that the transmitted wave is traveling at half velocity $v_2 = 1/2$ in the medium. This corresponds to a space-time angle of 22.5 degrees. Therefore, we obtain the expected physical behavior also in this scenario.

6.3 Propagation of a Wave through a Inhomogeneous Medium

Let us now discuss a special feature of the Trefftz method. In some cases it is possible to derive special Trefftz basis functions tailored to a specific problem. To demonstrate this, we derive Trefftz functions for partially filled cells (see.Section 4.4 of [48]).

To this end, we consider a centered reference space-time cell $(-\Delta_x/2, \Delta_x/2) \times(-\Delta_t/2, \Delta_t/2)$ with a material interface at some point $x = x_0$ inside the cell. The material parameters, medium velocities and intrinsic impedances on the left and the right side of the interface are $\epsilon_{1,2}$, $\mu_{1,2}$, $v_{1,2}$ and $Z_{1,2}$, respectively. The desired Trefftz function must describe a combination of an incident wave ('inc') and a reflected ('ref') / transmitted ('trs') wave at the interface. The fields in the considered cell are

$$\begin{aligned} E_{\text{inc}} &= \varphi_{\text{inc}}(x - v_1 t), & H_{\text{inc}} &= \frac{1}{Z_1}\varphi_{\text{inc}}(x - v_1 t); \\ E_{\text{ref}} &= \varphi_{\text{ref}}(-x - v_1 t), & H_{\text{ref}} &= \frac{1}{Z_1}\varphi_{\text{ref}}(-x - v_1 t); \\ E_{\text{trs}} &= \varphi_{\text{trs}}(x - v_2 t), & H_{\text{trs}} &= \frac{1}{Z_2}\varphi_{\text{trs}}(x - v_2 t). \end{aligned}$$

The tangential components of the fields inside the considered cell must be continuous. This is particularly true at the interface

$$\varphi_{\text{inc}}(x_0 - v_1 t) - \varphi_{\text{ref}}(-x_0 - v_1 t) = \varphi_{\text{trs}}(x_0 - v_2 t),$$

$$\frac{1}{Z_1}(\varphi_{\text{inc}}(x_0 - v_1 t) + \varphi_{\text{ref}}(-x_0 - v_1 t)) = \frac{1}{Z_2}\varphi_{\text{trs}}(x_0 - v_2 t).$$

By using the definition of the transmission and reflection coefficients (6.5) we can deduce

$$\varphi_{\text{ref}}(-x_0 - v_1 t) = R\varphi_{\text{inc}}(x_0 - v_1 t),$$

$$\varphi_{\text{trs}}(x_0 - v_2 t) = T\varphi_{\text{inc}}(x_0 - v_1 t).$$

In the next step we look for the wave forms at arbitrary positions x rather than just at x_0.

To this end we rewrite reflected wave forms

$$\varphi_{\text{ref}}(-x-v_1t) = \varphi_{\text{ref}}(-x_0-v_1t-(x-x_0)) \equiv \varphi_{\text{ref}}\left(-x_0-v_1t'\right)$$

$$= R\varphi_{\text{inc}}\left(x_0-v_1t'\right) = R\varphi_{\text{inc}}(2x_0-x-v_1t),$$

as well as the transmitted wave forms

$$\varphi_{\text{trs}}(x-v_2t) = \varphi_{\text{trs}}(x_0-v_2t+(x-x_0)) \equiv \varphi_{\text{trs}}\left(x_0-v_2t''\right)$$

$$= T\varphi_{\text{inc}}\left(x_0-v_1t''\right) = T\varphi_{\text{inc}}\left(\left(1-\frac{v_1}{v_2}\right)x_0+\frac{v_1}{v_2}x-v_1t\right),$$

in terms of the incident wave. The respective time variables of the reflected and transmitted wave forms contain an advance or delay

$$t' = t+\frac{(x-x_0)}{v_1} \qquad \text{and} \qquad t'' = t-\frac{(x-x_0)}{v_2},$$

as we expect from a common Lorentz transformation. More precisely we transform the fields from their moving reference frames to a static reference frame that is given by the cell.

Let us test this new basis for Problem III. We consider with the following scenario: A space-time domain consisting of two sub-domains $Q_1^{1\text{d}} = (-0.25,5)\times(0,20)$ and $Q_2^{1\text{d}} = (-5,-0.25)\times(0,20)$ subject to pec-boundary conditions with materials as given in the previous scenario (i.e. $\epsilon_1 = \mu_1 = \mu_2 = 1$ and $\epsilon_2 = 4$). Note that the medium interface now lies inside a cell. Consequently, we need three types of Trefftz basis functions: One for the vacuum, another for the medium, and a last one for the mixed cell. We initialize $E_0 = -H_0 = \Psi^{\text{Gauss}}(\mathbf{r},0)$ (c.f. (6.3)) with $\delta = 2$ and $x_0 = -3$.

The behavior of the propagation is similar to the previous case; after the incoming wave strikes the medium interface it splits into a reflected part and a transmitted part. In particular we obtain the same reflection and transmission coefficients close to $R = 1/3$ and $T = 2/3$. This means that we obtain the same physical behavior with the special Trefftz basis functions.

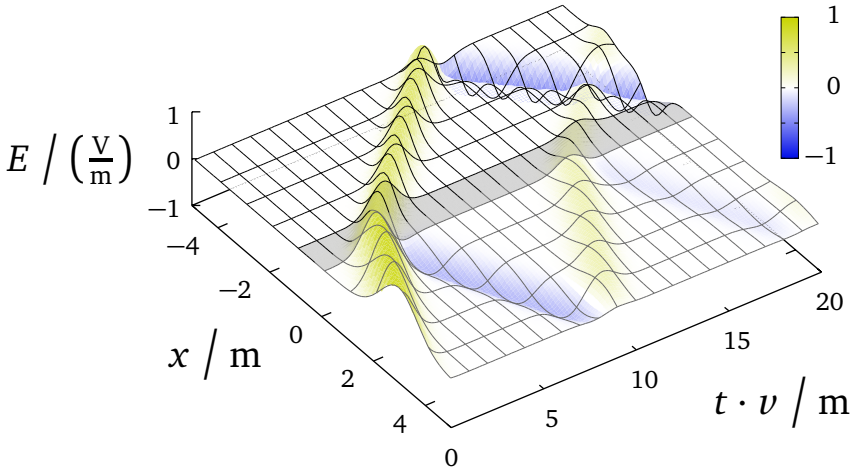

Figure 6.3.: Electric field of a one-dimensional wave with a Gaussian form with a medium interface at $x_0 = -0.25$; Note that the material interface lies inside an element. The solution in the whole space-time domain of interest $(x,t) \in (-5,5) \times (0,20)$ is displayed. The wave with $\delta = 2$ starts at $x_0 = -3$ and travels to the interface at $x = -0.25$. Here, one part of the wave is transmitted and travels trough the domain Ω_2 whereas another part is reflected back to domain Ω_1. Afterwards only reflections at the global boundaries occur.

6.4 Diffraction Experiments

Let us now consider two scenarios that are more involved: a single slit and a double slit. In both cases we consider Problem II with a spatial domain $\Omega^{2d} = (-5,5) \times (-20,20)$ that has PMC boundary conditions on the lateral boundaries (i.e. at $-5 \times (-20,20)$ and $5 \times (-20,20)$) and transparent boundary conditions[1] elsewhere (i.e. at $(-5,5) \times -20$ and $(-5,5) \times 20$). In both scenarios we initialize waves with box form as introduced in (6.4).

Single Slit Experiment

In the first scenario we place an infinitely thin PEC wall in the middle of the considered domain (i.e. at $x = 0$). This PEC wall has a small opening in its center (i.e. from $y = -1$ to $y = 1$), c.f. Section 6.4 of [15]. We initialize $H_y = E_z = \Psi^{\text{Box}}(\mathbf{r}, 0)$ and $H_x = 0$ with $\delta = 2$ and $\mathbf{r}_0 = (-4,0,0)^T$ over a time $T = 10$. In Fig. 6.4 we depict the evolution the wave through this slit.

[1] For further specifications see Chapter 8.

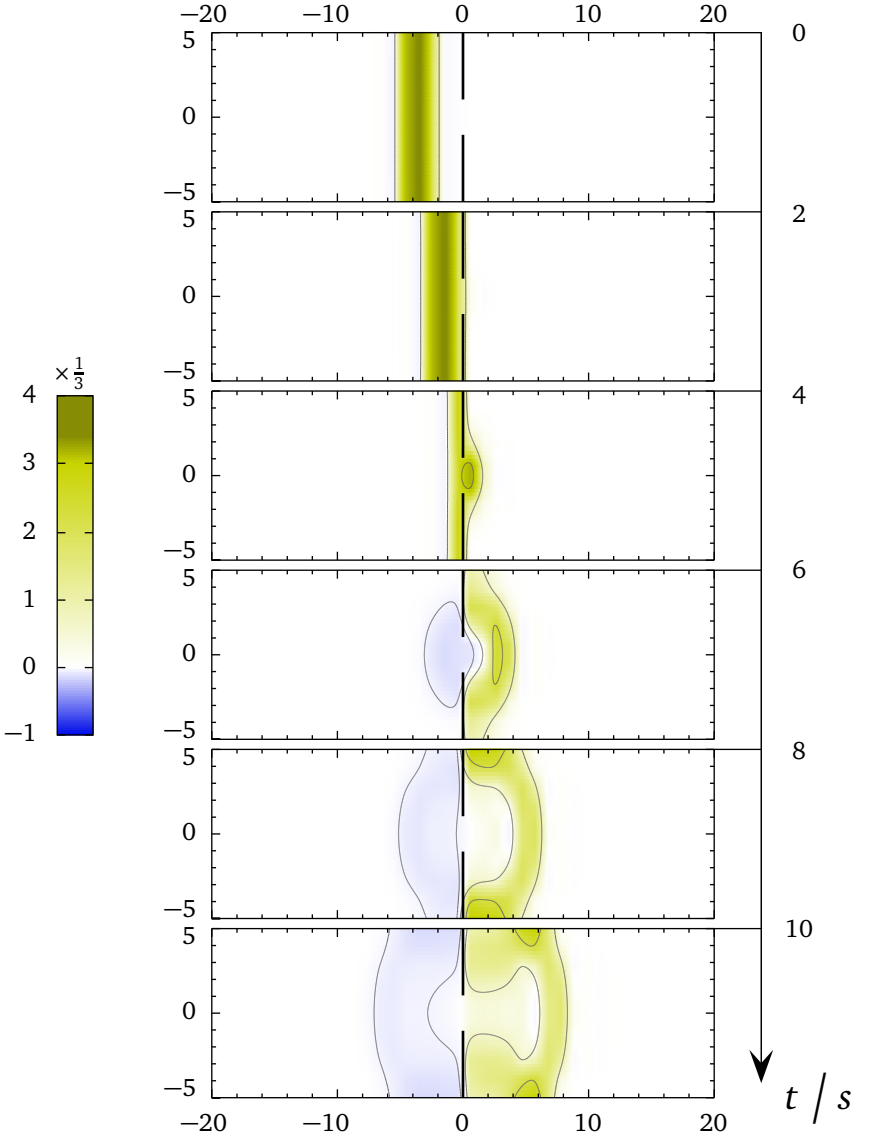

Figure 6.4.: Simulated electric field density E_z of a plane reflected at a PEC wall at $x = 0$. Most of the wave is reflected at the wall with change of sign of the electric field. The part propagating through the slit generates an almost cylindrical wave emanating from the center of the slit.

The simulation results show the expected physical behavior. At time-step $t = 4$ the wave strikes the wall. In the subsequent time-steps we obtain that the biggest part of the wave is reflected from the wall (blue portion) whereas a small portion propagates through the slit (green portion). In particular the diffraction at the corners of the slit is reproduced by the simulation. As a result waves of cylindrical shape begin to form on both sides of the slit.

Double Slit Experiment

In the second scenario, we insert a material block into the center of the considered domain. The block has a width of four cells, a height of ten cells and two small tunnels at $y = (-3, -2)$ and $y = (2, 3)$. The material in the block has relative permittivity $\epsilon = 4$ and $\mu = 1$ whereas the rest of the domain is filled with vacuum $\epsilon = \mu = 1$. The scenario corresponds to a double slit made of a material similar to concrete. We initialize $H_y = E_z = \Psi^{\text{Box}}(\mathbf{r}, 0)$ and $H_x = 0$ with $\delta = 4$ and $\mathbf{r}_0 = (-8, 0, 0)^T$ over $T = 20$, corresponding to a propagating wave. We show the snapshots of the wave evolution Fig. 6.5. At $t = 4$, the wave front impinges on the material; a portion of the wave is reflected at the material whereas a second part is reflected. We roughly obtain the correct reflection and transmission amplitudes of $R = 1/3$ and $T = 2/3$, respectively. At the subsequent time steps we obtain a propagation of the wave portion in the material at a lower velocity. In particular the wave portions in the slits propagate faster as can be deducted from the wavefronts at $t = 8$. In the remaining time-steps we observe secondary reflections and transmission at the material and the formation of a diffraction pattern that reflects our physical expectations.

Chapter Resumé

In this chapter we demonstrated that the solutions of our code have the correct physical behaviour. In Section 6.2 we first simulated the simple scenario of the propagation of a one-dimensional plane wave through a vacuum. Subsequently, we extended the simulation to the propagation of such a wave through a domain made of two piecewise homogeneous materials with an interface between two cells.

In Section 6.3 we then introduced special Trefftz basis functions for non-homogeneous materials and also verified the right physical behavior with a numerical experiment. These basis functions have been introduced as a special Trefftz feature in [48].

In the last Section 6.4 we discussed numerical single slit as well as double slit diffraction experiments. The outcome corresponds to the physical expectations.

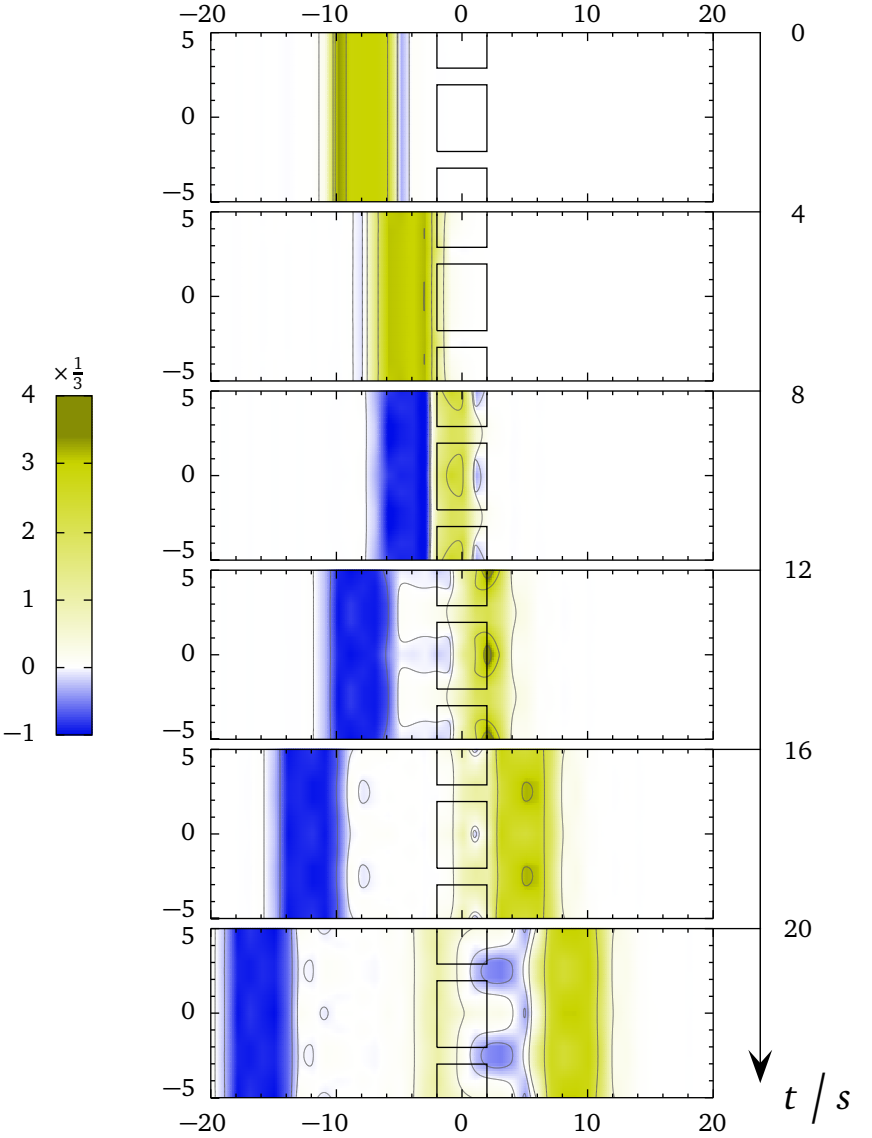

Figure 6.5.: Electric field density E_z of a plane wave propagating through a dielectric double slit with relative permittivity $\epsilon = 4$. In the free area the material parameters are set to $\epsilon = \mu = 1$. The wave is partially reflected at the boundaries of the material and propagates only with lower velocity within the inclusions.

7 Numerical Convergence Study

In [47], Moiola and Perugia have conducted an *a-priori* error analysis for the $(1+1)$-dimensional version of the DGT method. For higher dimensional versions of the method there exists no error analysis, so far. To nevertheless get an insight into the behaviour of the error we perform several numerical experiments.

In Section 7.1 we investigate the dispersion and dissipation behavior of the method. In Section 7.2 we carry out the required convergence studies and compare the Trefftz Method method to other schemes in Section 7.3.

7.1 Dispersion and Dissipation Errors

Let us consider an electromagnetic pulse that can be written as a superposition of plane waves with different frequencies ω_i. If such an electromagnetic pulse is propagating through a dispersive medium, its constituting plane waves propagate with different velocities v. Therefore, the velocities are frequency dependent $v(\omega)$. This effect is commonly known as dispersion. In addition to that, certain media can also exhibit damping, which can also be frequency dependent. In numerical simulations there exist discrete analoga which are called "*numerical dispersion*" and "*numerical dissipation*". These effects are parasitic and difficult to quantify in general. There are different ways to analyze the dispersion of a method such as the Neumann-Bloch analysis and various other Fourier analysis methods. The latter, for instance, is carried out by Van der Vegt in [83], where the eigenvalues of the system update matrix are used to extract the numerical frequencies ω_h. We use a more *experimental* approach to extract the ω_h.

In this section we investigate the dispersion and dissipation behavior of our method. To this end we study two different scenarios: an oscillating sinusoidal wave and a propagating wave with a box form. With these scenarios we numerically determine a dispersion relation of the Trefftz method.

Dispersion Relations

Dispersion relations provide one way to quantitatively investigate the numerical dispersion of a method. We simulate these dispersion relations by means of a sinusoidal wave

$$\Psi^{\text{Sinus}}(x,t) = \sin\left(k\frac{2\pi x}{L}\right)\cos(\omega t)\,. \tag{7.1}$$

Here, k is the wave-number of the oscillation, ω the frequency and L the length of the domain. In the following discussion we consider Problem III and restrict $\Omega^{1d} = (0, L)$ to $L = 20$ with $I = (0, 100)$. On the spatial boundaries we enforce PEC boundary conditions. With a sinusoidal initialization $E_0 = \Psi^{\text{Sinus}}(x, 0)$ and $H_0 = 0$, we can systematically study the numerical dispersion in our method by investigating initialization with different wave-numbers k. To this end we initialize a sinusoidal wave with a known wave-number k and let it propagate for a certain time. In Fig. 7.1 we exemplarily depict the temporal behavior of such an initialization. More precisely, of an simulation with $p = 1$ and $k = 5$ over 100 time-steps at one fixed point, i.e. $x = 2$ is plotted. Note that we have deliberately choosen an example with an (relatively) high damping factor here for demonstration purposes.

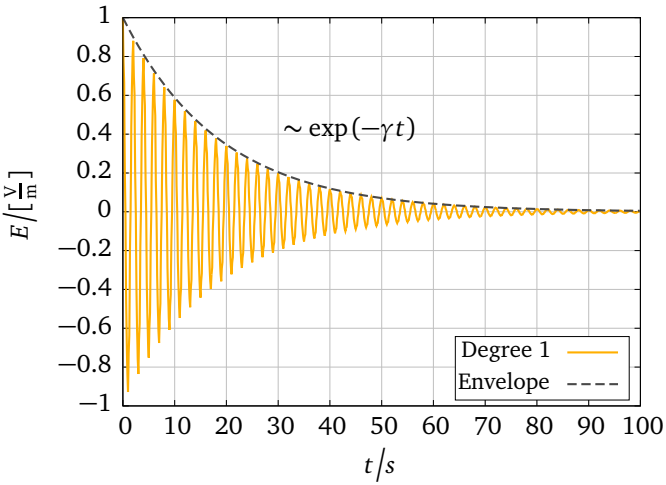

Figure 7.1.: Amplitude of the electric Field $E = E_x$ of a sinusoidal initialization (7.1) with $k = 5$ at a fixed point in space, i.e. $x = 2$, as a function of time. The order of the approximation is $p = 1$. The envelope decays exponentially $\sim \exp(-\gamma t)$, with γ being the damping factor.

From Fig. 7.1 one can obtain two things: the sinusoidal wave is oscillating at a frequency ω_h in time and the envelope of the oscillation is damped in time. By applying a Fourier Transformation with respect to time, we can extract the numerical frequency ω_h. The corresponding velocity then reads

$$v(\omega_h) = \frac{\omega_h}{k}. \tag{7.2}$$

The damping describes the decay of the amplitude envelope of the oscillation and can be described by

$$f(t) = \exp(-\gamma t), \tag{7.3}$$

with γ being the damping coefficient. γ can be obtained by fitting $f(t)$ to the envelope of the considered evolution. Due to the nature of our initialization that has only one wave-number per run, we can directly obtain the function $\omega(k)$ as shown in Fig. 7.2. Here, we plot the dependence of ω_h as a function of k for different approximation orders, i.e. one (orange upper triangles), two (green lower triangles) and three (blue boxes), independent of the discretization. For all simulations we obtain that the frequency ω_h depends linearly on k resulting in a (nearly) constant ratio $\omega_h(k)/k$ and therefore a (nearly) constant velocity for all modes. However, this velocity differs slightly from the expected speed of light in the medium. Therefore, in our numerical scheme modes propagate with a slightly wrong velocity than than the physically expected one. This effect is only minimal as can be seen from the plot. For the order one simulation the velocity $v_1 = 0.9938$ is slightly to low, whereas for the order two and three simulations the velocities $v_2 = 1.0007$ and $v_3 = 1.00005$ are slightly to high. The overall indication is that the velocity error decreases with increasing order and that there is (almost) no numerical dispersion present.

In the second part of this investigation we study the dependence of the damping factor $\gamma(k)$ as a function of k for orders one (orange line), two (green line) and three (blue line). The results are shown in Fig. 7.3 where the plot is in double logarithmic scale. Here, the damping factor is increasing linearly with k for a fixed order. This results in order dependent damping rates that decrease with increasing order. Since the damping is due to the numerical dissipation of the method, the findings of this plot have two implications: with increasing order the numerical dissipation decreases, and higher k modes are damped stronger than lower ones.

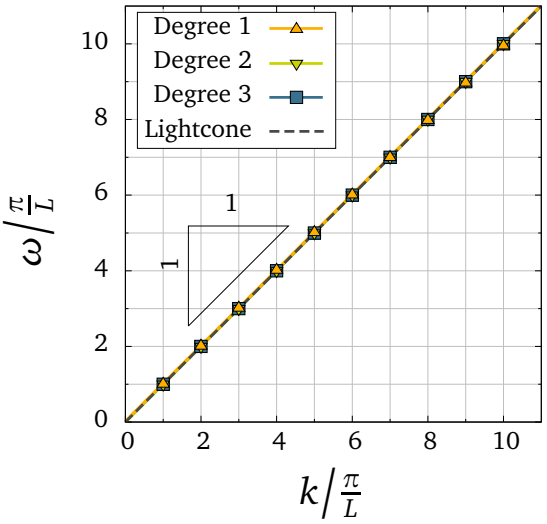

Figure 7.2.: Dispersion Relations of three sinusoidal initializations (7.1) with orders $p = 1, 2$ and 3. Both the wave-number k and the frequency ω are taken with respect to the grid. The light-cone (gray dashed line) is added as a reference.

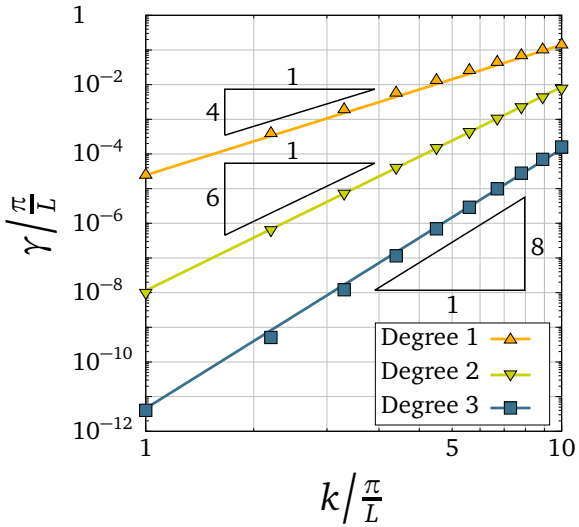

Figure 7.3.: Damping factors for a sinusoidal initialization (7.1) with orders $p = 1, 2$ and 3 obtained as in Fig. 7.1. Both the wave-number k and the damping factor γ are taken with respect to the grid.

Dispersion Behavior of a Heaviside Signal

In the second scenario we investigate the dispersion and dissipation in the propagation of a Heaviside shaped signal (see (6.4)). To this end we consider Problem II with $\Omega^{2d} = (0,3) \times (-10,10)$ over a time $T = 2000$. On the lateral boundaries (i.e. at $0 \times (-10,10)$ and $3 \times (-10,10)$) we apply PMC boundary conditions and PBC at the horizontal boundaries (i.e. at $(0,3) \times -10$ and $(0,3) \times 10$). We initialize $E_{x,0} = H_{y,0} = \Psi^{\text{Box}}(\mathbf{r},0)$ and $H_{z,0} = 0$ with $\delta = 5$ and $\mathbf{r}_0 = (-5,0,0)^T$. With this constellation we can study the long term behavior of our method: because of the PBC, the domain mimics an infinitely long expanded domain in which the wave is propagating. For correct propagation velocities the signal should re-appear at the same point in space after each period (i.e. after 20 time-steps).

Snapshots of the electric field over the first period are depicted in Fig. 7.4. Here, we have used polynomials of degree $p = 3$ and no further h-refinement. At $t = 0$ one obtains overshoots which are due to the Gibbs phenomenon[1] and almost completely vanish after the first period.

We display the long term behavior in Fig. 7.5. Here, we show the propagation after $0, 1, 10$ and 100 periods for orders one (orange line), two (green line) and three (blue line). To get an insight in the dissipation of the various modes we display the time domain picture as well as the (normalized) modulus of the Fourier transformed signals. At $t = 0$ overshoots at the edges of the box due to the Gibbs phenomenon are clearly visible. These are caused by oscillation modes corresponding to higher wave-numbers. Corresponding to Fig. 7.3 these modes are damped stronger than lower k modes and disappear after a short time. After one period the signals approximately reach their initial positions. Until now, we do not obtain an indication for wrong propagation velocities. In the Fourier plot that contains the corresponding k spectrum one already obtains a damping of the higher modes which is particularly visible in the first order approximation. In addition the signals broaden slightly. After ten periods we obtain a significant offset of the order $p = 1$ signal to the right while whereas the $p \geq 2$ signals approximately reach their initial positions. After one hundred periods the offset of the order one signal increases. For the higher order signals we observe a minimal tilts to the right. The visible offsets of the $p = 1$ simulations are due to a combination of two effects: the slightly wrong propagation velocities that were mentioned in the previous example and the fact that the Gibbs phenomenon is not symmetric at the front and read of the wave. More precisely, the shear wave (in front) has a higher depth. The fre-

[1] The Gibbs phenomenon is connected to the problem of approximating a discontinuous jump in terms of a series of continuous functions. At the location of the jump, the approximated solution oscillates.

quency dependent damping results in an immanent broadening of this shear wave and additionally pushes the overall wave forward.

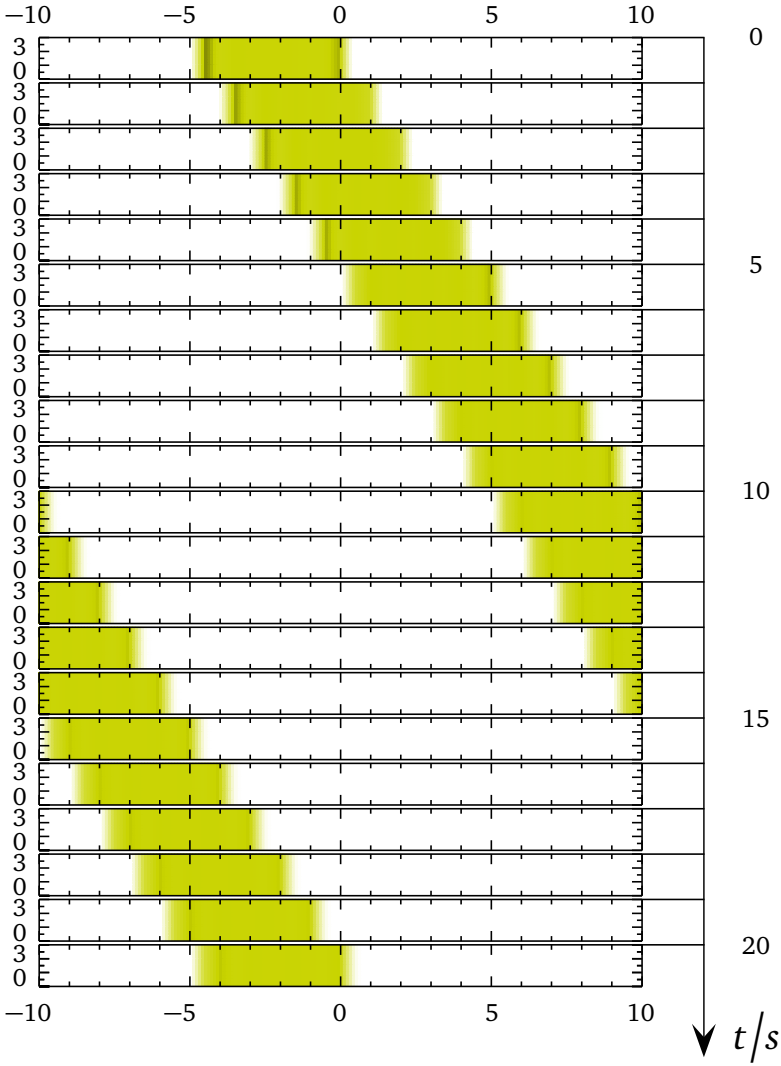

Figure 7.4.: Snapshots of the electric field amplitude E_z of a plane wave propagating from left to right through a homogeneous domain, simulated with order $p = 3$ on a mesh with $(0, 3) \times (-10, 10)$ elements and periodic boundary conditions.

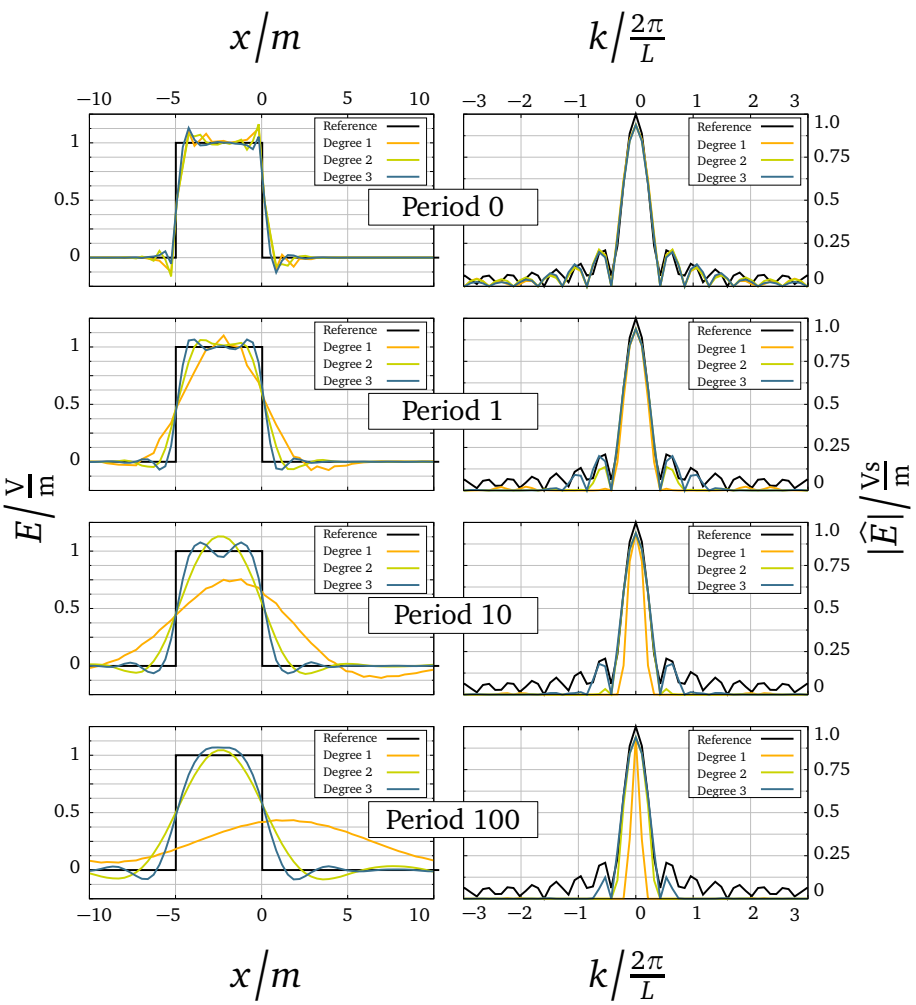

Figure 7.5.: Simulated electric field density $E = E_z$ corresponding to (6.4). Left: field amplitude $E_z(x,t)$ as a function of space. Right: normalized Fourier spectrum $\widehat{E}_z(k,t)$ as a function of the wave-number. The results for approximation orders $p = 1,2,3$ are respectively depicted in orange, green, and blue. The exact solution (6.4) is displayed in black. The plots are given at $t = 0, 20, 200, 2000$ corresponding to 0, 1, 10, and 100 periods.

7.2 Convergence Study

We now turn to a numerical study of the convergence of the DGT method. More precisely, we investigate the error convergence under p-enrichment, h-refinement, and d-enrichment. We use two different numerical setups, for which an analytic solutions exists; namely the propagation of a plane wave and the oscillation of a wave in a cavity. For this investigation we consider the relative error computed in the L_2-norm over the whole space-time domain Q

$$\epsilon_Q = \frac{\sqrt{\sum_{I^n \in I} \sum_{K \in \Omega_h} \int_K \int_{I^n} \left((\mathbf{E} - \mathbf{E}_h)^2 + (\mathbf{H} - \mathbf{H}_h)^2 \right) dt dV}}{\sqrt{\sum_{I^n \in I} \sum_{K \in \Omega_h} \int_K \int_{I^n} (\mathbf{E}^2 + \mathbf{H}^2) \, dt dV}}. \tag{7.4}$$

Propagation of a Plane Wave: The first example we consider Problem III in a domain $\Omega = (-20, 20)$ bounded by PEC boundary conditions over $I = 60$ time-steps. We initialize $E_0 = -H_0 = \Psi^{\text{Gauss}}(\mathbf{r}, 0)$ which corresponds to a plane wave that has a Gaussian shape (see (6.3)) with $\delta = 3$ and $\mathbf{r}_0 = -10$ and is propagating in negative direction (see Fig. 6.1 for similar illustration). In Fig. 7.6 we depict the error ϵ_Q for varying polynomial degrees p in a semi-logarithmic plot. From the occurring straight line we can deduce spectral convergence in the whole space-time domain of interest Q. To compare our method with a more conventional one we have simulated the same scenario with a method that uses a DG discretization in space while applying a Leapfrog time-stepping scheme. One obtains that the error of this method does not show spectral convergence which is due to the second-order accurate Leapfrog time integrator.

Let us now study the error of our method under h-refinement. Here, we separately study the error under refinement of the spatial cell size h_r and the temporal cell size h_t. In Fig. 7.7 (left side) we show the the error when we successively split the spatial cell size h_r in halves while keeping the temporal cell size at a sufficiently small fixed value of $h_t = 1/16$. In Fig. 7.7 (right side) we do the same for varying h_t while keeping the spatial cell size fixed $h_r = 1/16$. We study polynomial degrees $p = 0, 1, 2$ and 3 and obtain convergence rates of $p + 1$ for a polynomial order p in both scenarios. For further details we refer to [48] (Section 4.4).

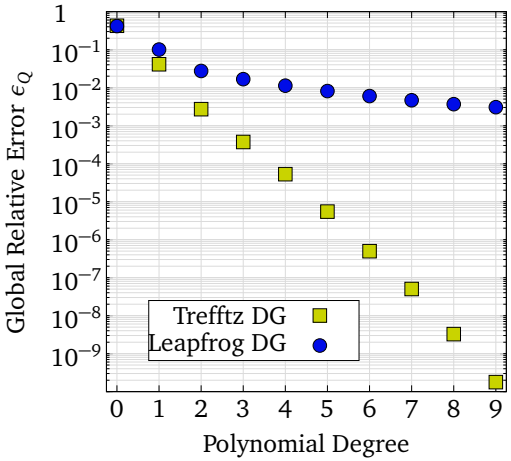

Figure 7.6.: Global relative errors ϵ_Q in the space-time L^2-norm (7.4) for the simulation of the wave propagation problem obtained with the discontinuous Galerkin Trefftz method (green boxes) and a DG method with a Leapfrog time-stepper (blue circles) on a mesh with 40×60 space-time cells for different polynomial orders p. The convergence curve of the Trefftz DG simulation indicates spectral convergence.

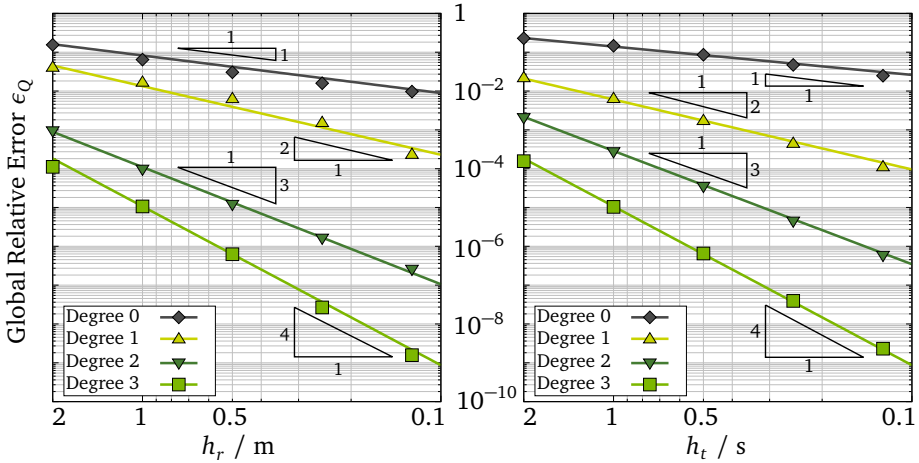

Figure 7.7.: Global relative errors ϵ_Q in the space-time L^2-norm (7.4) for the simulation of the wave propagation problem obtained with the discontinuous Galerkin Trefftz method with different polynomial degrees p. Left: convergence with respect to the spatial refinement; Right: convergence for temporal refinement. For both test series, the finest mesh was chosen to consist of 40×60 space-time cells.

Resonator Cavity: in the second example we study the error of a TM-mode which is oscillating in a rectangular cavity. To this end we consider Problem II with $\Omega = (-5,5) \times (-5,5)$ over $I = 50$ time-steps. Inside Ω we set the permittivity and permeability to $\epsilon = \mu = 1$. At the boundaries we apply PEC boundary conditions. The analytic solution of the problem is given by

$$
\begin{aligned}
H_x^{\mathrm{Cyl}} &= -\frac{n}{\omega L} \sin\left(\frac{\pi m x}{L}\right) \cos\left(\frac{\pi n y}{L}\right) \sin(\pi \omega t), \\
H_y^{\mathrm{Cyl}} &= \frac{m}{\omega L} \cos\left(\frac{\pi m x}{L}\right) \sin\left(\frac{\pi n y}{L}\right) \sin(\pi \omega t), \\
E_z^{\mathrm{Cyl}} &= \sin\left(\frac{\pi m x}{L}\right) \sin\left(\frac{\pi n y}{L}\right) \cos(\pi \omega t),
\end{aligned}
\tag{7.5}
$$

for arbitrary $m, n \in \mathbb{I}$ and $\omega = \sqrt{m^2 + n^2}$. We initialize the system at $t = 0$, with $E_{z,0}^{\mathrm{Cyl}}$ and $H_{x,0}^{\mathrm{Cyl}} = H_{y,0}^{\mathrm{Cyl}} = 0$. We execute the same investigation as was done in the previous example. The behavior of the error under p-enrichment is depicted in Fig. 7.8.

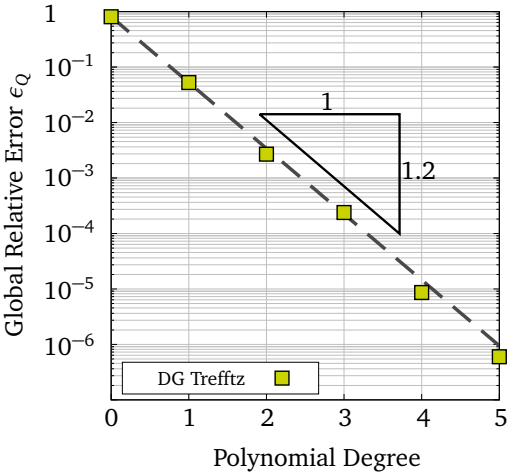

Figure 7.8.: Global relative errors ϵ_Q in the space-time L^2-norm (7.4) for the simulation of the cavity resonator problem obtained with the discontinuous Galerkin Trefftz method on a 10×10 mesh over 50 time-steps with different polynomial orders p. The convergence history indicates spectral convergence. Note that this figure corresponds to Figure 1 in [15].

We again receive spectral convergence in Q under p-enrichment. In Fig. 7.9 (left side) we study the behavior of the error under h_r refinement and in Fig. 7.9 (right side) the behavior of the error under h_t refinement, while keeping the respective other sufficiently small, namely $h_t, h_r = 1/16$. We observe convergence of order $p+1$ with respect to both, the spatial and temporal mesh-size. For further details we refer to [15] (Section 6.2).

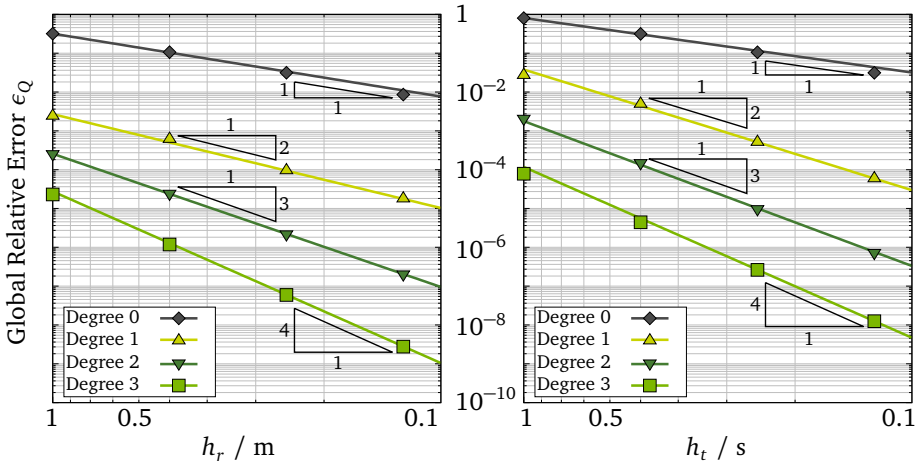

Figure 7.9.: Global relative errors ϵ_Q in the space-time L^2-norm (7.4) for the cavity resonator problem obtained with the discontinuous Galerkin Trefftz method with different polynomial degrees p. Left: convergence with respect to the spatial refinement; Right: convergence for temporal refinement. For both test series, the finest mesh was chosen to consist of 10×10 elements and 50 time steps. Note that this figure corresponds to Figure 2 in [15].

In the final part of this section we want to illustrate the effect of **d** enrichment for the previous scenario. For a given order p there exists a maximum of $2p+3$ polynomial Trefftz basis functions in this case (see (4.7)). In Fig. 7.10 we depict the behavior of the error while adding more directions according to the selection strategy that was introduced in Fig. 4.3 starting from three order zero polynomials (diamond bullet). The overall behavior of the error is illustrated by a linear fit of all values (gray dashed line). It results that the values of the full basis set, i.e. the last points of each polynomial degree lie on this fit curve. However, we can see an additional order-wise substructure in the convergence curve. In particular we obtain a jump in the convergence curve after a certain number of directions. For the order four values (pentagram bullets) the jump occurs between the 8^{th} and 9^{th}

value for instance. Here, the values of the last three directions are closer to the order five errors (circle bullets). Note that this effect is dependent on the nature of the problem and the strategy of the direction selection for the basis. If the direction of the actual solution is exactly represented by one of the basis functions, the error is at a minimum for the specific order.

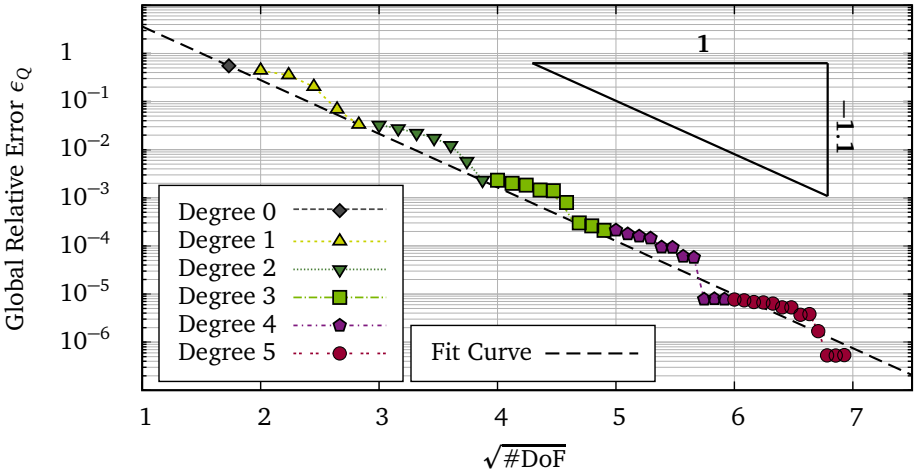

Figure 7.10.: Global relative errors ϵ_Q in the space-time L^2-norm (7.4) for the cavity resonator problem obtained with the discontinuous Galerkin Trefftz method on a 10×10 mesh over 50 time-steps. Behavior of the error under a d-enrichment, that has been introduced in Fig. 4.3, is shown.

7.3 Performance Study

So far we have studied the convergence of the error of the Trefftz method under refinement. In this context we have already indicated a comparison of our method with a *conventional* DG method that uses a Leapfrog time-stepper in Fig. 7.6 in terms of the obtained accuracy. However, this attempt is not sufficient to really compare the two methods since the execution time of the two schemes was simply ignored. Note at this point, that in any case it is difficult to compare different methods. For most "*real-world*" applications it is of major interest how long a certain

implementation of a method takes to produce results with a desired accuracy. For instance one can compare the relative error computed in the L_2-norm at time T

$$\epsilon_T = \frac{\sqrt{\sum_{K\in\Omega_h}\int_K \left((\mathbf{E}(T)-\mathbf{E}_h(T))^2+(\mathbf{H}(T)-\mathbf{H}_h(T))^2\right)dtdV}}{\sqrt{\sum_{K\in\Omega_h}\int_K (\mathbf{E}^2(T)+\mathbf{H}^2(T))\,dtdV}}, \tag{7.6}$$

for different methods in relation to their execution times. In Fig. 7.11 we show the simulation times of the previously considered one-dimensional problem (i.e. the propagation of a plane wave of Gaussian form).

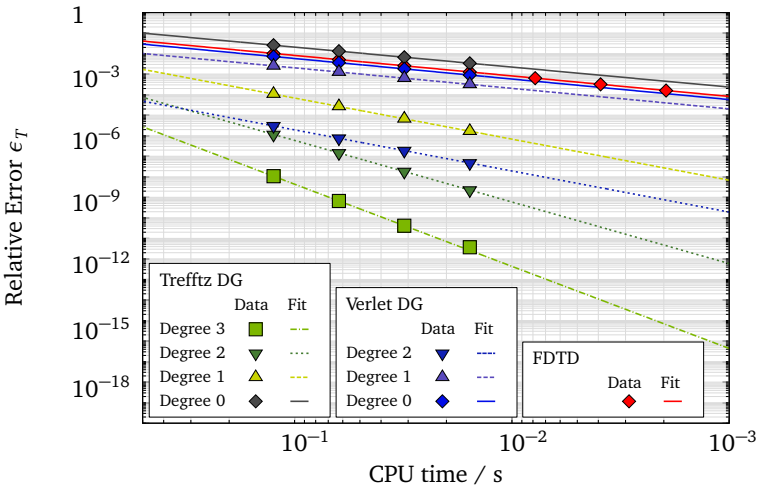

Figure 7.11.: Relative errors ϵ_T at the final time T in the L^2-norm (7.6) For the simulation of a one-dimensional wave propagation problem with the discontinuous Galerkin Trefftz method (green bullets), a discontinuous Galerkin method with a Verlet time-stepper (blue bullets) for different polynomial degrees as well as a FDTD method (red bullets) as function of CPU time.

The plot depicts the result of Matlab implementations of the DG Trefftz method (green bullets), a method that uses a DG discretization in combination with a Verlet time-stepper (blue bullets) and a FDTD method (red bullets). For the first two methods we show simulations with different polynomial degrees. We obtain that for relatively coarse accuracy (i.e. relative errors $\geq 10^{-3}$) the three methods seem to perform comparably well, whereas for fine accuracy (i.e. relative errors $< 10^{-3}$) the high order methods are better suited. Note at this point, that we do not want

to indicate that the DG Trefftz method is a more efficient method, since the performance of the method strongly depends on the numerical implementation as well as the considered problem. In addition, the direct comparison of low-order and high-order methods is dubious.

Let us now report about a more reasonable comparison, more precisely a direct comparison of a Trefftz and a comparable non-Trefftz method, see [47] (Section 7.3). To this end we consider Problem III in a domain $\Omega = (0, 60)$ bounded by PEC boundary conditions over a total time $T = 60$. We initialize $E_0 = -H_0 = \Psi^{\text{Gauss}}(\mathbf{r}, 0)$ with $\delta = 10$ and $x_0 = -10$ and simulate a wave propagation problem with an implementation of the space-time DG Method I in which we first employ Trefftz polynomials and tensorial non-Trefftz polynomials.

The results are depicted in Fig. 7.12. In both cases we observe (almost) the same spectral convergence as can be seen from Fig. 7.12 (left). However, the Trefftz space of order p has a smaller dimension. The error decreases exponentially with the number of degrees of freedom for the Trefftz method as can be seen from Fig. 7.12 (right), but exponentially only as a function of the square root of the number of degrees of freedom for the non-Trefftz method as can be seen from Fig. 7.12 (middle). The *a-priori* error analysis can be found in [47].

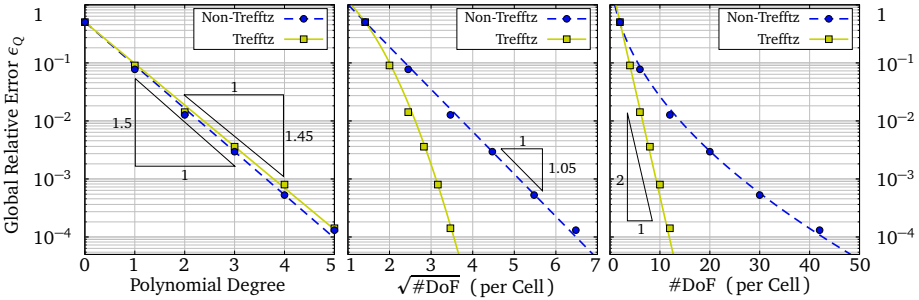

Figure 7.12.: Global relative errors ϵ_Q in the space-time L^2-norm (7.4) for the wave propagation problem for Trefftz and non-Trefftz basis functions against the polynomial degree (left), the square root of the number of degrees of freedom per element (middle), and the number of degrees of freedom per element (right), respectively.

Chapter Resumé

In this chapter we numerically investigated the error convergence of our method. In Section 7.1 we extracted dispersion relations as well as dissipation relations of our method from a sinusoidal wave simulation. We obtained a very small error due to dispersion. The dissipation of the method was found to increase with higher frequencies and decrease with higher polynomial approximations. In Section 7.1 we then used these findings to explain the behavior of a more involved example, i.e. the propagation of a box shaped signal.

In Section 7.2 we determined the error convergence behavior of our method. We found spectral convergence of the relative space-time error ϵ_Q (7.4) under p-enrichment and obtained optimal error convergence rates of $p+1$ under h-refinement. In addition we studied the behavior under a d-enrichment.

In Section 7.3 we compared an (one-dimensional) implementation of our method to established methods in terms of CPU time. In addition we have compared the errors of the space-time DG Trefftz method to an equivalent space-time DG method that uses conventional non-Trefftz basis functions. Here, the Trefftz method produces the same accuracy with considerably less degrees of freedom.

8 Transparent Boundary Conditions

In the numerical simulation of electromagnetic wave propagation problems one is commonly restricted to bounded computational domains, where two scenarios can appear: the domain of the underlying physical problem can either be restricted or unrestricted. The first scenario can be simulated by energy conserving boundary conditions such as PEC or PMC boundary conditions. The simulation of the second scenario is accompanied by the employment of artificial boundary conditions, that should minimize parasitic reflections into the domain.

In this chapter we will introduce an approach to these transparent boundary conditions in the context of the discontinuous Galerkin Trefftz method, see [14] for details. In Section 8.1 we survey some of the established methods. In Section 8.2 we introduce the new transparent Trefftz boundary conditions. After that we discuss their convergence behavior as well as some restrictions in Section 8.3. We conclude the chapter with the discussion of a more complicated example in Section 8.4.

8.1 Survey of Established Open Boundary Conditions

Silver Müller (First Order): in (2.16) we have already introduced the Silver Müller boundary conditions. This form of open boundary condition is widely used in practice due to its simple implementation. In their mixed form Silver Müller boundary conditions read

$$\frac{1}{2}\left(\mathbf{n}\times\mathbf{E}-Z^{-1}\,\mathbf{n}\times(\mathbf{H}\times\mathbf{n})\right)=0, \tag{8.1a}$$

$$\frac{1}{2}\left(\mathbf{n}\times\mathbf{H}+Z\,\mathbf{n}\times(\mathbf{E}\times\mathbf{n})\right)=0. \tag{8.1b}$$

The condition mimics the Silver-Müller radiation condition [6, 55, 70]. Plane waves that impinge normally on these boundaries exactly satisfy the Silver-Müller boundary condition. A brief inspection of the Pointing vector

$$\mathbf{n}\cdot\mathbf{S}=\mathbf{n}\cdot(\mathbf{E}\times\mathbf{H})=\mathbf{H}\cdot(\mathbf{n}\times\mathbf{E})=Z|\mathbf{n}\times\mathbf{H}|^2$$

yields that energy is dissipated at the boundaries, in other words, the energy is absorbed by the boundary. In their original form *Silver-Müller* boundary conditions

are *first-order absorbing* boundary conditions. An improvement to these classical *Silver-Müller* boundary conditions was formulated by Joly et al. in [45]. This formulation still involves only first order derivatives of the fields. A subsequent stability analysis has been given by Sonnendrücker et al. in [4].

Absorbing Boundary Conditions (High Order): other possibilities for open boundaries include the classical Bayliss-Turkel [8, 51] and Enquist-Majda [16, 17], which allow to systematically construct conditions for arbitrary order. However, due to lack of stability, these are hardly ever used in practice. Let us also mention more recent methods due to Warburton, Hagstrom, Higdon, and others [20–22, 28, 29], that are mainly based on the Enquist-Majda conditions.

Perfectly Matched Layers: another strategy to minimize reflections from the artificial boundaries is to add an exterior absorbing layer, in which the fields decay very fast. This approach, known as perfectly matched layers, has been used very widely and successfully [9, 10]. However, the appropriate choice of geometric and physical parameters of the absorbing layer is not always completely clear in practice. In some cases it may be necessary to extend the computational domain substantially. Therefore, the PML layers are difficult to implement and control in practice.

BEM Coupling Methods: In some cases it is possible to formulate exact boundary conditions and then couple them via a boundary integral formulation to the domain as has been done in [44, 85]. This treatment leads to boundary conditions that are non-local in space and/or time [30, 52], which substantially complicates numerical computations and is seldom used in practice.

For a review and a comparison of various kinds of non-absorbing, transparent, or non-reflecting boundary conditions, we refer to [13, 98].

8.2 Trefftz Transparent Boundary Conditions

Let us now report on a novel type of open boundary condition for our method that has been introduced in [14] and is based on a very simple idea, that is only applicable to certain Trefftz basis functions, i.e. those that have a distinct direction of propagation $\mathbf{d}_i$. In this case we can separate the basis functions at a boundary with outward normal $\mathbf{n}$ into "*ingoing*" and "*outgoing*" basis functions

$$\begin{aligned} \mathbf{F}_i &= \begin{pmatrix} \mathbf{E}_i \\ \mathbf{H}_i \end{pmatrix} = \begin{pmatrix} \mathbf{E}_i^{\text{in}} \\ \mathbf{H}_i^{\text{in}} \end{pmatrix} + \begin{pmatrix} \mathbf{E}_i^{\text{out}} \\ \mathbf{H}_i^{\text{out}} \end{pmatrix}, \\ \mathbf{v}_i &= \begin{pmatrix} \mathbf{v}_i^{\mathbf{E}} \\ \mathbf{v}_i^{\mathbf{H}} \end{pmatrix} = \begin{pmatrix} \mathbf{v}_i^{E,\text{in}} \\ \mathbf{v}_i^{H,\text{in}} \end{pmatrix} + \begin{pmatrix} \mathbf{v}_i^{E,\text{out}} \\ \mathbf{v}_i^{H,\text{out}} \end{pmatrix}, \end{aligned} \tag{8.2}$$

according to the sign of the scalar product of $\mathbf{d}_i \cdot \mathbf{n}$

$$\mathbf{F}_i = \begin{cases} \mathbf{F}_i^{\text{in}} & \text{if} \quad \mathbf{d}_i \cdot \mathbf{n} < 0 \\ \mathbf{F}_i^{\text{out}} & \text{if} \quad \mathbf{d}_i \cdot \mathbf{n} \geq 0 \end{cases} \qquad \text{and} \qquad \mathbf{v}_i = \begin{cases} \mathbf{v}_i^{\text{in}} & \text{if} \quad \mathbf{d}_i \cdot \mathbf{n} < 0 \\ \mathbf{v}_i^{\text{out}} & \text{if} \quad \mathbf{d}_i \cdot \mathbf{n} \geq 0. \end{cases} \tag{8.3}$$

The considered electromagnetic field at the boundary can be point-wisely expanded in terms of these basis functions and written as an expansion $\mathbf{F} = (\mathbf{E}, \mathbf{H}) = \sum_i c_i \ (\mathbf{e}_i, \mathbf{h}_i)$.

For ideal transparent boundaries there are no reflections back into the considered domain of interest. This means that there are no incoming field parts at the boundary. In analogy to this physical scenario, it would be an idea to simply extinct the incoming field parts. To check the stability of this condition, let us investigate the energy flux

$$\mathbf{n} \cdot \mathbf{S} = \sum_{i,j} c_i c_j \ \mathbf{n} \cdot \big(\mathbf{e}_i \times \mathbf{h}_j\big) = \sum_j c_j^2 \ \big(\mathbf{n} \cdot \mathbf{d}_j\big) + \sum_{i \neq j} c_i c_j \ \mathbf{n} \cdot \big(\mathbf{e}_i \times \mathbf{h}_j\big),$$

through the boundary. Here, the summation is only over $\mathbf{n} \cdot \mathbf{d}_i > 0$ and $\mathbf{n} \cdot \mathbf{d}_j > 0$. When the field at the boundary is mostly propagating outwards the first term is larger than the last, which guarantees an energy outflow. Such a direct approach has been incorperated in the FLAME framework by Tsukerman et al., for instance.

We pursue a slightly different approach, that is provided by the underlying DG framework: instead of extincting the incoming field parts we penalize them. More precisely we consider an averaged combination of PEC-like and PMC-like boundary conditions with respective penalization's given by $\beta, \beta' \geq 0$ that are only tested with $\mathbf{v}_{\text{in}}$ and result in the following contribution

$$\tfrac{1}{2}\Big(\mathbf{n} \times \mathbf{H}_{in} \cdot \mathbf{v}_{in}^{\mathbf{E}} - \mathbf{n} \times \mathbf{E}_{in} \cdot \mathbf{v}_{in}^{\mathbf{H}} + \beta'(\mathbf{n} \times \mathbf{E}_{in}) \cdot (\mathbf{n} \times \mathbf{v}_{in}^{\mathbf{E}}) + \beta(\mathbf{n} \times \mathbf{H}_{in}) \cdot (\mathbf{n} \times \mathbf{v}_{in}^{\mathbf{H}})\Big), \tag{8.4}$$

at the boundary. Let us now investigate the energy balance at the boundaries. To this end we proceed in a similar fashion as in the proof of Theorem X. First, we test Method II with $(\mathbf{E}_h^n, \mathbf{H}_h^n)$ and transform the expression by inserting

$$\begin{aligned} &2\|\epsilon^{1/2}\big(\mathbf{E}_h^n(t^{n-1})\mathbf{E}_h{}^{n-1}(t^{n-1})\big)\|_\Omega^2 \\ &\quad = \|\epsilon^{1/2}\mathbf{E}_h^n(t^{n-1})\|_\Omega^2 + \|\epsilon^{1/2}\mathbf{E}_h^{n-1}(t^{n-1})\|_\Omega^2 - \|\epsilon^{1/2}\big(\mathbf{E}_h^n(t^{n-1}) - \mathbf{E}_h^{n-1}(t^{n-1})\big)\|_\Omega^2, \end{aligned}$$

as well as a equivalent expression for $\mathbf{H}$. After an integration by parts we yield

$$\begin{aligned}
&\frac{1}{2}\left(\|\epsilon^{1/2}\mathbf{E}_h^n(t^{n-1})\|_\Omega^2 + \|\mu^{1/2}\mathbf{H}_h^n(t^{n-1})\|_\Omega^2\right) \\
&\qquad = \frac{1}{2}\left(\|\epsilon^{1/2}\mathbf{E}_h^{n-1}(t^{n-1})\|_\Omega^2 - \|\epsilon^{1/2}\big(\mathbf{E}_h^n(t^{n-1}) - \mathbf{E}_h^{n-1}(t^{n-1})\big)\|_\Omega^2\right) \\
&\qquad + \frac{1}{2}\left(\|\mu^{1/2}\mathbf{H}_h^{n-1}(t^{n-1})\|_\Omega^2 - \|\mu^{1/2}\big(\mathbf{H}_h^n(t^{n-1}) - \mathbf{H}_h^{n-1}(t^{n-1})\big)\|_\Omega^2\right) \\
&\qquad - \int_{\partial\Omega\times I^n} \mathbf{n}\times\mathbf{E}_h^n\cdot\mathbf{H}_h^n - \mathbf{n}\times\mathbf{E}_{h,\mathrm{in}}^n\cdot\mathbf{H}_{h,\mathrm{in}}^n - \beta|\mathbf{n}\times\mathbf{H}_{h,\mathrm{in}}^n|_\Omega^2 - \beta'|\mathbf{n}\times\mathbf{E}_{h,\mathrm{in}}^n|_\Omega^2.
\end{aligned}$$

Note again that we only consider points at the global boundaries here. By comparison with Theorem VIII (without boundary terms) we deduce that the condition

$$\int_{\partial\Omega\times I^n} \mathbf{n}\times\mathbf{E}_h^n\cdot\mathbf{H}_h^n - \mathbf{n}\times\mathbf{E}_{h,\mathrm{in}}^n\cdot\mathbf{H}_{h,\mathrm{in}}^n + \beta|\mathbf{n}\times\mathbf{H}_{h,\mathrm{in}}^n|_\Omega^2 + \beta'|\mathbf{n}\times\mathbf{E}_{h,\mathrm{in}}^n|_\Omega^2 \geq 0,$$

has to hold for an energy dissipation at the boundary. Here, the latter two terms are positive semi-definite by definition (i.e. $\beta, \beta' \geq 0$), whereas

$$\begin{aligned}
&\int_{\partial\Omega\times I^n} \mathbf{n}\times\mathbf{E}_h^n\cdot\mathbf{H}_h^n - \mathbf{n}\times\mathbf{E}_{h,\mathrm{in}}^n\cdot\mathbf{H}_{h,\mathrm{in}}^n \\
&\qquad = \int_{\partial\Omega\times I^n} \mathbf{n}\times\mathbf{E}_{h,\mathrm{in}}^n\cdot\mathbf{H}_{h,\mathrm{out}}^n + \mathbf{n}\times\mathbf{E}_{h,\mathrm{out}}^n\cdot\mathbf{H}_{h,\mathrm{in}}^n + \mathbf{n}\times\mathbf{E}_{h,\mathrm{out}}^n\cdot\mathbf{H}_{h,\mathrm{out}}^n,
\end{aligned}$$

are also positive if the simulated field is mainly directed outwards. This can be assumed in analogy to the continuous consideration, since the last term dominates the first two.

8.3 Convergence Study

In analogy to the previous chapter, we conduct a numerical error study of the method in the presence of the new transparent boundary conditions. We consider Problem II with a homogeneously filled (i.e. $\epsilon = \mu = 1$) domain $\Omega = (0,10) \times (0,10)$. Here we initialize $H_x = H_y = E_z = \Psi^{\text{Gauss}}(\mathbf{r},0)$ according to (6.3) with $\delta = 4$, $\mathbf{r}_0 = (4,4,0)$ which is propagating in direction $\mathbf{k} = 1/\sqrt{2}(-1,-1,0)$ over a total time $T = 100$. At $(x,0)$ and $(0,y)$ we utilize the new transparent boundary conditions whereas on the in-going boundaries at $(x,10)$ and $(10,y)$ we use pec-like impedance boundary conditions of the form

$$\mathbf{n} \times \mathbf{E} = \mathbf{n} \times \mathbf{g}(\mathbf{r},t).$$

Since this test scenario has got an analytic solution, i.e. (6.3), the function $\mathbf{g}(\mathbf{r},t)$ can be exactly determined from it. In Fig. 8.1 we depict the propagation of the wave at four stages.

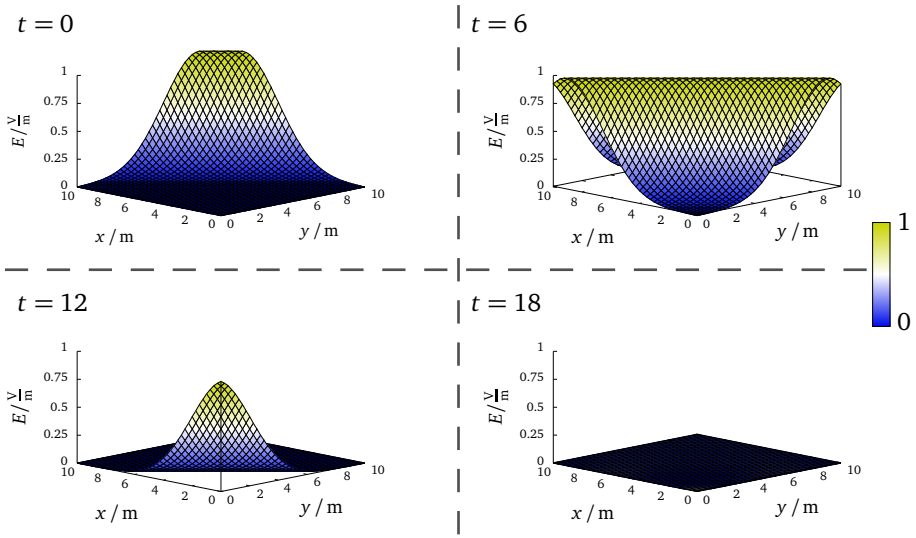

Figure 8.1.: Electric field of a plane wave propagating through the domain $(0,10) \times (0,10)$ covered by a homogeneous medium. At $x = 0$ and $y = 0$ the new transparent boundary conditions are applied, whereas at $x = 10$ and $y = 10$ exact boundary conditions are enforced. The solution is displayed at four relevant time steps: the start of the wave propagation (upper left), the first impinging of the wave at the transparent boundaries (upper right), the last outflow of the wave (lower left), and the remnants of the wave after the absorption (lower right).

Let us now conduct a convergence study similar to that of the preceeding chapter. As a first test we study the behavior of the error when enriching the polynomial degree p. The result is shown in Fig. 8.2. In this scenario we obtain spectral convergence for the new transparent boundary conditions (green boxes) if a proper choice of direction in the polynomial basis is applied as well as with the exact impedance boundary conditions (gray dashed line), which in practical scenarios are not available, of course. Here, the transparent boundary conditions perform almost as good. Transparent boundary conditions with a bad choice of directions in the polynomial basis (green diamonds) as well as the conventional SM boundary condition (blue circles) yield a saturation due to systematic consistency errors arising from the facts that the wave is not properly represented by the basis and that the wave does not impinge on the transparent boundary at a normal angle, respectively.

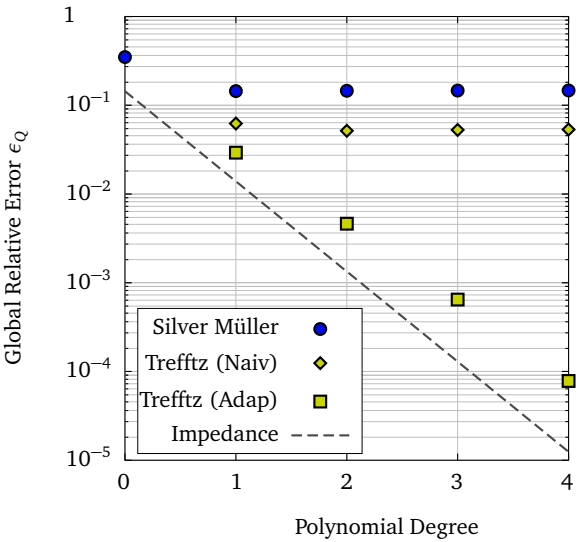

Figure 8.2.: Global relative errors ϵ_Q in the space-time L^2-norm (7.4) for a wave traveling at a 45° angle through the domain $(0, 10) \times (0, 10)$. The new Trefftz transparent boundary conditions with a naiv directional choice (green diamonds) as well as an adaptive directional choice (green boxes) are compared to conventional SM boundary conditions (blue circles) and impedance boundary conditions that use an 'analytic' function $\mathbf{g}(\mathbf{r}, t)$ at all boundaries. Here, one basis function coincides with the analytic field.

In the second test we study the convergence order for a proper choice of directions with fixed polynomial degrees under h-refinement. In contrast to the previous section we decrease the spatial cell size h_r and temporal cell size h_t simultaneously. The error convergence is visualized in Fig. 8.3.

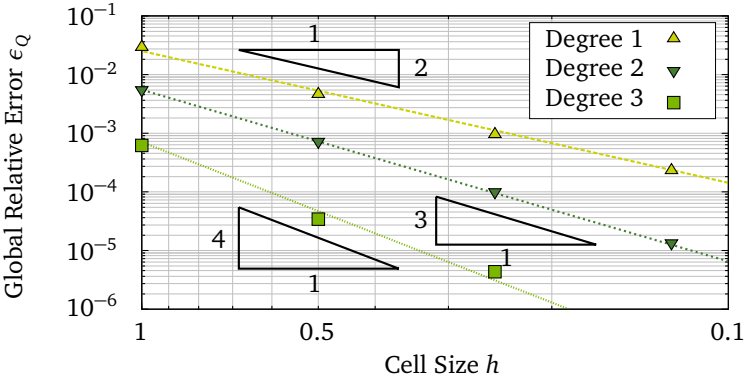

Figure 8.3.: Global relative errors ϵ_Q in the space-time L^2-norm (7.4) for a wave traveling at a 45° angle through the domain $(0, 10) \times (0, 10)$ for different polynomial degrees p under simultaneous refinement of h_t and h_r. Note that this figure corresponds to Figure 5 of [14].

In the previous tests we have chosen the basis functions according to the equidistant selection strategy that was mentioned in Fig. 4.3. In this case there exists one possibility to adapt the basis, direction-wise, i.e. by the choice of the first direction $\mathbf{d}_0^p$ of a certain order. In the previous tests this direction has been chosen in such a way, that it coincides with the direction of propagation of the simulated wave. Let us now study the behavior of the error if we change the corresponding offset angle γ. In Fig. 8.4 we depict the results for the Trefftz transparent boundary conditions (green bullets) and the conventional SM boundary conditions (blue bullets) for various polynomial degrees as a function of the angular difference between the offset of the basis function and the physical solution. For SM boundary conditions we do not see any dependence on this angle. However, for the Trefftz transparent boundary conditions there exists a dependence. The closer the direction of a function in the basis gets to the actual field, the lower gets the error. This dependence is getting more drastic when the polynomial degree is increased.

According to Fig. 8.4 one obtains that the $p+1$ convergence order is lost, when the directions of the basis functions are bigger than $\gamma = |\frac{\pi}{8}|$ (for $p = 3$) away from the actual direction of the propagation of the fields. However, the total error is still lower than that of the conventional SM boundaries.

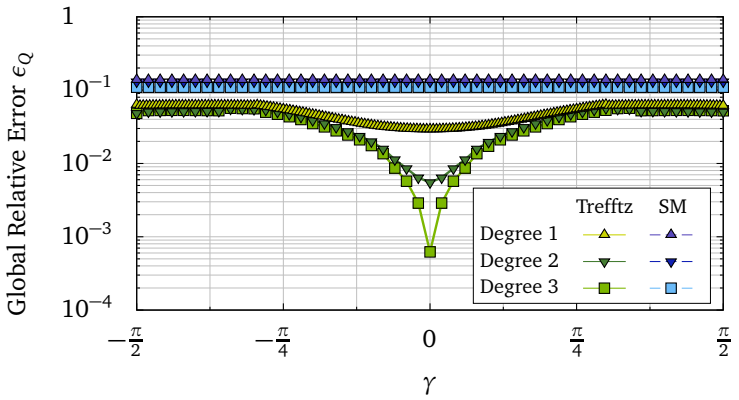

Figure 8.4.: Global relative errors ϵ_Q in the space-time L^2-norm (7.4) for a wave traveling at a 45° angle through the domain $(0, 10) \times (0, 10)$ for different offset angles of the basis functions. Both transparent Trefftz boundary conditions (green bullets) and conventional SM boundary conditions (blue bullets) with different polynomial degrees are shown.

Concludingly, we can state that spectral convergence can be obtained only if the directions $\mathbf{d}_i$ of the basis functions are chosen approximately.

8.4 Energy Dissipation Behaviour

Let us now study the behavior of the energy for a more complicated example. More precisely we consider Problem II in a homogeneous domain $\Omega = (-10, 10) \times (-10, 10)$ consisting of a vacuum, i.e. $\epsilon = \mu = 1$, with the new transparent Trefftz boundary conditions at all four boundaries. We initialize a cylindrical pulse

$$\Psi^{\text{Pulse}}(x, y) = \exp\left(-\left(x^2 + y^2\right)/\delta\right), \tag{8.5}$$

by setting $\mathbf{H}_{x,0} = \mathbf{H}_{y,0} = 0$ and $\mathbf{E}_{z,0} = \Psi^{\text{Pulse}}(x, y)$ with $\delta = 18$. Note that for this scenario there exists no analytic solution as we have stated in Sections 5.2 and 6.2 of [14]. The propagation is depicted in Fig. 8.5.

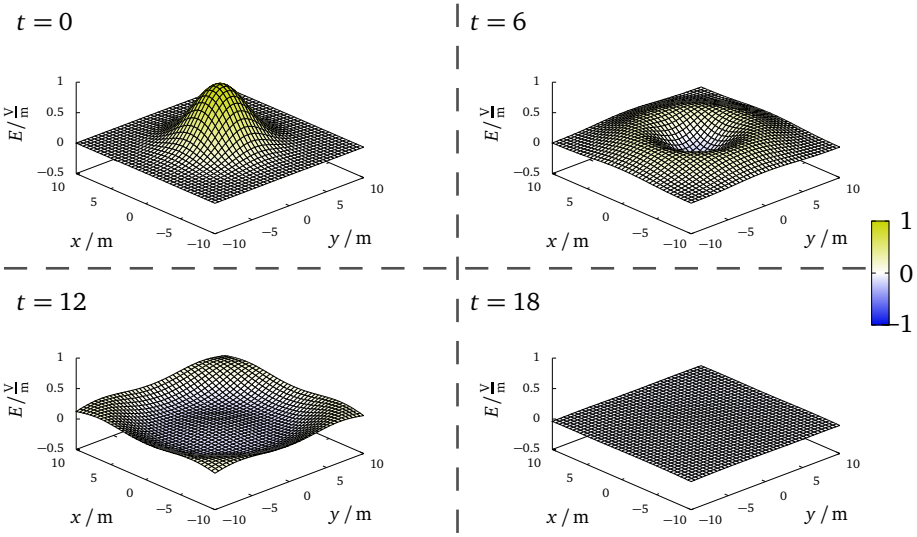

Figure 8.5.: Electric field of a cylindrical wave through the domain $(-10, 10) \times (-10, 10)$ covered by a homogeneous medium. The snapshot picture (upper left) depicts the start of the cylindrical wave propagation. The second picture (upper right) shows the time when the cylindrical wave is impinging at the transparent boundaries. In the third picture (lower left) most parts of the original cylindrical wave have left the domain through the transparent boundaries. The last picture (lower right) depicts the remnants of the cylindrical wave. Note that this figure corresponds to Figure 3 of [14].

Let us now investigate the evolution of the total electromagnetic energy contained in the computational domain. Here, we compare the decay of the energy simulated with the various versions Trefftz transparent boundary conditions (green dotted line, purple dotted line and green solid line) to a refference solution (gray dashed line) that has been done in a larger domain $(-30, 30) \times (-30, 30)$ which has then been truncated in Ω as well as a common SM boundary condition (blue solid line). The evolution of the energy is displayed in Fig. 8.6. We split the time evolution into four phases. In the first phase the wave is propagating freely inside the computational domain Ω. In this phase, the energy stays constant. In the second phase, the wave front hits the boundary; and energy starts to flow out of the system. In the third phase, the tail part of the wave front hits the boundary. In the last phase the remaining energy slowly flows out of the domain.

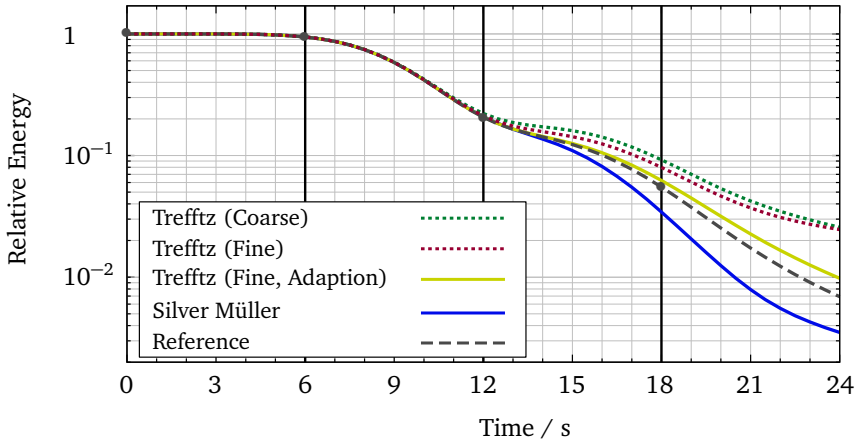

Figure 8.6.: Evolution of the total energy of a cylindrical wave pulse. All simulations are carried out with approximation order $p = 3$. The reference solution (gray dashed line) is computed on a larger domain $(-30, 30) \times (-30, 30)$. Simulations with transparent Trefftz boundary conditions are computed on a coarse mesh (green dotted line), a fine mesh (purple dotted line) and a fine mesh with addaption (solid green line) and compared to a simulation with SM boundary conditions (solid blue line), also on a fine mesh. The gray dots correspond to the fields displayed in Fig. 8.5.

After approximately 100 time-steps the energy of all Trefftz simulations converges to the reference solution. In the third and fourth phase we obtain effects of the previously mentioned consistency error, due to parasitic reflections, again

(c.f. coarse Trefftz simulation). If we apply a h-refinement, the solution becomes slightly better (c.f. fine Trefftz simulation). After an additional directional addaption (where the directions in the basis are aligned the the direction of propagation of the pulse), the simulation becomes almost identical to the reference solution (c.f. coarse addapted Trefftz simulation), meaning that the parasitic reflections are minimized.

Chapter Resumé

In this chapter we introduced a novel type of transparent boundary conditions that exploit the knowledge of the direction of propagation of the underlying Trefftz basis functions. In Section 8.2 we discussed the central idea of these boundary conditions, which is a penalization of in-going waves.

In Section 8.2 we studied the convergence of the error in certain scenarios. We obtained spectral convergence under p-enrichment and optimal convergence rates under h-refinement. However, the error was found to be dependent on the specific basis used. In some scenarios, i.e. where a directional adaption is possible, the error convergence can be improved. However, this is not possible in general.

In the last Section 8.1 we investigated the energy behavior of a pulse initialization. The energy was found to be strictly dissipative. However, an error due to parasitic reflections was obtained. This error was then decreased substentially by a mesh refinement and a directional addaption.

9 Conclusion

In this work we have developed and subsequently studied a novel numerical method in the context of electrodynamics. This method is based upon the discontinuous Galerkin framework; but employs polynomial Trefftz basis functions instead of generic tensorial basis functions that are commonly used in discontinuous Galerkin methods. The error of the method shows spectral convergence in space-time under p-enrichment with a reduced number of degrees of freedom compared to the tensorial version.

The main findings of this work are the following: we have introduced the concept of polynomial Trefftz functions, i.e. polynomial functions that exactly solve Maxwell's equations. These functions inherently depend on both space and time and exhibit a deterministic temporal behavior which we formally expressed in Lemma I. As a consequence we were able to separate the spatial and the temporal behavior of the basis and determine the dimension of the polynomial basis. We have found a way to systematically construct polynomial Trefftz functions from already existing polynomials by an iterative application of newly developed recurrence relations (4.4) and a subsequent application of the superposition principle (4.3). Aside from this construction we have introduced a second way to construct a polynomial Trefftz basis in terms of transport polynomials in Section 4.3 that we employed in the numerical examples described above.

We have introduced the underlying discontinuous Galerkin framework which is a ultra-weak form of a discontinuous Galerkin method (see Method I). Here, we have first employed an abstract vector space and studied some of the underlying properties such as the implicit nature (see Theorem V), consistency (see Theorem VI), and stability (see Theorem VII and Theorem VIII). By the subsequent restriction of the vector spaces to that of Trefftz functions (Definition III) we obtained the discontinuous Galerkin Trefftz method (see Method II). Here, all volume terms of the original method trivially vanished, leaving a method that is solely defined on the skeleton of the space-time mesh. The resulting method preserves all properties from the underlying discontinuous Galerkin method. In addition the solutions were found to be unique (see Theorem XI) from which the well-possedness of the method follows.

With the numerical implementation mentioned before we were able to reproduce physically correct results. Subsequently, we have numerically studied the error con-

vergence of the method for smooth solutions. Herein, we have obtained spectral convergence in the whole space-time domain under p-enrichment as well as the desired $p+1$ convergence rates under respective temporal and spatial h-refinement for various scenarios.

In addition we have studied miscellaneous features that are unique to Trefftz methods: we demonstrated a construction of problem tailored basis functions in Section 6.3 and the development of a new type of transparent boundary condition in Chapter 8.

With this we conclude this work.

A Natural Units

In this appendix we comment on the unit system that is applied in (most) of our derivations and in our numerical implementation. In particular we would like to motivate our choice that admittedly seems odd and unphysical on first sight.

In SI units a vacuum is described by the vacuum permitivity $\epsilon_0 = \sim 8.854 \cdot 10^{-12}$ measured in Farads per meter [F/m=As/Vm] and the vacuum permeability $\mu_0 = 4\pi \cdot 10^{-6}$ measured in Henries per meter [H/m=Vs/Am]. The resulting speed of light $c = 299792458$ is measured in meters per seconds [m/s] as has been stated in Table 2.2 already. The electric field $\mathbf{E}$ is measured in Volts per meter [V/m] and magnetic field $\mathbf{H}$ in Amperes per meter [A/m] (see Table 2.1). Therefore, the spacial and temporal dimensions differ by a factor $\sim 10^8$, i.e. c_0, and the fields by a factor $\sim 10^{2.5}$, i.e. the intrinsic impedance in the vacuum. As a result both Gram and system matrices would be bad conditioned and needed to be artificially rescaled.

To avoid this problem from the beginning, we apply a trick widely used in theoretical physics (see Peskin Schröder Introduction [73] for instance) and consider Maxwell's equations in "*natural units*". Here, we set

$$\mu_0 = \epsilon_0 = c_0 = 1, \tag{A.1}$$

which results in $[V/A] = [m/s] = [1]$. As a result space and time as well as the electric and the magnetic fields do have comparable scales. Moreover the fields have the same units as is stated in Table A.1, which is a convenient byproduct for calculations. At the end of a calculation all quantities can then be transformed back to physically meaningful SI units.

Property	SI units	Natural units
ϵ_0	[A s /(V m)]	[d.f.]
μ_0	[Vs/(Am)]	[d.f.]
c_0	[m/s]	[d.f.]
$\mathbf{E}(\mathbf{r}, t)$	[V/m]	[V/m]
$\mathbf{H}(\mathbf{r}, t)$	[A/m]	[V/m]

Table A.1.: Units of physical properties in the SI convention and the natural unit system convention. Dimension free properties are marked "*d.f.*".

B Second Order Polynomial Trefftz Basis

In this Appendix we explicitly list the second order polynomials that we omited in Section 4.2 for completeness. According to the dimension formulat (4.2), we need a total of 30 linearly independent polynomials here. For instance, we can choose the ones in Table B.1.

i	1	2	3	4	5	6
$\mathbf{e}_i^2$	$\begin{pmatrix} 0 \\ x^2 \\ 0 \end{pmatrix}$	$\begin{pmatrix} 0 \\ 0 \\ x^2 \end{pmatrix}$	$\begin{pmatrix} y^2 \\ 0 \\ 0 \end{pmatrix}$	$\begin{pmatrix} 0 \\ 0 \\ y^2 \end{pmatrix}$	$\begin{pmatrix} z^2 \\ 0 \\ 0 \end{pmatrix}$	$\begin{pmatrix} 0 \\ z^2 \\ 0 \end{pmatrix}$
$\mathbf{h}_i^2$	$\begin{pmatrix} 0 \\ 0 \\ 0 \end{pmatrix}$	$\begin{pmatrix} 0 \\ 0 \\ 0 \end{pmatrix}$	$\begin{pmatrix} 0 \\ 0 \\ 0 \end{pmatrix}$	$\begin{pmatrix} 0 \\ 0 \\ 0 \end{pmatrix}$	$\begin{pmatrix} 0 \\ 0 \\ 0 \end{pmatrix}$	$\begin{pmatrix} 0 \\ 0 \\ 0 \end{pmatrix}$
...	7	8	9	10	11	12
...	$\begin{pmatrix} 0 \\ xz \\ 0 \end{pmatrix}$	$\begin{pmatrix} 0 \\ 0 \\ xy \end{pmatrix}$	$\begin{pmatrix} yz \\ 0 \\ 0 \end{pmatrix}$	$\begin{pmatrix} 2xz \\ 0 \\ -z^2 \end{pmatrix}$	$\begin{pmatrix} -x^2 \\ 0 \\ 2xz \end{pmatrix}$	$\begin{pmatrix} -x^2 \\ 2xy \\ 0 \end{pmatrix}$
...	$\begin{pmatrix} 0 \\ 0 \\ 0 \end{pmatrix}$	$\begin{pmatrix} 0 \\ 0 \\ 0 \end{pmatrix}$	$\begin{pmatrix} 0 \\ 0 \\ 0 \end{pmatrix}$	$\begin{pmatrix} 0 \\ 0 \\ 0 \end{pmatrix}$	$\begin{pmatrix} 0 \\ 0 \\ 0 \end{pmatrix}$	$\begin{pmatrix} 0 \\ 0 \\ 0 \end{pmatrix}$
...	13	14	15	16	17	18
...	$\begin{pmatrix} 2xy \\ -y^2 \\ 0 \end{pmatrix}$	$\begin{pmatrix} 0 \\ 2yz \\ -z^2 \end{pmatrix}$	$\begin{pmatrix} 0 \\ -y^2 \\ 2yz \end{pmatrix}$	$\begin{pmatrix} 0 \\ 0 \\ 0 \end{pmatrix}$	$\begin{pmatrix} 0 \\ 0 \\ 0 \end{pmatrix}$	$\begin{pmatrix} 0 \\ 0 \\ 0 \end{pmatrix}$
...	$\begin{pmatrix} 0 \\ 0 \\ 0 \end{pmatrix}$	$\begin{pmatrix} 0 \\ 0 \\ 0 \end{pmatrix}$	$\begin{pmatrix} 0 \\ 0 \\ 0 \end{pmatrix}$	$\begin{pmatrix} 0 \\ x^2 \\ 0 \end{pmatrix}$	$\begin{pmatrix} 0 \\ 0 \\ x^2 \end{pmatrix}$	$\begin{pmatrix} y^2 \\ 0 \\ 0 \end{pmatrix}$

...	19	20	21	22	23	24
...	$\begin{pmatrix}0\\0\\0\end{pmatrix}$	$\begin{pmatrix}0\\0\\0\end{pmatrix}$	$\begin{pmatrix}0\\0\\0\end{pmatrix}$	$\begin{pmatrix}0\\0\\0\end{pmatrix}$	$\begin{pmatrix}0\\0\\0\end{pmatrix}$	$\begin{pmatrix}0\\0\\0\end{pmatrix}$
...	$\begin{pmatrix}0\\0\\y^2\end{pmatrix}$	$\begin{pmatrix}z^2\\0\\0\end{pmatrix}$	$\begin{pmatrix}0\\z^2\\0\end{pmatrix}$	$\begin{pmatrix}0\\xz\\0\end{pmatrix}$	$\begin{pmatrix}0\\0\\xy\end{pmatrix}$	$\begin{pmatrix}yz\\0\\0\end{pmatrix}$
...	25	26	27	28	29	30
...	$\begin{pmatrix}0\\0\\0\end{pmatrix}$	$\begin{pmatrix}0\\0\\0\end{pmatrix}$	$\begin{pmatrix}0\\0\\0\end{pmatrix}$	$\begin{pmatrix}0\\0\\0\end{pmatrix}$	$\begin{pmatrix}0\\0\\0\end{pmatrix}$	$\begin{pmatrix}0\\0\\0\end{pmatrix}$
...	$\begin{pmatrix}2xz\\0\\-z^2\end{pmatrix}$	$\begin{pmatrix}-x^2\\0\\2xz\end{pmatrix}$	$\begin{pmatrix}-x^2\\2xy\\0\end{pmatrix}$	$\begin{pmatrix}2xy\\-y^2\\0\end{pmatrix}$	$\begin{pmatrix}0\\2yz\\-z^2\end{pmatrix}$	$\begin{pmatrix}0\\-y^2\\2yz\end{pmatrix}$

Table B.1.: Linearly independent polynomials that form a basis of order two.

By applying the Trefftz construction procedure described in Section 4.2, meaning application of the expansion (4.3) and recurrence relations (4.4) we obtain the corresponding Trefftz basis in Table B.2.

i	1	2	3	4	5	6
$\mathbf{e}_i^2$	$\begin{pmatrix}0\\x^2+v^2t^2\\0\end{pmatrix}$	$\begin{pmatrix}0\\0\\x^2+v^2t^2\end{pmatrix}$	$\begin{pmatrix}y^2+v^2t^2\\0\\0\end{pmatrix}$	$\begin{pmatrix}0\\0\\y^2+v^2t^2\end{pmatrix}$	$\begin{pmatrix}z^2+v^2t^2\\0\\0\end{pmatrix}$	$\begin{pmatrix}0\\z^2+v^2t^2\\0\end{pmatrix}$
$\mathbf{h}_i^2$	$\begin{pmatrix}0\\0\\-2xvt\end{pmatrix}$	$\begin{pmatrix}0\\2xvt\\0\end{pmatrix}$	$\begin{pmatrix}0\\0\\2yvt\end{pmatrix}$	$\begin{pmatrix}-2yvt\\0\\0\end{pmatrix}$	$\begin{pmatrix}0\\-2zvt\\0\end{pmatrix}$	$\begin{pmatrix}2zvt\\0\\0\end{pmatrix}$
...	7	8	9	10	11	12
...	$\begin{pmatrix}0\\xz\\0\end{pmatrix}$	$\begin{pmatrix}0\\0\\xy\end{pmatrix}$	$\begin{pmatrix}yz\\0\\0\end{pmatrix}$	$\begin{pmatrix}2xz\\0\\-z^2-v^2t^2\end{pmatrix}$	$\begin{pmatrix}-x^2-v^2t^2\\0\\2xz\end{pmatrix}$	$\begin{pmatrix}-x^2-v^2t^2\\2xy\\0\end{pmatrix}$
...	$\begin{pmatrix}xvt\\0\\-zvt\end{pmatrix}$	$\begin{pmatrix}-xvt\\yvt\\0\end{pmatrix}$	$\begin{pmatrix}0\\-yvt\\zvt\end{pmatrix}$	$\begin{pmatrix}0\\-2xvt\\0\end{pmatrix}$	$\begin{pmatrix}0\\2zvt\\0\end{pmatrix}$	$\begin{pmatrix}0\\0\\-2yvt\end{pmatrix}$
...	13	14	15	16	17	18
...	$\begin{pmatrix}2xy\\-y^2-v^2t^2\\0\end{pmatrix}$	$\begin{pmatrix}0\\2yz\\-z^2-v^2t^2\end{pmatrix}$	$\begin{pmatrix}0\\-y^2-v^2t^2\\2yz\end{pmatrix}$	$\begin{pmatrix}0\\0\\2xvt\end{pmatrix}$	$\begin{pmatrix}0\\-2xvt\\0\end{pmatrix}$	$\begin{pmatrix}0\\0\\-2yvt\end{pmatrix}$
...	$\begin{pmatrix}0\\0\\2xvt\end{pmatrix}$	$\begin{pmatrix}2yvt\\0\\0\end{pmatrix}$	$\begin{pmatrix}-2zvt\\0\\0\end{pmatrix}$	$\begin{pmatrix}0\\x^2+v^2t^2\\0\end{pmatrix}$	$\begin{pmatrix}0\\0\\x^2+v^2t^2\end{pmatrix}$	$\begin{pmatrix}y^2+v^2t^2\\0\\0\end{pmatrix}$

…	19	20	21	22	23	24
…	$\begin{pmatrix} 2yvt \\ 0 \\ 0 \end{pmatrix}$	$\begin{pmatrix} 0 \\ 2zvt \\ 0 \end{pmatrix}$	$\begin{pmatrix} -2zvt \\ 0 \\ 0 \end{pmatrix}$	$\begin{pmatrix} -xvt \\ 0 \\ zvt \end{pmatrix}$	$\begin{pmatrix} xvt \\ -yvt \\ 0 \end{pmatrix}$	$\begin{pmatrix} 0 \\ yvt \\ -zvt \end{pmatrix}$
…	$\begin{pmatrix} 0 \\ 0 \\ y^2+v^2t^2 \end{pmatrix}$	$\begin{pmatrix} z^2+v^2t^2 \\ 0 \\ 0 \end{pmatrix}$	$\begin{pmatrix} 0 \\ z^2+v^2t^2 \\ 0 \end{pmatrix}$	$\begin{pmatrix} 0 \\ xz \\ 0 \end{pmatrix}$	$\begin{pmatrix} 0 \\ 0 \\ xy \end{pmatrix}$	$\begin{pmatrix} yz \\ 0 \\ 0 \end{pmatrix}$
…	25	26	27	28	29	30
…	$\begin{pmatrix} 0 \\ 2xvt \\ 0 \end{pmatrix}$	$\begin{pmatrix} 0 \\ -2zvt \\ 0 \end{pmatrix}$	$\begin{pmatrix} 0 \\ 0 \\ 2yvt \end{pmatrix}$	$\begin{pmatrix} 0 \\ 0 \\ -2xvt \end{pmatrix}$	$\begin{pmatrix} -2yvt \\ 0 \\ 0 \end{pmatrix}$	$\begin{pmatrix} 2zvt \\ 0 \\ 0 \end{pmatrix}$
…	$\begin{pmatrix} 2xz \\ 0 \\ -z^2-v^2t^2 \end{pmatrix}$	$\begin{pmatrix} -x^2-v^2t^2 \\ 0 \\ 2xz \end{pmatrix}$	$\begin{pmatrix} -x^2-v^2t^2 \\ 2xy \\ 0 \end{pmatrix}$	$\begin{pmatrix} 2xy \\ -y^2-v^2t^2 \\ 0 \end{pmatrix}$	$\begin{pmatrix} 0 \\ 2yz \\ -z^2-v^2t^2 \end{pmatrix}$	$\begin{pmatrix} 0 \\ -y^2-v^2t^2 \\ 2yz \end{pmatrix}$

Table B.2.: Polynomial Trefftz basis functions of order two corresponding to Table B.1 .

C Update Matrices

In this Appendix we explicitly state the element-wise constituents of the matrices used in the numerical scheme (5.13). We use fluxes that are centered in space and upwind in time. Let us consider the contributing terms in a example space-time with spatial index $\mathbf{k}$ at time n. First we obtain a contribution spatial flux term inside the cell

$$f_{\mathbf{k}}^{p,q,n} \sum_{k,l,m}^{x,y,z} \Bigg(\int\int\int \frac{1}{2}\epsilon_{klm} \left(u_k^{E,p}|_{\partial r_m^-} u_l^{H,q}|_{\partial r_m^-} - u_k^{E,p}|_{\partial r_m^+} u_l^{H,q}|_{\partial r_m^+} \right) dr_k dr_l dt \tag{C.1a}$$

$$- \int\int\int \frac{1}{2}\epsilon_{klm} \left(u_k^{H,p}|_{\partial r_m^-} u_l^{H,q}|_{\partial r_m^-} - u_k^{H,p}|_{\partial r_m^+} u_l^{E,q}|_{\partial r_m^+} \right) dr_k dr_l dt \Bigg). \tag{C.1b}$$

The Levi-Civita Symbol ϵ_{klm} denotes the rotation over all components $\{x, y, z\}$. Here, $u_y^q|_{\partial r_z^+}$ denotes the y component of $\mathbf{u}^{\mathbf{E},q}$ at the positive z interface of the cell (and analogously "$-$" for the left interface). In addition the spatial flux terms contribute to the neighboring cells. In x direction this reads

$$f_{\mathbf{k}\pm\hat{\mathbf{k}}_x}^{p,q,n} \Bigg(\pm \int\int\int \frac{1}{2} \left(u_{y,\mathbf{k}\pm\hat{\mathbf{k}}_x}^{E,p}|_{\partial x^\mp} u_{z,\mathbf{k}}^{H,q}|_{\partial x^\pm} - u_{z,\mathbf{k}\pm\hat{\mathbf{k}}_x}^{E,p}|_{\partial x^\mp} u_{y,\mathbf{k}}^{H,q}|_{\partial x^\pm} \right) dydzdt \tag{C.1c}$$

$$\mp \int\int\int \frac{1}{2} \left(u_{y,\mathbf{k}\pm\hat{\mathbf{k}}_x}^{H,p}|_{\partial x^\mp} u_{z,\mathbf{k}}^{E,q}|_{\partial x^\pm} - u_{z,\mathbf{k}\pm\hat{\mathbf{k}}_x}^{H,p}|_{\partial x^\mp} u_{y,\mathbf{k}}^{E,q}|_{\partial x^\pm} \right) dydzdt \Bigg).$$

For the neighboring cells in y direction we obtain

$$f_{\mathbf{k}\pm\hat{\mathbf{k}}_y}^{p,q,n} \Bigg(\pm \int\int\int \frac{1}{2} \left(u_{z,\mathbf{k}\pm\hat{\mathbf{k}}_y}^{E,p}|_{\partial y^\mp} u_{x,\mathbf{k}}^{H,q}|_{\partial y^\pm} - u_{x,\mathbf{k}\pm\hat{\mathbf{k}}_y}^{E,p}|_{\partial y^\mp} u_{z,\mathbf{k}}^{H,q}|_{\partial y^\pm} \right) dxdzdt \tag{C.1d}$$

$$\mp \int\int\int \frac{1}{2} \left(u_{z,\mathbf{k}\pm\hat{\mathbf{k}}_y}^{H,p}|_{\partial y^\mp} u_{x,\mathbf{k}}^{E,q}|_{\partial y^\pm} - u_{x,\mathbf{k}\pm\hat{\mathbf{k}}_y}^{H,p}|_{\partial y^\mp} u_{z,\mathbf{k}}^{E,q}|_{\partial y^\pm} \right) dxdzdt \Bigg).$$

And for the neighboring cells in z direction

$$f_{\mathbf{k}\pm\hat{\mathbf{k}}_z}^{p,q,n} \Bigg(\pm \int\int\int \frac{1}{2} \left(u_{x,\mathbf{k}\pm\hat{\mathbf{k}}_z}^{E,p}|_{\partial z^\mp} u_{y,\mathbf{k}}^{H,q}|_{\partial z^\pm} - u_{y,\mathbf{k}\pm\hat{\mathbf{k}}_z}^{E,p}|_{\partial z^\mp} u_{x,\mathbf{k}}^{H,q}|_{\partial z^\pm} \right) dxdydt \tag{C.1e}$$

$$\mp \int\int\int \frac{1}{2} \left(u_{x,\mathbf{k}\pm\hat{\mathbf{k}}_z}^{H,p}|_{\partial z^\mp} u_{y,\mathbf{k}}^{E,q}|_{\partial z^\pm} - u_{y,\mathbf{k}\pm\hat{\mathbf{k}}_z}^{H,p}|_{\partial z^\mp} u_{x,\mathbf{k}}^{E,q}|_{\partial z^\pm} \right) dxdydt \Bigg).$$

For cells at a global boundary $\partial\Omega$ these contributions will change. Let us outline the changes for PEC boundaries. Depending on the position of the PEC boundaries the contributions in the neighboring cells, (C.1c), (C.1d), (C.1e) as well as the part of the contribution in (C.1a) in the respective directions will vanish, respectively. From the temporal upwind flux we obtain two contributions. The contribution form time n reads

$$\mathbf{f}_{\mathbf{k}}^{p,q,n} \quad \int\int\int \left(\epsilon\, \mathbf{u}^{E,p,n}|_{\partial t^+} \cdot \mathbf{u}^{E,q,n}|_{\partial t^-} + \mu\, \mathbf{u}^{H,p,n}|_{\partial t^+} \cdot \mathbf{u}^{H,q,n}|_{\partial t^-}\right) dxdydz, \tag{C.2a}$$

whereas that from time $n-1$ reads

$$\mathbf{f}_{\mathbf{k}}^{p,q,n-1} \quad \int\int\int \left(\epsilon\, \mathbf{u}^{E,p,n-1}|_{\partial t^-} \cdot \mathbf{u}^{E,q,n}|_{\partial t^-} + \mu\, \mathbf{u}^{H,p,n-1}|_{\partial t^-} \cdot \mathbf{u}^{H,q,n}|_{\partial t^-}\right) dxdydz. \tag{C.2b}$$

To obtain a global scheme we assemble matrices with contributions over all cells $\mathbf{k}$ and all basis functions. At timestep t^n we obtain a contribution $\mathbf{f}^n\mathbf{A}$, with $\mathbf{f}^n$ being a coefficient vector and $\mathbf{A}$ a matrix. Here, the terms forms (C.1a), (C.1b) and (C.2a) contribute to the block diagonal of $\mathbf{A}$, whereas (C.1c), (C.1b), (C.1c) and possible boundary terms contribute to the off-block-diagonals. At time-step $n-1$ we obtain $\mathbf{f}^{n-1}\mathbf{R}$. Here, only (C.2b) contributes to the block diagonal of $\mathbf{R}$. In some scenarios we consider additional functions that need to be defined consistently with the scheme. As a final result, we obtain

$$\mathbf{A}\mathbf{f}^n = \mathbf{R}\mathbf{f}^{n-1} + \mathbf{G},$$

which is just (5.13) from Section 5.4.

Bibliography

[1] Mixed finite elements in R3. *Numerische Mathematik*, 35(3), 1980.

[2] M. Al Khatib and K. Grysa. Solving functions in problems of mathematical physics. *PAMM*, 3(1):374–375, 2003.

[3] M. Al Khatib, G. Krzysztof, and A. Maciąg. The method of solving polynomials in the beam vibration problem. *J Theor Appl Mech*, 46:347–366, 2008.

[4] F. Assous and E. Sonnendrücker. Joly-Mercier boundary condition for the finite element solution of 3D Maxwell equations. *Math Comput Model*, 51:935–943, 2010.

[5] Z. Badics. Trefftz Discontinuous Galerkin and Finite Element Multi Solver Technique for Modeling Time Harmonic EM Problems With High Conductivity Regions. *IEEE T Magn*, 50(2):1–125, 2 2014.

[6] H. Barucq and B. Hanouzet. Asymptotic behavior of solutions to Maxwell's system with absorbing Silver-Müller condition on the exterior boundary. *Asymptotic Anal.*, 15:25–40, 1997.

[7] D. Baumann, C. Fumeaux, P. Leuchtmann, and R. Vahldieck. Finite-volume time-domain (FVTD) modelling of a broadband double-ridged horn antenna. *Int. J. Numer. Model.*, 17:285–298, 2004.

[8] A. Bayliss, C. Goldstein, and E. Turkel. On accuracy conditions for the numerical computation of waves. *J Comp Phys*, 59(3):396–404, 1985.

[9] J. Berenger. A perfectly matched layer for the absorption of electromagnetic waves. *J Comput Phys*, (114):185–200, 1994.

[10] J. Berenger. Three-Dimensional Perfectly Matched Layer for the Absorption of Electromagnetic Waves. *J Comput Phys*, (127):363–379, 1996.

[11] F. Cajko and I. Tsukerman. Flexible approximation schemes for wave refraction in negative index materials. *IEEE Trans. Magn*, 44(6):1378–1381, 2008.

[12] J.-T. Chen, Y.-T. Lee, S.-R. Yu, and S.-C. Shieh. Equivalence between the Trefftz method and the method of fundamental solution for the annular Green's function using the addition theorem and image concept. *J Eng Anal Bound Elem*, 33:678–688, 2009.

[13] J. Dea. *High-order non-reflecting boundary conditions for the linearized euler equations*. PhD thesis, Naval Postgraduate School, Monterey, California, 2008.

[14] H. Egger, F. Kretzschmar, S. Schnepp, I. Tsukerman, and T. Weiland. Transparent boundary conditions in a discontinuous Galerkin Trefftz method. *ArXiv:1410.1899*, 2014.

[15] H. Egger, F. Kretzschmar, S. Schnepp, and T. Weiland. A space-time discontinuous galerkin trefftz method for time dependent maxwell's equations. *ArXiv:1412.2637*, 2014.

[16] B. Engquist and A. Majda. Absorbing boundary conditions for the numerical simulation of waves. *Math. Comp.*, (31):629–651, 1977.

[17] B. Engquist and A. Majda. Radiation boundary conditions for acoustic and elastic wave calculations. *Comm. Pure Appl. Math.*, (32):313–357, 1979.

[18] E. Gjonaj, T. Lau, S. Schnepp, F. Wolfheimer, and T. Weiland. Accurate Modelling of Charged Particle Beams in Linear Accelerators. *New J Phys*, 8:1–21, 2006.

[19] T. Griesmair and P. Monk. Discretization of the wave equation using continuous elements in time and a hybridizable discontinuous Galerkin method in space. *J Sci Comput*, 58:472–498, 2014.

[20] T. Hagstrom, M. De Castro, D. Givoli, and D. Tzemach. Local high-order absorbing boundary conditions for time-dependent waves in guides. *J Comput Acoust*, 15(01):1–22, 2007.

[21] T. Hagstrom and S. Hariharan. A formulation of asymptotic and exact boundary conditions using local operators. *Appl Numer Math*, 27:403–416, 1998.

[22] T. Hagstrom and T. Warburton. A new auxiliary variable formulation of high-order local radiation boundary conditions: corner compatibility conditions and extensions to frst-order systems. *Wave Motion*, 39(04):327–338, 2004.

[23] I. Herrera. Trefftz Herrera domain decomposition. *Adv Eng Softw*, 24:43–56, 1995.

[24] I. Herrera. Trefftz Herrera Method. *cames*, 4:369–382, 1997.

[25] I. Herrera. Trefftz Method: A General Theory. *Numer Methods Partial Differ Equ*, 16:561–580, 2000.

[26] I. Herrera. On Jirousek Method and its Generalizations. *Comp Ass Mech Eng Sci*, 8:325–342, 2001.

[27] J. Hesthaven and T. Warburton. *Nodal Discontinuous Galerkin Methods*. Springer, first edition, 2008.

[28] R. Higdon. Absorbing boundary conditions for difference approximations to the multidimensional wave equation. *Math. Comp.*, 47(176):437–459, 1986.

[29] R. Higdon. Numerical absorbing boundary conditions for the wave equation. *Math. Comp.*, 49(179):65–90, 1987.

[30] R. Hiptmair. Coupling of Finite Elements and Boundary Elements in Electromagnetic Scattering. *SIAM J Numer Anal*, 41(3):919–944, 2003.

[31] R. Hiptmair, A. Moiola, and I. Perugia. Plane wave discontinuous Galerkin methods for the 2D Helmholtz equation: analysis of the p-version. *SIAM J Numer Anal*, 49(1):264–284, 2011.

[32] R. Hiptmair, A. Moiola, and I. Perugia. Error analysis of Trefftz-discontinuous Galerkin methods for the time-harmonic Maxwell equations. *Math Comp*, 82:247–268, 2013.

[33] R. Hiptmair, A. Moiola, and I. Perugia. Trefftz discontinuous galerkin methods for acoustic scattering on locally refined meshes. *Applied Numerical Mathematics*, 79(0):79–91, 2014.

[34] J. Horvát. Basic Sets of Polynomial Solutions for Partial Differential Equations. *P Am Math Soc*, 6(2):569–575, 1958.

[35] T. Huttunen, M. Malinen, and P. Monk. Solving Maxwell's equations using the ultra weak variational formulation. *J Comput Phys*, 223(2):731–758, 2007.

[36] T. Huttunen, P. Monk, and P. K. Jari. Computational Aspects of the Ultra Weak Variational Formulation. *J Comput Phys*, 182:27–46, 2002.

[37] J. D. Jackson. *Classical Electrodynamics*. Wiley, 1999.

[38] I. T. Jianhua Dai. Flexible approximation schemes with adaptive grid refinement. *Magnetics, IEEE Transactions on*, 44(6):1206–1209, 7 2008.

[39] J. Jirousek. Basis for development of large finite elements locally satisfying all field equations. *Computer Methods in Applied Mechanics and Engineering*, 14(1):65–92, 4 1978.

[40] J. Jirousek and L. Guex. The Hybrid-Trefftz Finite Element Model and its Application to Plate Bending. *Int J Numer Meth Eng*, 23:651–693, 1986.

[41] J. Jirousek and N. Leon. A powerful finite element for plate bending. *Computer Methods in Applied Mechanics and Engineering*, 12(12):201–213, 9 1977.

[42] J. Jirousek and Q. Qin. Application of Hybrid Trefftz Element Approach to Transient Heat Conduction Analysis. *Comput Struct*, 58(1):195–201, 1994.

[43] J. Jirousek and A. Zielinski. Survey of Trefftz-type element formulations. *Comput Struct*, 63(2):225 – 242, 1997.

[44] C. Johnson and J. C. Nedelec. On the coupling of boundary integral and finite element methods. *Mathematics of Computation*, 35(152):1063–1079, 1980.

[45] P. Joly and B. Mercier. A new second order absorbing boundary condition for Maxwell's equations in dimension 3. *INRIA Res. Report*, 1047, 1989.

[46] E. Kita and N. Kamiya. Trefftz method: an overview. *Adv Eng Softw*, 24:3–12, 1995.

[47] F. Kretzschmar, A. Moiola, I. Perugia, and S. Schnepp. A priori error analysis of space-time trefftz discontinuous galerkin methods for wave problems. *ArXiv:1412.2637*, 2014.

[48] F. Kretzschmar, S. Schnepp, I. Tsukerman, and T. Weiland. Discontinuous Galerkin methods with Trefftz approximations. *J Comput Appl Math*, 270:211–222, 2014.

[49] G. Krzysztof and A. Maciąg. Solving Direct and Inverse Thermoelasticity Problems by Means of Trefftz Base Functions for Finite Element Method. *J Therm Stress*, 34:378–393, 2011.

[50] G. Krzysztof and A. Maciąg. Trefftz Functions For a Plate Vibration Problem. *J Theor Appl Mech*, 34:378–393, 2011.

[51] S. Kurz and S. Russenschuck. The application of the bem-fem coupling method for the accurate calculation of fields in superconducting magnets. *Electrical Engineering*, 82(1):1–10, 1980.

[52] S. Kurz and S. Russenschuck. *The application of the BEM-FEM coupling method for the accurate calculation of fields in superconducting magnets*, volume 82. Springer-Verlag, 1999.

[53] P. LeSaint and P.-A. Raviart. *On a finite element method for solving the neutron transport equation*. Academic Press, New York, 1974.

[54] Lev Davidovich Landau and Evgeny Mikhailovich Lifshitz. *Lehrbuch der Theoretischen Physik II - Klassische Feldtheorie*. Akademie Varlag, german edition, 1982.

[55] L. Li, S. Lanteri, and R. Perrussel. A hybridizable discontinuous Galerkin method combined to a Schwarz algorithm for the solution of 3d time-harmonic Maxwell's equation. *J Comput Phys*, 256:563–581, 2014.

[56] M. Lilienthal, S. Schnepp, and T. Weiland. Non-dissipative space-time hp - discontinuous galerkin method for the time-dependent maxwell equations. *Journal of Computational Physics*, 275:589–607, 2014.

[57] A. Maciąg. Three-dimensional wave polynomials. *Math Probl Eng*, 5:583–598, 2005.

[58] A. Maciąg. The usage of wave polynomials in solving direct and inverse problems for two dimensional wave equation. *Int J Numer Method Biomed Eng*, 27:1107–1125, 2009.

[59] A. Maciąg. Solving thermoelasticity problems by means of Trefftz functions. *Compute Assisted Mechanics and Engineering Sciences*, 16:193–208, 2010.

[60] A. Maciąg and Pawinska. Solving direct and inverse problems of plate vibrations by using the Treffz functions . *J Theor Appl Mech*, 51:543–552, 2013.

[61] A. Maciąg and J. Wauer. Solution of the two-dimensional wave equation by using wave polynomials. *J Eng Math*, 51:339–350, 2005.

[62] J. Maxwell. A Dynamical Theory of the Electromagnetic Field. *Phil Trans R Soc Lond*, 155:459–512, 1864.

[63] J. Maxwell. *A treatise on electricity and magnetism.* Clarendon Press, 1. edition edition, 1873.

[64] E. Miles and E. Williams. A Basic Set of Homogeneous Harmonic Polynomials in k Variables. *P Am Math Soc*, 6(2):191–194, 1955.

[65] E. Miles and E. Williams. A note on basic sets of homogeneous harmonic polynomials. *P Am Math Soc*, 6(2):769–770, 1955.

[66] E. Miles and E. Williams. The Cauchy problem for linear partial differential equations with restricted boundary conditions . *Canad J Math*, 8:426–431, 1956.

[67] T. Milligan. *Modern Antenna Design*. Wiley, New Jersey, 2005.

[68] A. Moiola. *Trefftz-discontinuous Galerkin methods for time-harmonic wave problems* . PhD thesis, ETH Zuerich, 2011.

[69] A. Moiola, R. Hiptmair, and I. Perugia. Plane wave approximation of homogeneous Helmholtz solutions. *Z Angew Math Phys*, 62(5):809–837, 2011.

[70] C. Muller. Randwertprobleme der Theorie elektromagnetischer Schwingungen. *Math Z*, 56:261–270, 1952.

[71] I. Muntenau and T. Weiland. RF & microwave simulation with the finite integration technique – from component to system design. In *SCEE 2006*, volume 11 of *Mathematics in Industry*, pages 247–260. 2007.

[72] J. Novak, A. Kucerova, and J. Zeman. Microstructural enrichment functions based on stochastic Wang tilings. *Modelling Simul Mater Sci Eng*, 21, 2013.

[73] M. Peskin and D. Schröeder. *An Introduction to Quantum Field Theory* . Basic Books, 1993.

[74] S. Petersen, C. Farhat, and R. Tezaur. A space-time discontinuous Galerkin method for the solution of the wave equation in the time domain. *Int J Numer Meth Eng*, 78(3):275–295, april 2009.

[75] J. Petrolito. Triangular Thick Plate Elements Based on a Hybrid-Trefftz Approach. *Comput Struct*, 60(6):883–894, 1996.

[76] R. Piltner. On the representation of three-dimensional elasticity solutions with the aid of complex valued functions . *Int J Numer Meth Eng*, 22:45–55, 1989.

[77] R. Piltner. Recent developments in the Trefftz method for finite element and boundary element applications. *Adv Eng Softw*, 24:107–115, 1995.

[78] H. Pinheiro, J. Webb, and I. Tsukerman. Flexible Local Approximation Models for Wave Scattering in Photonic Crystal Devices. *Magnetics, IEEE Transactions on*, 43(4):1321 –1324, april 2007.

[79] W. Reed and T. Hill. Triangular mesh methods for the neutron transport equation. Technical report, Los Alamos Scientific Laboratory Report, 1973.

[80] W. Ritz. Über eine neue Methode zur Lösung gewisser Variationsprobleme der mathematischen Physik. *J Reine Angew Math*, 135:1–61, 1909.

[81] P. Rosenbloom and D. Widder. Expansions in Terms of Heat Polynomials and Associated Functions. *T Am Math Soc*, pages 220–266, 1958.

[82] P. Runge. The complete Trefftz method. *Acta Mech*, 78(3-4):235–242, 1978.

[83] D. Sarmany, M. Botchev, and J. Vandervegt. Dispersion and Dissipation Error in High-Order Runge-Kutta Discontinuous Galerkin Discretisations of the Maxwell Equations. *J Sci Comput*, 33:47–74, 2007.

[84] I. Sloan and R. Womersley. Extremal systems of points and numerical integration on the sphere. *Advances in Computational Mathematics*, 21(1-2):107–125, 2004.

[85] J. Song and K. Li. The coupling of finite element method and boundary element method for two-dimensional helmholtz equation in an exterior domain. *J Comput Math*, 5(1):21–37, 1987.

[86] E. Stein. *Die Kombination der erweiterten Methode der finiten Elemente und direkter Variationsmethoden in grossen Bereichen bei der elastostatischen Berechnung von Flächentragwerken*. PhD thesis, University of Stuttgart, 1973.

[87] J. Stratton. *Electromagnetic theory*. McGraw-Hill Book Company, New York, 1941.

[88] E. Trefftz. *Ein Gegenstueck zum Ritzschen Verfahren*. Number 2. Internationaler Kongress fuer Technische Mechanik, Zurich, 1926.

[89] I. Tsukerman. A Flexible Local Approximation Method for Electro- and Magnetostatics. *IEEE T Magn*, 40(2), 2004.

[90] I. Tsukerman. A class of difference schemes with flexible local approximation. *J Comput Phys*, 211:659–699, 2006.

[91] I. Tsukerman and F. Cajko. Photonic Band Structure Computation Using FLAME. *Magnetics, IEEE Transactions on*, 44(6):1382 –1385, june 2008.

[92] D. Wang, C. Farhat, and R. Tezaur. A hybrid discontinuous in space and time Galerkin method for wave propagation problems. *Int J Num Meth Eng*, 99(4):263–289, 2014.

[93] T. Weiland. A discretization method for the solution of Maxwell's equations for six-component fields. *Electronics and Communications AEUE*, 31:116–120, 1977.

[94] K. Yee. Numerical solution of initial boundary value problems involving maxwell's equations in isotropic media. *IEEE T Antenn Propag*, 14(3):302–307, 1966.

[95] A. Zieliǹski and I. Herrera. Trefftz Method: Fitting Boundary Conditions. *Int J Numer Meth Eng*, 24:871–891, 1987.

[96] A. Zieliǹski and O. Zienkiewicz. Generalized finite Element Analysis with T-Complete Boundary Solution Functions. *Int J Numer Meth Eng*, 21:509–528, 1985.

[97] O. Zienkiewicz, R. Taylor, and J. Zhu. *The Finite Element Method, Its Basis and Fundamentals*. McGraw-Hill, Oxford, 1967.

[98] L. Zschiedrich. *Transparent Boundary Conditions for Maxwell's Equations: Numerical Concepts beyond the PML Method*. PhD thesis, FU Berlin, 2009.

List of Symbols

$\mathbf{h}^{2d}$ Unit vector in direction of the magnetic field for two-dimensional scenarios.. 41, 42
$\mathbf{H}_h^0$ Discretized intial magnetic field. 49, 54
$\mathbf{H}_0$ Initial magentic field. 29, 32, 49, 54
$\tilde{\mathbf{H}}$ Temporal magnetic flux. 47

I Total time interval. 17, 29, 31, 63–66, 76, 82, 84, III, V
Z Intrinsic impedance. 11, 12, 16, 32–35, 37, 38, 42, 68, 69, 91
I^n Time slab n. 30, 31, 35, 41, 46–49, 51–56, 82, 94

K Spatial element. 30–32, 35, 46–49, 51–55, 82, 87
K Two dimensional spatial element. 41
∂K Spatial boundary of element K. 51
k Wave vector. 76–79, 81

ϵ Electric permitivity. 9–14, 17, 29, 31, 35, 37, 42, 43, 47, 49, 51–55, 63–70, 73, 74, 84, 93–95, 99, 105
μ Magnetic permeability. 9–14, 17, 35, 37, 42, 43, 47, 49, 51–55, 63–70, 73, 74, 94, 95, 105

Ω Spatial domain. 13–17, 21, 29, 35, 48, 52, 54, 55, 63–66, 68, 71, 76, 79, 82, 84, 88, 93–95, 99, 112, III, V
$\partial\Omega_h$ Discretized spatial domain boundary. 51, 52, 55
Ω_h Discretized spatial domain. 35, 48, 49, 51–55, 82, 87

ω Frequency. 75–78, 84
ω_h Discrete frequency. 75, 77
$\mathbf{n}$ Outward normal. 6–8, 10, 13–17, 35, 47–52, 54, 55, 91–95

$\mathbf{r}$ Position vector. 6–9, 11, 12, 16, 17, 30–33, 35, 37, 41, 49, 50, 52, 54, 55, 66, 67, 70, 71, 73, 79, 82, 88, 95, 97

$\mathbf{v}$ First abstract test function. 47, 49–52, 54, 55, 92, 93
Q Space-time domain. 29, 31, 32, 41, 54, 66–68, 70, 82–86, 88, 89, 97–99
Q_h^n Discretized space-time at time n. 48, 51, 53–56
Q^n Discretized space-time at time n. 30, 31, 35, 41, 48, 53

t Time variable. 6–9, 11, 12, 16, 17, 29–35, 37, 41, 42, 47, 49–55, 63–71, 76, 77, 81, 84, 93–95, 97
$\mathbf{w}$ Second abstract test function. 22, 47, 49–52, 54, 55
$\mathbb{T}$ Polynomial Trefftz space for wave propagation problems. 29–32, 35, 41, 53–56
T Trefftz space for wave propagation problems. 29
n Time step n.. 30, 31, 35, 47, 49–56, 93, 94, 111, 112

$\mathcal{V}_n^E$ Abstract vector space. 48, 49, 51–54
$\mathcal{V}_n^H$ Abstract vector space. 48, 49, 51–54

List of Abbreviations

BC Boundary Conditions. 14

DG Discontinuous Galerkin. 1–3, 23, 25, 26, 45, 46, 82, 83, 86–89, 93
DGT Discontinuous Galerkin Trefftz. 2, 3, 45, 75, 82
DoF Degrees of Freedom. 25, 53

FDTD Finite Difference Time Domain. 1, 24, 26, 45, 46, 58, 87
FEM Finite Element Methods. 1, 23, 46, 58
FIT Finite Integration Technique. 45, 46, 58
FLAME Flexible Local Approximation Method. 24, 26, 46, 93

PBC Periodic Boundary Conditions. 15, 64, 65, 79
PDE Partial Differential Equation. 1, 7, 21, 28, 29
PEC Perfect Electric Conductor. 14, 15, 64–66, 71, 76, 82, 84, 88, 91, 93, 112
PMC Perfect Magnetic Conductor. 15, 64, 65, 71, 79, 91, 93

SI Systeme International. 7, 9, 105
SM Silver Müller Boundary Conditions. 16, 96–101

TBC Transparent Boundary Conditions. 16, 25

Acknowledgement

First of all I want to thank Laura, my family and my friends for supporting me during my research with non-topic specific support and thereby making this work possible.

I would like to thank Thomas Weiland for his excellent supervision. In particular I would like to thank for the constant practical advices, motivation and for the enduring support.

My greatest thanks go to Sascha Schnepp for providing this dissertation topic. Moreover I would like to thank, for introducing me into the field of discontinuous Galerkin methods and for always supporting me. I would like to thank for his constant endurance during our endless discussions that finally made this thesis possible.

I would like to thank our collaborators, Igor Tsukerman, Andrea Moiola and Ilaria Perugia for all the great joint works in a very productive enviroment.

A special thank goes to Sascha Schnepp, Martin Lilienthal, Innocent Niyonzima, Herbert Egger, Dominik Smith, Nikolai Schmitt and Friedrich Helm for reading and correcting this work.

In addition I would like to thank Markus Lazanowski and Carina Schuster for the great management; And our administrator Christian Schmitt for smoothly manageing our comoutational infrastructure and installing countless Geek programs.

I would like to thank the 'Excellence Initiative' of the German Federal and State Governments and the Graduate School of Computational Engineering at Technische Universität Darmstadt for financially supporting this work.

Last but not least I would like to thank the reader for reading this thesis !